NASA CR-121208

GASL TR-781

A MATHEMATICAL MODEL FOR JET ENGINE

COMBUSTOR POLLUTANT EMISSIONS

by J. L. Boccio, G. Weilerstein and R. B. Edelman

GENERAL APPLIED SCIENCE LABORATORIES, INC.

CASE FILE
COPY

prepared for

NATIONAL AERONAUTICS AND SPACE ADMINISTRATION

NASA Lewis Research Center
Contract NASW-2235

GASL
516 333 6960
GENERAL APPLIED SCIENCE LABORATORIES, INC.

MERRICK AND STEWART AVENUES
WESTBURY, L. I., NEW YORK 11590

A MATHEMATICAL MODEL FOR JET ENGINE

COMBUSTOR POLLUTANT EMISSIONS
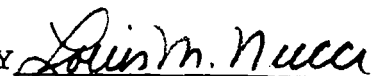
By J. L. Boccio
G. Weilerstein
R. B. Edelman

Prepared for

Prepared by

APPROVED BY _____
Louis M. Nucci
President

March 1973

Report No. NASA CR-121208	2. Government Accession No.	3. Recipient's Catalog No.
Title and Subtitle A MATHEMATICAL MODEL FOR JET ENGINE COMBUSTOR POLLUTANT EMISSIONS		5. Report Date March 1973
		6. Performing Organization Code
Author(s) J.L.Boccio, G. Weilerstein and R.B.Edelman		8. Performing Organization Report No. GASL TR-781
		10. Work Unit No.
Performing Organization Name and Address General Applied Science Labs.,Inc. Merrick and Stewart Avenues Westbury, New York 11590		11. Contract or Grant No. NASW-2235 Mod.1
Sponsoring Agency Name and Address National Aeronautics and Space Administration Lewis Research Center Cleveland, Ohio 44135		13. Type of Report and Period Covered 7/19/71-1/31/73 Contractor Report
		14. Sponsoring Agency Code

Supplementary Notes

Project Manager, David Anderson

Abstract Mathematical modeling for the description of the origin and disposition of combustion-generated pollutants in gas turbines is presented. A unified model in modular form is proposed which includes kinetics, recirculation, turbulent mixing, multiphase flow effects, swirl and secondary air injection. Subelements of the overall model have been applied to data relevant to laboratory reactors and practical combustor configurations. Comparisons between the theory and available data show excellent agreement for basic $CO/H_2/Air$ chemical systems. For hydrocarbons the trends are predicted well including higher-than-equilibrium NO levels within the fuel-rich regime. Although the need for improved accuracy in fuel-rich combustion is indicated, comparisons with actual jet-engine data in terms of the effect of combustor-inlet temperature is excellent. In addition, excellent agreement with data is obtained regarding reduced NO emissions with water droplet and steam injection.

Comparisons of predictions made on swirling flame data show that while good agreement can be obtained additional work is required in terms of the turbulent transport properties.

In general, the modeling presented herein has aided in the understanding of the emissions problem and has delineated areas needing further study.

17. Key Words (Suggested by Author(s)) Turbojet Pollution Mathematical Modeling Mixing Fluid Dynamics Chemistry		18. Distribution Statement Unclassified - Unlimited	
19. Security Classif. (of this report) Unclassified	20. Security Classif. (of this page) Unclassified		21. No. of Pages 96	22. Price

TABLE OF CONTENTS

1. SUMMARY

Mathematical modeling for the description of the origin
and disposition of combustion-generated pollutants in gas
turbines is presented. A unified model in modular form is
proposed which includes kinetics, recirculation, turbulent
mixing, multiphase flow effects, swirl and secondary air
injection. Subelements of the overall model have been applied
to data relevant to laboratory reactors and practical combustor
configurations. Comparisons between the theory and available
data show excellent agreement for basic $CO/H_2/Air$ chemical
systems. For hydrocarbons the trends are predicted well
including higher-than-equilibrium NO levels within the fuel-
rich regime. Although the need for improved accuracy in fuel-
rich combustion is indicated, comparisons with actual jet-
engine data in terms of the effect of combustor-inlet temperature
is excellent. In addition, excellent agreement with data is
obtained regarding reduced NO emissions with water droplet and
steam injection.

Comparisons of predictions made on swirling flame data
show that while good agreement can be obtained additional work
is required in terms of the turbulent transport properties.

In general, the modeling presented herein has aided in the
understanding of the emissions problem and has delineated areas
needing further study.

2. INTRODUCTION

Recent studies[1,2,3] have established that the density of pollutant emissions from aircraft turbine engines, particularly in the vicinity of airports, is a matter of increasing public concern and will become even more important in future years. This is a problem which has stimulated the output of a large body of data on the emission characteristics of existing as well as advanced combustor concepts[4,5,6,7,8]. However, the data itself has not been sufficient to explain all the trends exhibited by the observations. Part of this difficulty is due to instrumentation problems and part has been due to the lack of appropriate mathematical models useful in providing the insight necessary to understand the data. The emissions problem arises out of past engine developmental procedures which have emphasized overall combustion efficiency and performance while giving little attention to the resulting pollutant generation and emissions.

The conventional treatment of the combustor process involves one-dimensional concepts and only recently has some consideration been given to the inclusion of the kinetics process as an improvement over the equilibrium assumption. Very little work has been done in the past to couple valid kinetics with the appropriate fluid mechanics.

It is generally recognized that the pollutant emission characteristics of aircraft turbine engines are related to the failure of the exhaust gases to attain chemical equilibrium. Analysis of exhaust gas samples indicate that the departure from equilibrium, especially for species such as nitric oxide, CO and hydrocarbons, is extremely high. In actual practice, the effect is to produce greater quantities of these pollutants than would exist if equilibrium prevailed throughout the engine. Thus, the exhaust composition of these pollutants is dependent upon the rate limiting processes within the combustor. In order to formulate a realistic mathematical model of these processes, a knowledge of the detailed flow field within the combustor is required.

The combustion process in such annular and canannular combustors can be described in terms of the flow pattern in two zones; a primary and secondary, which are shown schematically in Figure 1.

In the primary zone, air enters through swirlers (bladed passages which impart a swirl to the air flowing through) around the fuel spray nozzles and air holes in the combustor liner. In this zone, the fuel and air are mixed and partially burned at near stoichiometric conditions ($\Phi = 0.8 - 1.2$). However, the discrete injection of the fuel results in a wide spectrum of equivalence ratios in this region. This provides for nonuniform fuel evaporation and mixing giving rise to locally fuel-rich and fuel-lean domains. This equivalence ratio variation together with the associated temperature variation will lead to: (1) partial oxidation and thermal cracking (pyrolysis) with the attendant formation of hydrocarbon fragments, CO, and soot in the fuel-rich regions, (2) maximum formation of NO_x on the lean side, near stoichiometric regions, and (3) quenching in the colder very lean regions. In practice, the concentration levels of these species depends upon the mixing and kinetic rates relative to the local residence times. A mathematical model representing the overall primary zone must account for the mechanisms controlling these rates as a function of initial fuel and air properties.

In the secondary zone, Figure 1, the main bulk of the air is added and the reaction is continued. Further dilution occurs in the secondary zone to reduce the product gas temperature to the desired turbine inlet conditions. For an overall combustor equivalence ratio of about 0.25, approximately 75 percent of the total air flow is introduced in the secondary zone. Part of the air from the secondary holes recirculates upstream into the primary zone and improves the combustion stability and part is injected close to the flame-tube wall providing film cooling (Figure 1).

The assumption of one-dimensional flow is inadequate in the treatment of the secondary zone because air is being injected through holes and cooling slots along the combustor length. The one-dimensional flow assumption which implies flow properties are uniform across any cross-section requires the very poor hypothesis that the injected air mixes instantaneously with the bulk flow. In reality, the injected air can require appreciable distances to mix with the bulk flow. Thus, in addition to the nonuniform initial condition generated by the primary zone flow field, the boundary conditions along the secondary zone walls will force a persistence of the nonuniformity throughout the chamber. The effect of this nonuniformity includes possible quenching of the reactions due to the cooling near the walls.

Again, as in the primary zone, the velocity, concentration, and thermal fields in the secondary zone depend upon the relative importance of the mixing, chemical and flow times. Thus, a mathematical model for the secondary zone must include the inter-relationship of these processes and take account of their dependence upon the primary zone characteristics as well as the dilution and coolant air distributions and states of flow.

Thus, the objective of this work was to develop a modular computer program for the description of gas turbine combustor flow and chemical fields for the prediction of combustion efficiency and pollutant formation and disposition.

3. MATHEMATICAL MODEL FORMULATION

a. General Model Requirements

The jet engine combustor involves perhaps one of the most complex reacting flow fields of practical interest. The complexity arises out of the number of discrete mechanisms which occur simultaneously including heterogeneous reaction kinetics and turbulent mixing with recirculation patterns all taking place in a subsonic flow. Such a problem is in general elliptic and would require a Navier-Stokes treatment to thoroughly represent the flow field. To completely model the complex flow pattern existing in the primary zone of a real combustor is beyond the capability of present analytical methods. However, several approximate models can be postulated which characterize this zone in terms of mixing rates, reaction rates, and residence times. For example, one limit of operation of this zone is characterized by a "stirred reactor." That is, a well established recirculation zone exists and the process in terms of the degree of reaction is controlled by the chemical kinetic rates. Another limiting representation of this zone is characterized by a discrete jet mixing and combustion process. In this case, a parabolic analysis would be appropriate. The more general representation involves a combination of stirred reactor and jet type flows as shown in Figure 1. That is, a local region involving a recirculation, or stirred reactor zone, surrounded by a jet type mixing and combustion zone. Fuel injection and spray patterns must be accounted for in terms of the nozzle characteristics.

4

The analysis of the <u>secondary zone</u> must include the following principal effects:

1. Turbulent mixing and diffusion of the gases, droplets (if they should still exist), and carbon particles, including the effect of mixing of the injected air (injected through the cooling slots and dilution holes) and the bulk reacting gases;

2. Finite-rate chemical kinetics which describe not only the reactions between the combustion products (CO_2, CO, NO_x, etc.) but also the further oxidation of the unburned hydrocarbon and of the carbon particles.

b. The Modular Concept

The modular concept proposed here includes a rather general set of discrete mechanisms which control combustion efficiency and pollutant emissions. These mechanisms can be conveniently represented in terms of chemical kinetics and fluid mechanics processes as shown in Figure 2. However, it should be noted that these ingredients are coupled in the actual combustor. Thus Figure 2 shows that the <u>reaction kinetics</u> include droplet combustion and involves the exothermic reactions associated with the production of CO_2 and H_2O, the non-exothermic reactions involving combustion intermediates, as well as NO_x and SO_x (appropriate for sulfur bearing fuels), and finally, CO, C_xH_y , and soot, $C_{(s)}$, which can be associated with the combustion efficiency. In terms of pollutants, the net output of the chemical reaction processes are the concentrations of CO , C_xH_y , $C_{(s)}$, NO_x and SO_x . Of course, the reaction processes are ocurring with a complex flow field involving fuel droplets (and soot) suspended in the gas. Thus the <u>multiphase fluid mechanics</u> includes both gas and droplet mixing in the presence of swirl and recirculation.

The primary virtue of the proposed model lies in its inherent ability to respond to changes in many of the operating conditions and geometric factors which are of practical interest. This capability is summarized in TABLE I.

In general, the model will predict the details of the flow including the local velocity components, concentrations of gas and droplets, temperature and pressure (for a specified liner contour). In addition, mean properties within a recirculation zone are predicted. These variables are displayed in Column I while Column II shows their initial conditions which are arbitrarily specified. Columns III, IV and V detail the boundary conditions where it is worth noting that the area contour or wall pressure distributions may be specified. This option is of particular interest for advanced high speed combustors where sufficient dynamic head is available for significant pressure conversion. Thus, it may be desirable to determine a liner contour for some specified pressure distribution that provides control of the velocity field as well as of the kinetics. In particular, control of mixing rates, residence times, and combustion rates can be studied with the option as outlined in Column III. Column IV outlines the treatment of slots and holes. The "lateral" injection process through the holes is treated as a unit problem for the determination of the penetration into the main flow at the particular combustor cross section. The depth of penetration defines the radial location at which the injected flow becomes essentially parallel to the main combustor flow. Here, the flow is circumferentially mass averaged after taking into account the acceleration of the main combustor flow due to the area occupied by the injected air. The "new" profiles of the flow variables provide the information required to continue the solution downstream.

c. Chemical Kinetics

It is well established that in high performance systems the chemical equilibrium assumption is not valid for most species of interest. This is particularly true of NO_x even for residence times well beyond the millisecond range. Carbon monoxide is a problem since in many systems its oxidation to CO_2 is halted due to quenching at reduced temperatures or dissociation at peak temperatures. Only a few points of combustion inefficiency are associated with unacceptable CO emission levels. This is also true of the unburned hydrocarbons (UHC).

One of the most significant findings associated with recent pollution-oriented kinetics modeling is the extreme importance of many of the intermediate atoms and free radicals that are an inherent part of any oxidation process, Reference 9. Super-equilibrium levels of such species occur during the early stages

of combustion and they persist, due to the relatively slow three-body recombination reactions, even beyond what is normally considered the overall reaction time. This behavior accounts, at least in part, for such observations as "Prompt NO", Reference 10.

Perhaps the single most important consideration in the formulation of appropriate kinetic mechanisms is the recognition of the spectrum of local states that are encountered in various combustor flow fields. This includes the distribution of fuel/air ratios, temperatures, pressure ratios, and residence times. A rather general consideration must be given to species and reactions each of which may become important under the varying conditions encountered in practical combustor configurations.

It is common to distinguish between combustion reactions involving the exothermic formation of CO_2 and H_2O , and the NO_x formation reactions. In practice, however, the two processes cannot be distinguished and they are coupled. For example, under many combustion conditions of interest the Zeldovich mechanism appears to govern the formation of NO through the rate controlling reactions:

$$O + N_2 \rightleftharpoons NO + N \tag{1}$$

Now, the assumption that O is at its equilibrium level is generally not valid. Superequilibrium levels of atomic oxygen as well as other intermediates are predicted which is totally consistent with observed ignition delay and reaction time data. In view of these observations we have developed models which treat the combustion and NO_x formation mechanisms within the framework of a unified scheme. All reactions are coupled and neither equilibrium nor steady-state assumptions are made.

Our early work, Reference 11, demonstrated that many observations on the rate of combustion of hydrocarbons could be predicted by a relatively simple kinetic scheme. We termed the mechanism "quasi-global" which has as a key element a subglobal partial oxidation step:

$$C_n H_m + \frac{n}{2} O_2 \longrightarrow \frac{m}{2} H_2 + nCO \tag{2}$$
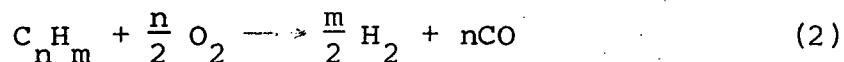
This reaction is unidirectional with an empirically determined rate (grams of fuel /cc /sec) given by

$$5.52 (10)^8 (p)^{-.825} (T) [C_n H_m]^{\frac{1}{2}} [O_2] \exp (-12,200/T) \tag{3}$$

where p must be given in atmospheres, T in degrees Kelvin and [ ] denotes molar concentration.

7

Coupled to this subglobal step are the intermediate reversible reactions given in TABLE II. Some observations on this scheme should be noted. First, it is generally agreed that in hydrogen bearing systems carbon monoxide is most rapidly oxidized to CO_2 via the reaction

$$CO + OH \rightleftharpoons CO_2 + H \qquad (4)$$
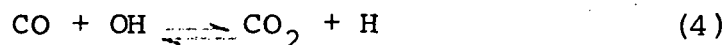
We have, however, included other reactions involving CO and oxygen for completeness including,

$$CO + O_2 \rightleftharpoons CO_2 + O \qquad (5)$$

and

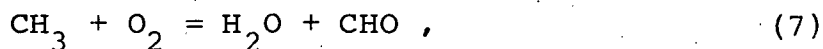$$CO + O + M \rightleftharpoons CO_2 + M \qquad (6)$$
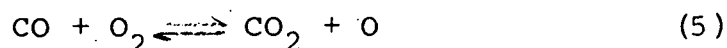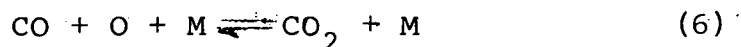
where M is the general third body. Reactions 5 and 6 are much slower than reaction 4 but their inclusion was necessary for basic studies performed on systems including the CO/Air system such as reported upon in Reference 12. In addition, a number of reactions involving NO_x are included which represent a necessary extension of the basic Zeldovich mechanism to account for certain of the ambient long time NO-to-NO_2 conversion reactions which occur in the 'atmosphere particularly when coupled with appropriate daylight photochemical mechanisms.

There are, however, other species of interest which can play an important role in the hydrocarbon oxidation process. A problem remains and this is mostly in fuel-rich hydrocarbon combustion. Hydrocarbon fragments, radicals, and a variety of oxygenated species are produced during the combustion process and accounting for them is of potential importance in adquately representing the fuel oxidation process as well as the NO_x formation process.

Perhaps one of the most exhaustively studied hydrocarbon oxidation mechanisms is associated with the methane/air system, References 13, 14 and 15. Although there is an apparent controversy over the importance of certain species and reactions governing the fuel oxidation process agreement on several aspects are worth noting: (1) A basic H_2/Air mechanism is crucial, (2) CO oxidation is controlled by the hydroxyl radical (OH) concentration level, and (3) the methyl radical (CH_3) dominates the initial phases of the oxidation process. The points in question relate to (1) the relevance of formaldyhyde, (2) the importance of hydrogen peroxide (H_2O_2) and the hydroperoxyl

8

radical (HO_2), and (3) the appearance of higher hydrocarbons such as ethane (C_2H_6) as experimentally observed in Reference 13. Finally, little work has been done to quantify the effects of other intermediates including CN and HCN type species in terms of their influence on NO_x formation. Fenimore, Reference 10, has suggested that such species may play a role in the "early" formation of NO.

To answer some of these questions we have initiated a study on certain aspects of the methane oxidation process. To date, the in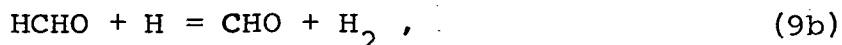vestigation has been limited to a scheme we have postulated and the scheme proposed by Bowman and Seery, Reference 14. These are given in **TABLES III and IV**. respectively. We have kept a number of reactions not included in Reference 14 but the major difference is our retention of formaldehyde (HCHO). As cited above, a question regarding the importance of the explicit appearance of HCHO exists and has led to deleting it by employing the subglobal steps, Reference 14.

$$CH_3 + O_2 = H_2O + CHO ,\qquad\qquad (7)$$

and

$$CH_3 + O = CHO + H_2 ,\qquad\qquad (8)$$

in place of the sets,

$$CH_3 + O = HCHO + H ,\qquad\qquad (9a)$$

$$HCHO + H = CHO + H_2 ,\qquad\qquad (9b)$$

and

$$CH_3 + O_2 = HCHO + OH ,\qquad\qquad (10a)$$

$$HCHO + OH = CHO + H_2O\qquad\qquad (10b)$$
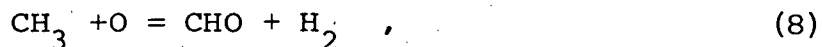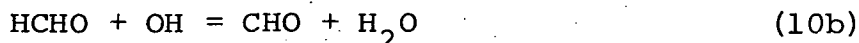
By retaining reactions 9 and 10, together with additional reactions involving HCHO, TABLE III not only provides a means of assessing its importance as an intermediate but also permits the prediction of the HCHO emission level which is an important pollutant entering into the atmospheric chemistry problem.

Now, the above mechanisms have been investigated in a variety of flows comprising the elements of our modular concept. Emphasis here is on the "quasi-global" model.

d. Recirculation Zone Model

The existence of recirculating regions in the primary zone of turbine combustors provides a mechanism for rapid mixing. If the backmixing is sufficiently intense this local zone will tend toward a homogeneous state. As the limit of essentially complete mixing is approached the principal mechanism defining the state of flow becomes the chemical kinetics of the fuel oxidation process. The residence time becomes the controlling parameter for a given fuel and air state entering such a recirculating zone.

The equations describing the process are straightforward and are deduced directly by application of the conservation of mass, energy and species. The conditions are: steady state, homogeneity within the reacting volume, and that the efflux state is identical to the state existing within the reaction zone. The resulting describing equations are:

Global Conservation of Mass:

$$\dot{m} = \text{constant} = \sum_{k} \dot{m}_{k}^{I} = \sum_{k} \dot{m}_{k}^{O} \tag{11}$$

where k is the kth component and includes i gas-phase species, and j droplet types. A droplet type (or class) is defined by its composition (fuel, water, etc.) and its size. The superscripts I and o refer to inflow and outflow, respectively.

Conservation of Energy:

$$h = h^{I} + \dot{Q}/\dot{m} \tag{12}$$

where $\dot{Q}$ is the net rate of external heat addition to the reactor and the inflow of enthalpy is written to allow each component to enter the reactor with an arbitrary temperature. In particular,

$$h = \sum_{i} \alpha_{i} h_{i}(T) + \sum_{j} \alpha_{j} h_{j}(T_{j}) , \tag{13}$$

and

$$h^{I} = \sum_{i} \alpha_{i}^{I} h_{i}(T_{i}^{I}) + \sum_{j} \alpha_{j}^{I} h_{j}(T_{j}^{I}) \tag{14}$$

where

$\quad$ T = Local gas-phase temperature

$\quad$ T_j = Local j^{th} droplet temperature

$\quad$ T_i^I = Injection temperature of the ith gas-phase specie

$\quad$ T_j^I = Injection temperature of the jth droplet

To complete the specification of the thermal field some constraint governing the conservation of droplet energy is required. For the present it will be assumed that each droplet type is at its respective boiling-point temperature, i.e., $T_j = T_{j\ B.P.}$

Conservation of Species:

$\quad$ The conservation of species k requires that its net outflow be equal to the rate of production due to chemical and phase transition processes. Formally, this principle gives k equations of the form:

$$\alpha_k = \alpha_k^I + \frac{V}{\dot{m}} [\dot{W}_k^G + \dot{W}_k^P] \tag{15}$$

where superscripts G and P refer to homogeneous gas-phase and dropwise production rates, respectively.

Homogeneous Gas Phase Reactions

$\quad$ The volumetric production rates are given as follows:

$$\dot{W}_i^G = W_i \sum_{p=1}^{R} (\nu_{ip}'' - \nu_{ip}') k_{f_p} \rho^{m_p} \prod_{i=1}^{N} \left(\frac{\alpha_i}{W_i}\right)^{\nu_{ip}'} \left[1 - \frac{\rho^{N_p}}{k_{c,p}} \prod_{i=1}^{N} \left(\frac{\alpha_i}{W_i}\right)^{(\nu_{ip}'' - \nu_{ip}')}\right] \tag{16}$$

where

$$m_p = \sum_i^N \nu_{ip}' \quad ; \quad N_p = \sum_i^N (\nu_{ip}'' - \nu_{ip}') \tag{17}$$

11

for a chemical system containing N gas-phase species entering into R elementary reversible reactions given by:

$$\sum_{i=1}^{N} \nu'_{ip} M_i \underset{k_{b_p}}{\overset{k_{f_p}}{\rightleftharpoons}} \sum_{i=1}^{N} \nu''_{ip} M_i \quad , \quad p = 1, \ldots R \tag{18}$$
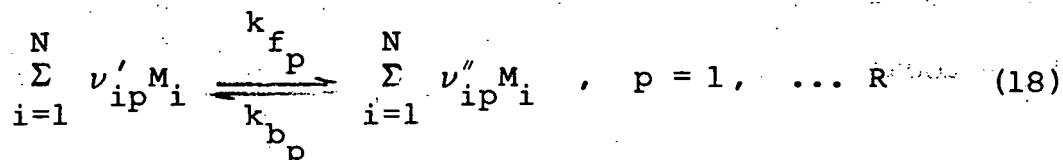
Dropwise Combustion and Evaporation

For now, the droplet types will be specialized to fuel and water. Two limiting modes of consumption will be considered for the fuel droplet: (1) diffusion-controlled combustion and (2) evaporation only. In both cases a detailed homogeneous gas phase kinetics mechanism will be in effect. Of course, for the water only evaporation is relevant.

Fuel:

The two reactions considered are:

$$1. \quad C_n H_m + (n + \frac{m}{4}) \; O_2 \rightarrow nCO_2 + \frac{m}{2} H_2O \tag{19}$$

$$2. \quad (C_n H_m)_{Liquid} \rightarrow (C_n H_m)_{gas} \tag{20}$$
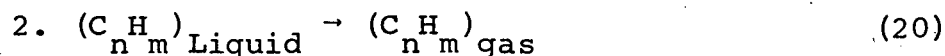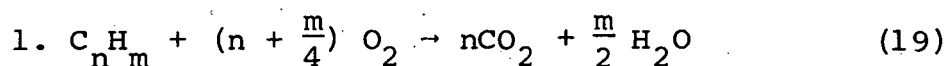
In both cases, the rate of consumption of the liquid fuel is given by diffusion-controlled theory; viz:

$$(\dot{W}_{C_n H_m})^P = - \; 3/2 \; \rho \; d_{C_n H_m} \left(\frac{\alpha^I}{d_{C_n H_m}^{I^3}} \right) \lambda_{C_n H_m} \tag{21}$$

where

$$d_{C_n H_m}^{3} = d_{C_n H_m}^{I^3} \; \frac{\alpha_{C_n H_m \ell}}{\alpha_{C_n H_m \ell}^{I}} \tag{22}$$

and d is the droplet diameter. In addition,

$$\lambda_{C_n H_m} = 8 \; (\frac{k}{c_p \delta})_{C_n H_m} \; \ell n \; (1 + B_{C_n H_m}) \tag{23}$$

12

where

$$B_{C_n H_m} = \frac{A(Y_{O_2})_g \left(\frac{\bar{\bar{H}}}{\bar{N}}\right)_{C_n H_m} + C_{P_{C_n H_m}} \left(T - T_{C_n H_m}^{B.P.}\right)}{Q_{C_n H_m}} \qquad (24)$$

and k and C_p are the thermal conductivity and specific heat of the vapor, respectively; $\bar{\bar{H}}$ is the heat of combustion, $\bar{N}$ is the stoichiometric O/F ratio, δ is the droplet density, Q is the latent heat of vaporization, and A is a factor which differentiates between diffusion-controlled combustion (A=1) and droplet evaporation (A=0).

Now, <u>for A = 1</u> we have:

$$(\dot{W}_{O_2})^P = \frac{(n + \frac{m}{4}) W_{O_2}}{n W_C + m W_H} (\dot{W}_{C_n H_m})^P \qquad (25)$$

$$(\dot{W}_{CO_2})^P = - \frac{n W_{CO_2}}{n W_C + m W_H} (\dot{W}_{C_n H_m})^P \qquad (26)$$

$$(\dot{W}_{H_2O})^P_g = - \frac{\frac{m}{2} W_{H_2O}}{n W_C + m W_H} (\dot{W}_{C_n H_m})^P - (\dot{W}_{H_2O})^P \qquad (27)$$

and <u>for A = 0</u>:

$$(\dot{W}_{C_n H_m})^P_g = - (\dot{W}_{C_n H_m})^P \qquad (28)$$

In addition,

$$(Y_{O_2})_g = \frac{\alpha_{O_2}}{\sum_i \alpha_i} \qquad , \; i = \text{all gases} \qquad (29)$$

where $(Y_{O_2})_g$ is the mass fraction of O_2 in the gas-phase subsystem.
<u>Water:</u>

Here the reaction is:

$$(H_2O)_\ell \rightarrow (H_2O)_g \qquad (30)$$

where

$$(\dot{W}_{H_2O})^P = - 3/2 \, \rho \, d_{H_2O} \left(\frac{\alpha^I}{d^{I^3}}_{H_2O}\right) \lambda_{H_2O} \qquad (31)$$

13

and

$$\lambda_{H_2O} = 8 \left(\frac{k}{C_p \delta}\right)_{H_2O} \ln (1 + B_{H_2O}) \qquad (32)$$

with

$$B_{H_2O} = \frac{C_{p_{H_2O}} (T - T_{H_2O}^{B.P.})}{Q_{H_2O}} \qquad (33)$$

and

$$d_{H_2O}^3 = d_{H_2O}^{I^3} \cdot \frac{\alpha_{H_2Ol}}{\alpha_{H_2Ol}^I} \qquad (34)$$

State:

$$\rho = \frac{p}{RT \sum_i \frac{\alpha_i}{W_i}} \qquad , \quad i = \text{all gases} \quad \dots \qquad (35)$$

where ρ is the mixture density and T is the gas-phase temperature.

Although there exist more or less standard techniques for the solution of such algebraic equations, an alternative approach is that of seeking the asymptotic (steady state) solution to a transient problem wherein the "boundary conditions" are held fixed at the desired steady state values. In essence, our approach involves the use of the non-steady form of the species conservation equations, viz:

$$\frac{d\alpha_k}{dt} = \frac{\dot{m}}{\rho V} (\alpha_k^I - \alpha_k) + \left(\frac{\dot{W}_k}{\rho}\right)^G + \left(\frac{\dot{W}_k}{\rho}\right)^P \qquad (36)$$

where t is the time variable of significance only during the transient period. Thus, Equation (36) is identical to Equation (15) when:

$$\frac{d\alpha_k}{dt} \rightarrow 0 . \qquad (37)$$

14

The remaining working equations retain their steady state form. To initiate a calculation requires the specification of the α_k's at t = 0. We start with the equilibrium state although this "initial" composition may be chosen arbitrarily.

The above formulation represents only part of the overall combustor model. In general the recirculation zone is imbedded within a "directed" flow in the primary zone and the two zones are coupled through diffusive transport across the dividing streamline. Furthermore, in the downstream secondary zone the mixing and kinetics processes are continued and in some cases must include the effects of secondary air injection for cooling and dilution.

e. Mixing Model

The principal element forming the framework of the unified combustor model is the mixing analysis. It is within this framework that recirculation zones, additional kinetics, secondary injection and combustor geometry are coupled. Figure 3 shows a schematic of the flow where the inner separating streamline boundary may either enclose a recirculation zone or represent the inner wall of an annular combustor. Swirl is included in the domain outside of the recirculation zone. The various elements of the unified model are coupled together either through source terms or through the initial and boundary conditions.

The features of the mixing analysis including assumptions are summarized below, (see also TABLE I):

- The fuel droplets and other particulates form a dilute, continuum-like suspension in the multi-component gas phase carrier.

- The volume occupied by the particulates is negligible.

- The particulates are classified in terms of size and composition and each class mixes at a rate determined by its ability to respond to the dynamics of the gas-phase motion.

- Turbulent transport is important only in the direction normal to the primary burner flow direction.

- Non-isotropy is accounted for by assigning appropriate transport coefficients to the axial and tangential components of the shear stress.

The describing equations are parabolic and for steady turbulent flow are given as follows:

Global Continuity:

$$\frac{\partial y^N \rho u}{\partial x} + \frac{\partial y^N \rho v}{\partial y} = 0 \tag{38}$$

Species Diffusion:

i^{th} gas-phase specie

$$\rho u \frac{\partial \alpha_i}{\partial x} + \rho v \frac{\partial \alpha_i}{\partial y} = \frac{1}{y^N} \frac{\partial}{\partial y} \left\{ y^N \rho \epsilon_{D_g} \left[\frac{\partial \alpha_i}{\partial y} - \alpha_i \left(\frac{1 - \sum_j \theta_j \beta_j}{\alpha_g} \frac{\partial \alpha_g}{\partial y} \right. \right. \right.$$

$$\left. \left. \left. + \sum_j \theta_j \frac{\partial \beta_j}{\partial y} \right) \right] \right\} + (\dot{w}_g)_i + \sum_j (\dot{w}_p)^F_{ij} \tag{39}$$

j^{th} particulate class

$$\rho u \frac{\partial \beta_j}{\partial x} + \rho v \frac{\partial \beta_j}{\partial y} = \frac{1}{y^N} \frac{\partial}{\partial y} \left\{ y^N \rho \epsilon_{D_g} \theta_j \left[\frac{\partial \beta_j}{\partial y} - \beta_j \left(\frac{1 - \sum_k \frac{\theta_k}{\theta_j} \beta_k}{\alpha_g} \left(\frac{\partial \alpha_g}{\partial y} \right) \right. \right. \right.$$

$$\left. \left. \left. + \sum_k (\theta_k/\theta_j)(\partial \beta_k/\partial y) \right) \right] \right\} + (\dot{w}_p)^F_j \tag{40}$$

16

where:

N = 0 for two-dimensional flow; N = 1 for axisymmetric flow

$(\dot{w}_g)_i \equiv$ production of the ith gas-phase specie due to homogeneous gas-phase reactions;

$(\dot{w}_p)^F_{ij} \equiv$ production of the ith gas-phase specie from the jth particle class due to evaporation or heterogeneous reactions;

$(\dot{w}_p)^F_j \equiv$ production of the jth particle class;

Momentum Equations:

x component

$$\rho u \frac{\partial u}{\partial x} + \rho v \frac{\partial u}{\partial y} = \frac{1}{y^N} \frac{\partial}{\partial y} \left\{ y^N \rho (\epsilon_v)_g^{(rx)} \left[\alpha_g + \Sigma_j \sigma_j \beta_j \right] \frac{\partial u}{\partial y} \right\} - \frac{\partial p}{\partial x}$$

(41)

y component

$$\frac{\partial p}{\partial y} = \frac{\rho w^2}{y} = \frac{\rho \Gamma^2}{y^3} \quad ; \quad \Gamma \equiv yw \text{ (circulation)}$$

(42)

θ component

$$\rho u \frac{\partial \Gamma}{\partial x} + \rho v \frac{\partial \Gamma}{\partial y} = \frac{1}{y} \frac{\partial}{\partial y} \left\{ y \rho (\epsilon_v)_g^{(r\theta)} \left[\alpha_g + \Sigma_j \sigma_j^{(r\theta)} \beta_j \right] \left[\frac{\partial \Gamma}{\partial y} - \frac{2\Gamma}{y} \right] \right\}$$

(43)

where for swirling flows only N = 1 has significance.

Energy Equations:

mixture energy equation

$$\rho u \frac{\partial H}{\partial x} + \rho v \frac{\partial H}{\partial y} = \frac{1}{y^N} \frac{\partial}{\partial y} \left\{ y^N \rho (\epsilon_v)_g^{(rx)} \left\{ \left[\left(\frac{1}{P_r} \right) \frac{\partial H}{\partial y} + \left(\frac{h_g}{S_c} \sum_j \theta_j \beta_j - \frac{H_g}{P_r} - \frac{1}{P_r} \left(\frac{P_r}{S_c} - 1 \right) h_g \right. \right. \right. \right.$$

$$\left. - \frac{1}{S_c} \sum_j \theta_j h_j \beta_j \left[\frac{1 - \sum_k (\theta_k/\theta_j) \rho_k}{\alpha_g} \right] \right) \frac{\partial \alpha_g}{\partial y}$$

$$+ \frac{1}{P_r} \left(\sum_j \beta_j (\delta_j - 1) \frac{\partial H_j}{\partial y} + \left(\frac{P_r}{S_c} - 1 \right) \sum_i h_i \frac{\partial \alpha_i}{\partial y} \right)$$

$$+ \left(\sum_j \left[\frac{\theta_j (h_j - h_g \alpha_g)}{S_c} - \frac{H_j}{P_r} \right] \frac{\partial \beta_j}{\partial y} \right)$$

$$+ \left(\alpha_g (1 - 1/P_r) - \sum \frac{\beta_j \delta_j}{P_r} \right) \frac{\partial q^2/2}{\partial y} - \frac{1}{Sc} \left(\sum_j \beta_j h_j \right) \left(\sum_k \theta_k \partial \beta_k / \partial y \right)$$

$$+ \left(\alpha_g (\tilde{\epsilon}_g - 1) - \sum_j \beta_j \frac{\tilde{\epsilon}_j}{\tilde{\epsilon}_g} \sigma_j \right) \frac{\partial w^2/2}{\partial y}$$

$$- (\alpha_g \tilde{\epsilon}_g + \sum_i \beta_j \frac{\tilde{\epsilon}_j \sigma_j}{\tilde{\epsilon}_g}) w^2 \right\} \right\} \tag{44}$$

where in the above describing equations the quantities θ_j , δ_j and σ_j respectively define the ratio of the particle-to-gas phase eddy diffusivities of mass, momentum and energy, i.e.,

$$\theta_j = \epsilon_{D_j}/\epsilon_{D_g} \quad , \quad \sigma_j = \epsilon_{v_j}/\epsilon_{v_g} \quad , \quad \delta_j = \epsilon_{T_j}/\epsilon_{T_g}$$

and P_r, S_c $\equiv$ gas phase Prandtl and Schmidt numbers, respectively.

18

Also, the gas phase mass fraction, α_i, and the particle-phase mass fraction β_j are defined such that

$$\alpha_g \equiv \sum_i \alpha_i = 1 - \sum_j \beta_j = 1 - \beta_p$$

where the subscript i covers each gas-phase species and the subscript j denotes each particle class.

Note also that the energy equation, Equation (44), may not, in general, be sufficient to define the thermal state of the system. Although dynamic equilibrium may be appropriate, the temperature associated with each particle class can be sensibly different from the gas-phase temperature depending on the process occurring on the particle scale. For example, for evaporating droplets the local saturation temperature is appropriate while if metallic particles are part of the multicomponent system and surface reactions are occurring then some other temperature is appropriate. Only in the case of inert particles (non-radiating) is there similarity in particle drag and heating processes for which "near" dynamic equilibrium would imply near thermal equilibrium. In cases where the thermal equilibrium assumption does not apply, Equation (44) must be augmented by either the gas-phase or particulate-phase energy equation.

In the present study the formulation for the mixing zone is limited to the thermal equilibrium assumption. Additional details of the treatment given to these equations can be found in Appendix A.

Initial and Boundary Conditions

The problem is set with the specification of the dependent property profiles at some initial x-station together with appropriate boundary conditions invoked along the inner and outer "walls."

These conditions are presented in TABLE I. There are, however, several implications associated with these boundary conditions as we have specified them:

Inner Wall - When the inner surface bounds an imbedded, recirculation zone the state of flow along the surface is defined by the stirred reactor analysis. This state will generally be different from that in the surrounding directed flow. As a result diffusion across the dividing streamline, y_{IW},

19

occurs which provides the coupling mechanism between the inner and outer flow regimes. Of particular interest are the transport of species and energy. Since there is no net mass transfer across this boundary the respective species and energy fluxes out of the imbedded recirculation zone are given by:

Species Flux, $\dot{m}_{i,j}$

i^{th} gas phase specie:

$$\dot{m}_i = - \rho \epsilon_{Dg} \left\{ \frac{\partial \alpha_i}{\partial y} - \alpha_i \left[\frac{1 - \Sigma_j \theta_j \alpha_j}{\alpha_y} \frac{\partial \alpha_q}{\partial y} + \Sigma_j \theta_j \frac{\partial \alpha_i}{\partial y} \right] \right\}$$

(45)

j^{th} particulate phase specie:

$$\dot{m}_j = - \rho \epsilon_{Dg} \theta_j \left\{ \frac{\partial \alpha_j}{\partial y} - \alpha_j \left[\frac{1 - \Sigma_\mu \theta_\mu \, \alpha_{\beta\mu} / \theta_j}{\alpha_g} \frac{\partial \alpha_q}{\partial y} + \Sigma_\mu \frac{\theta_\mu}{\theta_j} \frac{\partial \beta_\mu}{\partial y} \right] \right\}$$

(46)

Energy Flux, $\dot{e}$

$$\dot{e} = \frac{\rho \epsilon_{vg}^{(rx)}}{Pr} \left[\frac{\partial H}{\partial y} - \frac{\partial q^2/2}{\partial y} - \Sigma_{i \, gas} h_i \frac{\partial \alpha_i}{\partial y} - \frac{\partial \beta_p h_p}{\partial y} + \Sigma_j \beta_j \delta_j \frac{\partial h_{pj}}{\partial y} \right] +$$

$$+ \Sigma_i \dot{m}_i h_i (T_g) + \Sigma_j \dot{m}_j h_j (T_{pj})$$

(47)

Once the above fluxes have been determined over the entire dividing stream surface the total rate of transport for each specie and the energy may be found:

$$\dot{M}_{Ti,j} = 2\pi \int_0^{L_r} \dot{m}_{i,j} \, Y_{IW} \, dx$$

(48)

$$\dot{E} = 2\pi \int_0^{L_r} \dot{e} \, Y_{IW} \, dx$$

(49)

20

These specie and energy flow rates can now be (re)introduced into the stirred-reactor analysis providing an iterative method of bilaterally coupling the outer directed flow with the internal recirculating flow. Of course, a new average pressure level exerted upon the recirculation zone is also made available for updating the recirculation zone state. Finally, the contour of the recirculation zone must be specified and some data for basic swirling flows exits, Reference 16.

Outer Wall - Lateral Injection - When the combustor flow encounters secondary injection through holes, the problem is reinitialized as described in TABLE I. The penetrations are determined by empirical correlations using the work of References 17 and 18. Although several secondary injection analyses have pervaded the literature the aforementioned works were chosen arbitrarily, and the following discussion does not preclude the implementation of any other injection analyses. In fact, most of these empirical analyses treat the secondary injection problem in somewhat similar fashion. In particular, the interaction of a secondary jet and the subsequent dispersion in the primary (combustor field) fluid is assumed to be a two stage process - the penetration and mixing stages. In the penetration stage, the jet retains its identity while being accelerated and turned in the flow direction of the primary fluid. Here it is assumed that the jet emerging from the dilution hole acts as some "solid" body which is subsequently bent downstream by drag and distorted in cross section by pressure differences on the front and back faces and viscous shear. Accordingly, the jet trajectory using an analysis described in Reference 17 is obtained from

$$y_p/d_j = y_{IW}/d_j - (14.4)(\dot{q})^{\frac{1}{2}} \ell_g \left\{ 1 + 0.1 \ (\Delta x/d_j) \left[1 + \left(1 + \frac{20}{(\Delta x/d_j)} \right)^{\frac{1}{2}} \right] \right\}$$

(50)

where the quantity, $\dot{q}$, defines the ratio of the dilution hole momentum flux to the primary stream momentum flux and the quantity, Δx, defines the difference between the local axial distance and the axial location of the jet-dilution hole of diameter d_j. Furthermore, the jet is assumed to deform from its otherwise initial circular cross section into an ellipse having a 5 to 1 ratio between its major to minor axis, Reference 18. The variation of the jet width or minor axis with distance is based upon subsonic experiments, Reference 17, and is given by

$$h/d_j = 2.25 + 0.22(\Delta x/d_j)$$

(51)

21

with the jet cross section area given by

$$A_j(x)/A_j(o) = (^1/5) (h/d_j)^2 \tag{52}$$

Thus, for given dilution-hole jet efflux conditions, the above three equations are sufficient to describe the penetration height, width and cross-sectional area once a ($\Delta x/d_j$) value has been chosen. Consideration of mass conservation and the fact that usually more than one dilution hole is located along the periphery of the combustor wall then allows us to determine the geometric and physical properties of jet fluid effectively contained within an annulus having a radius as determined by Equation (50) with a width given by

$$\Delta y/d_j = (N_j/8) \left[(V_j)_{\Delta x=0} / (V_j)_{\Delta x} \right] \left[y_p/d_j \right]^{-1} \tag{53}$$

where N_j defines the total number of dilution holes at the axial station in question.

Once this annulus is defined and the jet fluid properties within it determine the mixing analysis, or so-called second stage, is re-initiated. It is noted however that since the effective maximum penetration is assumed to be achieved quite quickly the distance that the jet traverses downstream of the port is considered to be small. Hence the second stage or re-initialization procedure occurs at the dilution hole axial station.

Turbulent Transport Coefficients

The method employed here to represent the effect of turbulence involves the specification of eddy transport coefficients. This implies a gradient mechanism of diffusion in direct analogy with molecular transport and this assumption is reflected in the form of the describing equations (38) - (44).

Now, since the description of the turbulence field is extremely complex a semi-empirical representation is required in expressing the eddy transport coefficients as functions of the state of flow. The presence of swirl further complicates the problem by introducing a tangential component of shear into the flow.

Although a complete description of the turbulent mechanism is not available there are some observations which are relevant to the present problem. First of all the effect of swirl enhances the axial component of shear and secondly, the shear distribution is anisotropic, References 19 and 20.

These observations have been incorporated in the present turbulent transport property representations where the anisotropy is accounted for by specifying axial and tangential viscosities, respectively.

Axial Viscosity, $\mu^{(rx)} = \rho\epsilon^{(rx)}$

For small to moderate swirl where the axial velocity profiles are monotonic the work of Reference 21 has been found appropriate in representing available data. In particular, this model has the form:

$$\mu^{(rx)} = k(s)\ r_{\frac{1}{2}}\ \rho_g(u)_{\mathcal{L}} \tag{54}$$

where $k(s)$ is an empirically determined function of the swirl parameter, s, and $r_{\frac{1}{2}}$ is the half radius based upon the location of the mean velocity. Here, the data of Reference 20 has been used to define $k(s)$.

Values of $k(s)$ found to represent non-reacting (isothermal) and flame data are as follows:

• Isothermal runs	• Flame
$k = 0.025\ \{s=0\}$	$k = 0.0225$
$= 0.033\ \{s=.1\}$	$= 0.0225$
$= 0.066\ \{s=.2\}$	$= 0.0450$

For large swirl, the axial velocity attains its maximum off the axis where the tangential component of the shear is zero. This suggests that the turbulent eddy scale on either side of the zero shear contour is different and that a two layer transport model is required. A limited study of such a representation was made using a model of the following type:

$$\mu^{(rx)} = \mu_1 \text{ for } y < y \text{ peak}$$

$$\mu^{(rx)} = \mu_2 \text{ for } y \geq y \text{ peak}$$

where

$$y \ \text{peak} = y @ (\rho u)_{\text{max}} .$$

The results of this study are encouraging and comparisons with data are presented later.

Tangential Viscosity, $\mu^{(r\theta)} = \rho \ \epsilon^{(r\theta)}$:

The previously cited work of Reference 19 has shown the anisotropic character of the shear distribution. This observation was based upon analysis of the measured axial and tangential velocity profiles indicating that the tangential viscosity is on the order of 10 to 20 percent of the axial viscosity. This conclusion is in general agreement with previous studies on vortex decay wherein a model of the following type was suggested, Reference 22:

$$\mu^{(r\theta)} = 0.185 \ \nu_g \left(\frac{\Gamma_o/\nu_g}{}^{2/3} \right) , \tag{55}$$

where Γ_o is an initial value of the circulation $(wy)_{\text{init.}}$ and ν_g is the gas phase molecular kinematic viscosity.

Now, to complete the description of the turbulent transport properties, representations for the eddy diffusivity and eddy conductivity are required. For this purpose it is convenient to represent these coefficients in terms of the Schmidt No. and Prandtl No. respectively, viz:

$$\rho_g \epsilon_{Dg} = \mu^{(rx)}/Sc ,$$

and,

$$\rho_g \epsilon_{Tg} = \mu^{(rx)}/Pr .$$

Finally, the relationship between gas phase and particulate phase transport properties are expressed in terms of the parameters, σ_j , θ_j and δ_j , viz:

$$\left. \begin{array}{l} \sigma_j = \dfrac{\epsilon_{Vj}}{\epsilon_{Vg}} \\[12pt] \theta_j = \dfrac{\epsilon_{Dj}}{\epsilon_{Dg}} \\[12pt] \delta_j = \dfrac{\epsilon_{Tj}}{\epsilon_{Tg}} \end{array} \right\} \tag{56}$$

24

Although in the present study these parameters must be speci-
fied some work on particulate dispersion in turbulent flows
has been reported and is summarized in Reference 23.

Now, the preceeding formulations have been applied
to a range of configurations with particular attention given
to the analysis of available data.

4. MODEL APPLICATIONS

To date the primary application of the model has been in
terms of unit configurations involving both well-controlled
laboratory combustors and actual systems.

Pollutant emissions are most often measured at levels
commonly considered as "trace" concentrations relative to the
major products of combustion. Thus, their determination is a
matter of great delicacy. Consequently, to establish a basic
understanding of the mechanism(s) controlling the formation
and disposition of pollutants has required well-controlled
laboratory experiments.

Now, during the course of the present study basic data
was concurrently becoming available to us under a joint effort
with ESSO Research and Engineering Company. In this regard,
the work of Reference 12 should be noted. That study marked
the first time that such basic systems as the H_2/Air and CO/Air
systems were studied experimentally and theoretically in terms
of NO_x emissions. A jet stirred reactor of the type developed
by Longwell and Weiss, Reference 24, together with the above
analysis were employed in that investigation. The results for
the H_2/Air and CO/Air systems are given in Figures 4 and 5
where very good agreement between theory and experiment is
shown for both systems. The significance of these results
is two-fold: First, the model can be used with confidence
to accurately define the effects of variations in the con-
trollable parameters. Insight gained from these two basic
chemical systems can be applied to more complex fuels.
Secondly, the H_2/Air and CO/Air mechanisms are basic to any
hydrocarbon/air oxidation mechanism. Thus, verification of
these two systems provides a firm basis for postulating and
developing schemes to represent the oxidation of hydrocarbons.
Figure 6 shows a comparison of calculations using our quasi-
global mechanism with data for the propane/air system.
Included are equilibrium predictions and kinetic predictions
also made assuming that free atomic nitrogen is present.

25

The latter is an artifice to establish the upper limit for the conversion of fuel "bound" nitrogen to NO_x. In addition, adiabatic as well as specified temperature results are presented, and the relative importance of the $N+OH \rightleftharpoons NO+H$ reaction is also shown.

The adiabatic stirred reactor predictions are in good agreement with the fuel lean data but poor agreement is obtained in the fuel rich regime.

The calculations determined by using temperatures deduced from the experimental data yield low NO values throughout.

The predictions are sensitive to small added amounts of free atomic nitrogen entering with the fuel. The conversion efficiency is high and can be traced to the fast $N + O_2 = NO + O$ reaction.

The $N + OH = NO + H$ reaction is most significant in the rich regime where [OH] > [O], where [ ] is the concentration.

Finally, the equilibrium results are as expected in the leaner regions but in the rich regime the measurements as well as the predictions of NO are higher than the corresponding equilibrium levels. This is apparently due to the dominance in this regime of free radical overshoots.

In general, the above results are extremely encouraging and although more work is required in hydrocarbon kinetics modeling the results indicate that many of the observed trends are predicted with the quasi-global representation. Nevertheless, our quasi-global mechanism does involve replacing many intermediate reactions and species high up in the oxidation chain with a subglobal partial oxidation step. The results presented so far have implied the importance of the non-equilibrium free radical overshoots on the generation of NO_x. In terms of the NO reactions considered in the present work O , OH and N are crucial to NO formation mechanism. Of these species the combustion generated atomic oxygen appears to be the controlling one. For hydrocarbons, such superequilibrium values of atomic oxygen can account for an "early" formation of NO in the milli-second range that would not be predicted assuming the equilibrium level of atomic oxygen existed throughout. Figures 7 and 8 give an example of this for isothermal plug flow of octane and hydrogen assuming two models for the combustion process. In both models, the full system given in TABLE II was employed. However, the "coupled kinetics"

results were obtained by initiating the calculation with
pure fuel and air whereas the "Equilibrium Fuel/O_2 - Non-
equilibrium NO_x" results were obtained by initiating the
calculation assuming equilibrium Fuel/O_2 wherein the N_2
was assumed inert. Figure 7 shows that the atomic oxygen
overshoot for the hydrogen/air occurs earlier than in the
corresponding octane/air case. Of course, for pure air the
growth of O is monotonic. The fact that hydrogen is more
reactive than the hydrocarbon is the reason for "shift" in
the overshoot and Figure 8 shows the consequences of this
behavior. Thus, the early formation of NO is significant
for the hydrocarbon but not so for hydrogen (or pure air).
The higher "final" pure air level of NO is due to the avail-
able O_2 that would otherwise be consumed by the fuel.
Although this result does not cover a wide range of possible
states that would be encountered in a practical system, it
demonstrates, for a typical condition, that a coupled com-
bustion/NO_x mechanism is necessary to explain and predict
certain observations. Moreover, the question that arises
is whether any of the additional intermediates not included
in the quasi-global mechanism play a significant role in the
NO formation process where hydrocarbons are concerned.

To gain some insight into this we directed our attention
to the methane/air system. It seemed appropriate to start
with this system since of the many hydrocarbons of interest
this one appeared to be best understood in terms of its
oxidation kinetics. The mechanisms used in this study are
those given in TABLES III and IV. The results assuming
adiabatic combustion are shown in Figure 9 where the data
is from Reference 25. The jet stirred reactor previously
cited was employed here. The Bowman-Seery mechanism pre-
dicts the fuel lean NO emissions very well while poor agreement
is obtained in the rich regime. This behavior is remarkably
similar to the results obtained for the propane/air system using
our quasi-global mechanism. What is equally significant is
the effect obtained when formaldehyde is included in our mech-
anism. The comparison with the data is somewhat poorer than
that obtained with the Bowman-Seery mechanism, although some
improvement is observed in the fuel rich region. Although
improved rate data for the formaldehyde chain may improve our
predictions, these results support the contention that fast N
producing reactions are missing as suggested by Fenimore,
Reference 10. In any case, the common behavior between the
quasi-global predictions and predictions made using "detailed"
mechanisms suggests that the quasi-global concept itself should
not be ruled out at this time.

27

There is an additional point regarding the effect of turbulence and the degree of "unmixedness" on the microscale in practical systems as well as within laboratory reactors. Studies on various aspects of this problem have indicated the potential importance of microscale inhomogeneities upon the combustion process, References 26, 27 and 28. In Reference 28, Bowman, Pratt and Crowe introduce an empirical representation to account for incomplete mixing in their stirred reactor work. They showed parametrically that the temperature and NO emission levels are lower than would be predicted on the basis of assuming all fuel and oxidizer reacted within the geometrically defined combustion volume. This is, of course, the expected behavior when the fuel and oxidizer are premixed prior to injection into the reaction zone. In our work we have assumed a perfectly stirred configuration which for the Longwell reactor seems to be valid on the basis of the results obtained for the highly reactive H_2/Air system, Figure 4. Now, in terms of the propane and methane results it is clear that if the model had assumed any level of inhomogeneity the predictions would have been displaced even further below the data. These results lend evidence to the observation that representing the kinetics rather than the effect of "unmixedness" is the most important consideration here.

Now, all of the above comparisons with available data indicate that the models employed in our studies provide predictions in complete agreement with the observed trends. These results have implied that insight into the effect of liquid fuel injection could be obtained and therefore might suggest some of the controlling parameters in droplet combustion. Accordingly, some calculations have been made for a situation where the fuel enters the recirculation zone in a partially vaporized state. The effect of residence time upon fuel-droplet consumption, recirculation-zone temperature, and NO concentration as a function of the droplet size at injection, are shown in Figures 10, 11 and 12. The complete set of operating conditions are given in TABLE V. Two values of the mass flow-to-volume ratio were selected to provide a range of residence times. The resulting residence times are about 2 msec and 17 msec.

Figure 10 shows the importance of residence time upon droplet consumption. It is also interesting to note that the effect of dropwise combustion is small for both residence times meaning that the primary effect upon droplet consumption

28

is the heat conduction to the droplet. This effect is dominant
for our conditions because of the relatively high temperatures
in the surrounding gas phase due to the homogeneous gas-phase
oxidation of the vapor-phase component of the fuel. These
temperatures are shown in Figure 11 where it is interesting
to note that at the larger residence time the amount of
unconsumed liquid fuel is small enough for the entire range
of initial droplet diameters that dropsize has little effect
upon the combustion temperature. Finally, Figure 12 shows
the concentration of NO. The extreme sensitivity of NO to the
temperature is clearly evident here. Of particular interest,
however, is that at the larger residence time the NO levels
are somewhat higher where the droplets are assumed to evaporate
(with no dropwise burning). This is a reversal in the trend
observed at the shorter residence time. This is apparently
associated with the fact that the difference in temperature
between the two modes of droplet consumption is small. How-
ever, the atomic oxygen levels are higher for the pure evap-
oration mode of droplet consumption. Thus, under these con-
ditions the important reaction:

$$O + N_2 = NO + N$$
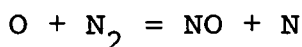
proceeds toward the right at a somewhat higher rate even
though the temperature is slightly lower. This result
further indicates the importance of the coupling between
the combustion kinetics and the NO_x formation kinetics
particularly where fuel droplets are involved.

So far in our discussions emphasis has been on the emis-
sions problem in terms of parameters controlling the fuel
oxidation process. It is of interest, however, to examine
other control measures of potential interest for NO_x reduction.
In view of the preceding discussion involving liquid fuel
injection it is appropriate to extend that analysis to include
water injection here.

Water injection is regarded as one possible control
measure for NO_x emissions. We have applied our multiphase
stirred reactor model to the jet engine combustor data of
Reference 29 and the comparison is shown in Figure 13.
Excellent agreement is shown for the smaller size droplets
and for the steam injection. The small difference between
steam and the small droplet size predictions are in complete
agreement with the experimental observations. The predictions
also show that the effectiveness of liquid water injection
decreases rapidly with increasing droplet size. Indirect

confirmation of this latter prediction has been noted recently by Shaw, Reference 30, wherein he was able, upon becoming aware of the present results to explain the small reduction in NO_x emissions on the basis of his dealing with large droplets.

To further demonstrate the utility of this basic model element further comparisons with engine emissions data have been made. For this purpose, we have simply assumed that the primary zone is the source of NO and that the entire primary zone is a single perfectly stirred reactor.

Figure 14 shows comparisons of predictions with measured NO_x emissions from a variety of jet engines. The data as represented is a correlation as determined by Lipfert, Reference 31. The predictions were made assuming an equivalence ratio of unity ($\Phi=1$) and a constant residence time of about 2 msec. Lipfert showed the importance of combustor inlet temperature with his correlation and the predictions are in complete agreement with this observation. The above comparisons of theory with data demonstrate that while certain questions on hydrocarbon combustion remain open much can be done with basic models to explain and quantify observations from practical system configurations. However, while this seems to apply to certain systems many practical burners depend upon simultaneous mixing and burning for effective operation. When reaction rates and mixing rates are of the same order of magnitude different modeling is required. In particular, most practical systems involve discrete injection of fuel and oxidizer which may involve imbedded recirculation zones and such systems are characterized by the existence of distinct diffusion flame regions. To analyze such flows the submodel which couples the reaction kinetics with the appropriate turbulent mixing processes is required. In these mixing regions it is assumed that convection dominates in the primary flow direction and that diffusive processes are most important in the direction normal to the primary flow direction as previously described.

Initial applications of the mixing model analysis were made to non-reacting free swirling gas jet flows for direct comparisons of the results found in Reference (32). That experimental investigation involved a series of tests on free, non-reacting, turbulent jets with degrees of swirl covering the weak, moderate and strong ranges. The relevant data used for the comparisons found herein are given in Table VII. Measurements

30

of mean axial and swirl velocities, static pressure and jet widths are reported at axial stations up to 15 orifice diameters. Figures 15, 16, 17 typify the agreement between the experiment and the analysis for the case where the swirl parameter, s, is equal to 0.6.

Figure 15 depicts the decay in the maximum axial velocity for the so-called high and low swirl levels. Depending on the swirl level, the maximum axial velocity need not be located along the jet axis. In particular, for the large swirl case, s = 0.6, the axial velocity achieves a maximum off the jet axis for a distance of approximately 10 jet diameters. This can be seen by examining Figure 16 which shows the radial distribution of axial velocity at several downs stations along with the theoretical predictions. The reason for such a behavior is that the presence of the swirl results in the setting up of radial and axial pressure gradients which, in turn, influence the flow field. In cases of strong swirl, the adverse pressure gradient along the jet cannot be overcome by the kinetic energy of the fluid flowing in the axial direction and a recirculating flow is set up in the central portion of the jet between two stagnation points. This recirculation region extends downstream approximately 1.25 jet diameters, Reference 16. Corresponding to Figure 16, Figure 17 shows the radial distribution of the tangential, or swirl, velocities along with the theoretical predictions. The agreement is quite good within the inner region where the tangential velocity behaves like a solid body rotation; however, in the outer region the analysis somewhat under-predicts the experiments.

On the overall the agreement is quite good and although not shown fully similar comparative agreement has been indicated for the experiments involving the low and moderate swirl levels.

Noteworthy also is that the theoretical results depicted have been obtained by utilizing a turbulent eddy transport that is both radially and axially dependent. This model described in some detail previously was devised by examining the axial velocity profile histories for several degrees of swirl as well as the findings of Reference 19 where, through hot-wire measurements, it is shown that the nonisotropic character of the turbulent stress distributions increase with increasing swirl. The results of our theoretical efforts in attempting to establish closer agreement between theory and experiment have also indicated that the turbulent transport processes are strongly dependent upon the change in the character of

31

the flow as the level of swirl increases. For example, for low to moderate levels of swirl, i.e., for values of s < 0.6 as adjudged by Beer and Chigier, Reference 16, the function k(s) found in Equation (54) was determined by deducing the value of eddy viscosity on the axis from the experimental profiles of velocity and pressure at a given axial station. Basically, the procedure was to solve Equation (41) for $\rho(\epsilon_v)_g^{(rx)}$ ($= \mu^{(rx)}$) at the axis where the derivatives of p and u required for this evaluation were obtained from the experimental profile information.

For the non-reacting swirling flows, the results of these calculations are shown in TABLE VI. The same procedure was initially tried for the large swirl case (s = 0.6). However, it became readily apparent that one value of the function k(s) was not sufficient to provide a correspondingly comparative agreement indicative of the lower swirl results. In this connection it became clear that at least two mixing length scales and hence two levels of turbulent eddy viscosity are appropriate in the region of the flow where the velocity maxima occurs off the axis. In this case a preliminary two layer model, previously described, was utilized where the viscosity in the outer layer was predetermined to be related to the viscosity in the inner region which was deduced by the procedure described above. The values used for these comparisons are shown in TABLE VI as well.

In addition, it was found that within the fully developed regions of the flow, the value of $\tilde{\mu}$, i.e., the ratio between $\mu^{(r\theta)}$ and $\mu^{(rx)}$, of between 0 to 0.3 gave essentially the same results. Whereas, in the initial regions of the flow where the axial decay in tangential velocity and pressure is quite rapid, the agreement between the predictions and the experiment were more sensitive to the ratio.

Accordingly, these basic studies which were performed primarily to establish the accuracy of the mixing model to represent the measured mean-flow properties in flows strictly governed by turbulent transport have clearly demonstrated that the non-isotropic character of the shear stress, alluded to previously, indeed had to be taken into account. Although good agreement was obtained with the available experiments, this required treating the turbulent transport coefficients with a certain degree of delicacy.

32

These observations notwithstanding, we have proceeded to make comparisons with swirling flame data. The experiments were performed using a swirl burner fueled by liquified petroleum gas, Reference 33. The flame was unconfined and the measurements included velocity, pressure and temperature data along the flame. The results are shown in Figures 18 through 25, and they include comparisons with data at two swirl levels where the assumptions regarding turbulent transport properties are given in TABLE VI.

Figures 18 and 19 show the axial distributions of the streamwise and tangential components of velocity, respectively. The agreement is quite good at both swirl levels although a slightly slower decay in the predicted tangential velocity is observed in the downstream portion of the flames, Figure 19. Figure 20 shows a radial profile of the streamwise component of velocity and here also a somewhat slower decay is observed in the outer regions of the flow. Figure 21 shows the static pressure distributions along the flame axis. The agreement here is generally excellent.

Perhaps of most interest are the temperature field and the NO_x emissions from these flames.

Figure 22 gives a comparison of the measurement and predicted radial temperature distributions for the large swirl level. Here the profile is just downstream of the flame closure point on the axis and the agreement is good.

Figures 23 and 24 show the axial temperature distributions and again the agreeement is quite good although the measured peak temperature in the small swirl case, Figure 24, is somewhat lower than predicted.

Although pollutant emissions were not measured, Figure 25 shows the emission index (E.I.) for NO obtained by integrating the NO flux across the flame at their respective closure points. The substantially longer residence time associated with the low swirl flame accounts for the higher NO emission level.

Some comments are in order here with regard to both experimental procedure and the modeling of the problem. In the experiments, air was introduced within the swirl burner both

axially and tangentially with the degree of swirl changed by
independently varying the axial and tangential flow rates.
The fuel rich liquified petroleum gas/air mixture issued from
the burner orifice and was subsequently ignited by means of a
portable pilot flame. Accordingly, ignition was obtained by
applying an "external" source which was removed upon establish-
ing the flame. Thus, the calculations were performed by
assuming a chemically frozen system from the burner exit to
the experimentally determined flame stabilization point, i.e.,
$x \approx 0.085$ meters. An equilibrium chemistry calculation was
then performed in the neighborhood of where the stoichiometric
ratio was unity to simulate the pilot ignition as it occurred
in the experimental system. The products of combustion from
this adjunct calculation provided an annulus of high-temperature
gases which subsequently diffused into the inner fuel-rich
regions and outer fuel-lean regions providing a simulation of
the actual ignition source.

It should be noted that for these reacting flow calcula-
tions the function $k(s)$ could not be determined from profile
information as was described previously because there was
insufficient profile information for these experiments. As such,
the values of $k(s)$ reported in Reference 19 were used both for
the initial non-reacting region and subsequent reacting regions.

In addition, some preliminary work was done in utilizing
the mixing analysis to predict the flow field development within
annular-type combusters. Figures 26 and 27 highlight some of
the pertinent results obtained when the "centerbody option" as
previously discussed (see also Appendix A) was exercised.
Table VIII presents the initial data used with this option of
the program and shows that the numerical experiment under con-
sideration involves the subsequent mixing between air and a
propane fuel jet issuing within an annulus at a speed of
61 m/sec. The fuel is considered to be at ambient temperature
while the air enters the annulus at a temperature of 1500° K.
The initial pressure is assumed to be 10 atmospheres; and,
depending on the option employed the pressure either is held
constant or an axial variation is allowed to develope as
dictated by a prescribed area-contour. The duct outer radius
is 0.328 m. (1 foot); the center-body radius being $3/4$ of the
outer duct radius. The centerbody radius was held constant
albeit the computer program can treat variable contour annuli.
The fuel jet ring is located 0.254 m from the axis and has a
ring width of $0.68(10)^{-3}$ m, or approximately 0.3% of the total
width of the annulus.

34

The relatively small width of the fuel-jet ring brings
out another interesting aspect of the flexibility of the
computer program and that is with regard to mesh size required
for intial profile definition. For example, if one wishes to
input into the program data across the entire annulus while
still maintaining good profile resolution between the airstream
and fuel stream an inordinate amount of input information, due
to the small grid spacing needed, would be required. However,
because the flow field bounding the jet initially is uniform
all that is required is detailed information in the regions
just surrounding the jet. Accordingly, as mixing procceds,
grid points are added from above and below the fuel-jet center-
line as required to bring into proper perspective the necessary
definition of the potential flow regions. Thus, as indicated
in TABLE VIII, information at only eight grid points are supplied
initially; four points to define the fuel jet and four points
(two on each side of the fuel jet) to define the surrounding air
stream. Further details pertaining to this option can be found
in Appendix A.

Figure 26 shows the downstream development of the tempera-
ture within the annulus due to mixing of the high-temperature
air stream with the cold fuel jet. These results were based
upon imposing a constant wall pressure (10 atm) along the duct
and allowing the outer wall to adjust to this constant value of
pressure.

The numerical results show that the outer-wall contour did
not vary markedly within the 1 radii of duct length considered.
The figure also shows that the mixing process has reached the
inner, center-body wall before spreading across the entire duct
width. This asymmetry is due primarily to the closer proximity
of the fuel jet to the inner wall than the outer wall and because
the eddy-viscosity value is assumed constant throughout the duct.

As indicated previously, the other option investigated was
one in which the outer-wall contour is prescribed a priori'
(equal to 0.328 m., and constant) and hence the pressure field
within the duct is adjusted at each diffusion step to reflect
this constraint as well as fulfilling the requirement of mass
conservation. Figure 27 shows the temperature-profile develop-
ment under these conditions and when compared to Figure 26 shows
the effect of the adverse pressure gradient that arises due to
viscous mixing. In the previous case, no pressure gradient
is set up because of the imposed constraint of constant wall
pressure.

Overall, these results were encouraging from the standpoint of having established a model capable of lending insight into unit-problem behavior.

In general all of the above studies have demonstrated that much can be done with basic models to aid not only in understanding the parameters controlling flame-generated pollutants but also in defining areas in kinetics and turbulent mixing needing additional experimental and theoretical work.

5. SUMMARY OF RESULTS

The study performed here has resulted in the development of some of the basic elements required in turbojet combustor modeling. Application of subelements of the unified model has provided needed insight into the NO_x formation process while also establishing the validity of many of the included mechanisms. In particular, the following constitute the major observations of the study:

1. The kinetics mechanisms for the H_2/Air and CO/Air systems appear adequate for combustion and NO emissions predictions for temperatures at least in the 1500 to 2200° K range.

2. The quasi-global mechanism underpredicts the observed NO emission levels in the fuel rich region. Preliminary studies with detailed methane mechanisms show the same behavior suggesting that the quasi-global concept is not at fault but rather certain fast N producing species and reactions are required.

3. Preliminary studies with liquid fuel injection and comparisons with data for the effect of water injection on NO emissions show the strong influence of droplet size. Excellent agreement with water injection data was obtained.

4. All studies made here show NO_2 levels to be from two-to-three orders of magnitude smaller than NO.

5. The stirred reactor concept with appropriate kinetic mechanisms explains much of the observed data obtained from both laboratory reactors and practical engine configurations.

6. The mixing model predicts the observations made on non-reacting and reacting swirling flows but better agreement between theory and experiment requires treating the transport properties with great delicacy. More work in required here.

7. The unified model has been completed but its application and further development are required.

In general, the study not only has provided much needed insight into the NO_x formation and disposition mechanisms but has also delineated areas in the kinetics and fluid mechanics needing additional work.

6. APPENDICES

APPENDIX A - MIXING EQUATIONS IN

VON-MISES COORDINATES

The starting point for the coupled mixing and kinetics model is the boundary-layer form of the conservation equations for global mass, momentum and energy and species diffusion, i.e., Equations (38) through (44). A solution of this system provides the details of the flow field including axial and tangential velocity, pressure, temperature and species fields.

Now, by introducing a stream function such that

$$\psi^M \, \partial\psi/\partial y = \rho u y^N$$

and

$$\psi^M \, \partial\psi/\partial x = -\rho v y^N \tag{A-1}$$

global continuity is automatically satisfied and the resulting coordinate transformation from the physical (x,y) system to a (x,ψ) system yields a set of differential equations which are more amenable to finite-difference solution techniques. Application of this generalized stream function yields the following set of parabolic, partial differential equations:

Species Diffusion (i^{th} gas phase)

$$\frac{\partial \alpha_i}{\partial x} = \frac{1}{\psi^M} \frac{\partial}{\partial \psi} \left\{ \left[\frac{y^{2N} \rho u \, \mu_g^{(rx)}}{\psi^M} \right] \left(\frac{Le}{Pr}\right)_g \frac{\partial \alpha_i}{\partial \psi} \left[1 - (J_D)_i \right] \right\} +$$

$$+ \frac{(\dot{w}_g)_i}{\rho u} + \frac{\Sigma (\dot{w}_p)_{ij}}{\rho u} \tag{A-2}$$

Species Diffusion (j^{th} particle class)

$$\frac{\partial \beta_j}{\partial x} = \frac{1}{\psi^M} \frac{\partial}{\partial \psi} \left\{ \left[\frac{y^{2N} \rho u \; \mu_g^{(rx)}}{\psi^M} \right] \left(\frac{Le}{Pr} \right)_g \theta_j \frac{\partial \beta_j}{\partial \psi} \left[1 - (J_D)_j \right] \right\} +$$

$$+ \frac{(\dot{w}_p)_j}{\rho u} \tag{A-3}$$

x Momentum

$$\frac{\partial u}{\partial x} = \frac{1}{\psi^M} \frac{\partial}{\partial \psi} \left\{ \left[\frac{y^{2N} \mu_g^{(rx)} \rho u}{\psi^M} \right] (J_M^{(x)}) \left(\frac{\partial u}{\partial \psi} \right) \right\} -$$

$$- \left(\frac{\partial p}{\partial x} \right) \left(\frac{1}{\rho u} \right) + \left(\frac{dy}{dx} \right) \frac{\Gamma^2}{y^3 u} \tag{A-4}$$

y Momentum

$$\frac{\partial p}{\partial \psi} = \frac{\psi^M \Gamma^2}{u y^4} \tag{A-5}$$

θ Momentum

$$\frac{\partial \Gamma}{\partial x} = \frac{1}{\psi^M} \frac{\partial}{\partial \psi} \left\{ \left[\frac{y^{2N} \mu_g^{(rx)} \rho u}{\psi^M} \right] \tilde{\mu} (J_M^{(\theta)}) \frac{\partial \Gamma}{\partial \psi} - 2\Gamma \tilde{\mu} \mu^{(rx)} \right\} \tag{A-6}$$

39

Mixture Energy Equation

$$\frac{\partial H}{\partial x} = \frac{1}{\psi M} \frac{\partial}{\partial \psi} \left\{ \left[\frac{y^{2N}\rho u\, \mu_g^{(rx)}}{\psi M} \right] \left\{ \left(\frac{J_T}{Pr}\right)\left(\frac{\partial H}{\partial \psi}\right) - \frac{J_D^{(g)}}{S_c} h_g \alpha_g \right. \right.$$

$$- \frac{J_D^{(p)}}{S_c} \sum_j \theta_j h_j \beta_j + \frac{(Le-1)}{P_r} \sum_i h_i \frac{\partial \alpha_i}{\partial \psi} + \frac{(Le-1)}{P_r} \sum_j \bar{\theta}_j h_j \frac{\partial \beta_j}{\partial \psi}$$

$$+ \left[\alpha_g (1-1/P_r) - \sum_j \beta_j \delta_j / P_r \right] (\partial (q^2/2)/\partial \psi)$$

$$\left. + \left[\alpha_g (\tilde{\mu}_g - 1) - \sum_j \beta_j \sigma_j \tilde{\mu}_j / \tilde{\mu}_g \right] (\partial (w^2/2)/\partial \psi) \right\}$$

$$\left. - \mu^{(r\theta)} J_M^{(\theta)} \tilde{\mu} \quad (w^2) \right\} \qquad (A-7)$$

Once initial and boundary conditions are specified, and assuming thermal equilibrium for the particulate phase, the above set of equations, along with the equation of state, i.e.,

$$\rho = p / \{ RT (\sum_i \alpha_i / W_i + \sum_j \beta_j / W_j) \} \qquad (A-8)$$

together with thermochemical data for the specific enthalpies in the form

$$h_i = h_i (T)$$

for the gas-phase species and

$$h_j = h_j (T)$$

for the particular-phase species and expressions describing the volumetric production rates of each specie properly define

the problem. In the above system of equations the quantities, J, reflect the interaction between the various phases within this multiphase system. Accordingly the J's are defined as follows:

$$(J_D)_i \equiv \left[\alpha_i / (\partial \alpha_i / \partial \psi) \right] \left[(1 - \sum_j \theta_j \beta_j) (\sum_i (\partial \alpha_i / \partial \psi) / \alpha_g) \right.$$

$$\left. + \sum_j \theta_j (\partial \beta_j / \partial \psi) \right] \qquad (A-9)$$

$$(J_D)_j \equiv \left[\beta_j / (\partial \beta_j / \partial \psi) \right] \left[(1 - \sum_k \theta_k \beta_k / \theta_j) (\sum_i (\partial \alpha_i / \partial \psi) / \alpha_g) \right.$$

$$\left. + \sum_k \theta_k / \theta_j) (\partial \beta_k / \partial \psi) \right] \qquad (A-10)$$

$$J_M^{(x)} \equiv \sum_i \alpha_i + \sum_j \sigma_j^{(yx)} \beta_j \qquad (A-11)$$

$$J_M^{(\theta)} \equiv \sum_i \alpha_i + \sum_j \sigma_j^{(y\theta)} \beta_j \qquad (A-12)$$

$$J_T \equiv 1 + \left[\sum_j (H_g - H_j)(\partial \beta_j / \partial \psi) + \sum_j \beta_j (\delta_j - 1)(\partial H_j / \partial \psi) \right] / (\partial H / \partial \psi)$$

$$(A-13)$$

$$J_D^{(g)} = \sum_i J_{D_i} (\partial \alpha_i / \partial \psi) / \alpha_i \qquad (A-14)$$

$$J_D^{(p)} = \sum_i J_{D_j} (\partial \beta_j / \partial \psi) / \beta_j \qquad (A-15)$$

Also, for simplicity, the parameter $\bar{\theta}_j$ appearing in Equation (A-7) is defined by

$$\bar{\theta}_j = \left[Le \theta_j - (h_g / h_j) \right] / (Le - 1)$$

An interesting feature of the analysis written in this form is that it suggests an appropriate modification of the gas-phase transport coefficients making it applicable to "near" dynamic equilibrium multiphase flows. For example, Equations (A-4) and (A-11) show

41

$$\mu_T = (J_M^{(x)}/\alpha_g)\ \mu_g^{(rx)} = (1 + \sum_j \sigma_j^{(rx)} \beta_j/\alpha_g)\ \mu_g^{(rx)} \qquad \text{(A-16)}$$

is the gas-phase turbulent viscosity. Thus, assuming that
the functional form of the gas-phase transport coefficient,
i.e., Equation (54) is unchanged due to the presence of
the particles one can apply an appropriate model for $\mu_q^{(rx)}$
and arrive at an effective global model for μ_T according to
the above equation.

Likewise, Equations (A-9) and (A-10) can be thought of
as being used to define the "effective" gas phase and par-
ticulate phase Schmidt numbers in that one could define

$$(^1/Sc)_{g,eff} = (^1/Sc)_g \ [1-(J_D)_i]$$

$$\text{(A-17)}$$

$$(^1/Sc)_{p,eff} = \theta_j/(Sc)_g \ [1-(J_D)_j]$$

These equations can be readily put into a finite-difference
form where "backward-difference" scheme is employed for the
axial derivatives and where central-difference scheme is
used for the derivatives in the radial direction. But,
before this is discussed, the various boundary and initial
conditions which one can implement with the above analyses
will be documented.

As mentioned in the body of this report several types
of jet configurations can be analyzed with the above mentioned
scheme. These included:

- free jets
- ducted jets
- ducted annular jets

For the latter problems the annulus could be either a
physical center body, which is relevant to combustors or
the "center-body" might be the outer boundary of a recir-
culation zone. Although, from a geometric standpoint both
of these submodels are similar, the boundary conditions along
the "center-body" for each must be treated differently as
will be discussed later on.

42

For the initial conditions for each of these models one must specify the distributions of velocities, species, pressure and temperature, i.e.,

$x = 0$:

$$u = u(o,\psi)$$

$$\Gamma = \Gamma(o,\psi)$$

$$p = p(o,\psi)^*$$

$$\alpha_i = \alpha_i(o,\psi)$$

$$\beta_i = \beta_i(o,\psi)$$

$$T = T(o,\psi)^{**}$$

(A-18)

In addition to this standard set of profile information one requires an initial distribution of

$$dy/dx = dy/dx \ (o,\psi)$$

$$dp/dx = dp/dx \ (o,\psi)$$

$$\theta_j,\delta_j,\sigma_j = \theta_j,\delta_j,\sigma_j(o,\psi)$$

$$\tilde{\mu} = \tilde{\mu} \ (o,\psi)$$

(A-19)

where the latter two forms of profile information are assumed to be unchanged as the mixing proceeds.

As mentioned previously the boundary conditions for the various jet configurations must be handled separately depending whether an axis of symmetry or a centerbody exists. Thus the boundary

---

*   Note: if the initial distribution of tangential velocity
             or $\Gamma(\Gamma = wy)$ is specified then $p(o,\psi)$ can be
             determined by quadrature (see Equation (A-5))

**   Note: Although one of the dependent variables is the
             total enthalpy, H, the idea of requiring an initial
             temperature distribution instead is totally con-
             sistent since $H(o,\psi)$ can be determined from this
             and the other profile information.

conditions for the free-jet mixing properties are in effect:

Free Jet Boundary Conditions

$$\psi = 0: \quad \partial u/\partial \psi = \partial \alpha_i/\partial \psi = \partial \beta_j/\partial \psi = \partial H/\partial \psi = \Gamma = 0$$

$$p_e - p(x,o) = \int_0^\infty \psi^M \, \Gamma^2/uy^4 \; d\psi \tag{A-20}$$

$$\psi \to \infty \quad u = u_e \quad , \quad \alpha_i = \alpha_{i_e} \quad , \quad \beta_j = \beta_{j_e} \quad , \quad H = H_e \quad , \quad p=p_e, \; w=0$$

$$\tag{A-21}$$

The governing equations, i.e., Equations (A-2) - (A-7) must be treated differently along an axis of symmetry. For as the axis is approached

$$\psi \to 0$$

and

$$\partial/\partial \psi \to 0$$

Accordingly, by applying L'Hospital's rule, the governing equations applicable along an axis of symmetry are

$$\frac{\partial \alpha_i}{\partial x} = 2^N (\rho u)^{1-N} \, \mu^{(rx)} \left(\frac{Le}{Pr}\right)_g [1-(J_D)_i] \, \frac{\partial^{M+1} \alpha_i}{\partial \psi^{M+1}} + \frac{(\dot{w}_q)_i}{\rho u} + \frac{\Sigma(\dot{w}_p)_{ij}}{\rho u} \tag{A-2$'$}$$

$$\frac{\partial \beta_j}{\partial x} = 2^N (\rho u)^{1-N} \, \mu^{(rx)} \left(\frac{Le}{Pr}\right)_g \theta_j [1-(J_D)_j] \, \frac{\partial^{M+1} \beta_j}{\partial \psi^{M+1}} + \frac{(\dot{w}_p)_j}{\rho u} \tag{A-3$'$}$$

44

$$\frac{\partial u}{\partial x} = 2^N (\rho u)^{1-N} \mu \ (rx) \ J_M \ (x) \ \frac{\partial^{M+1} u}{\partial \psi^{M+1}} - \frac{1}{\rho u} \left(\frac{\partial p}{\partial x} \right) \qquad \text{(A-4\,$''$)}$$

$$\Gamma = 0 \qquad \text{(A-6$'$)}$$

$$\frac{\partial H}{\partial x} = 2^N (\rho u)^{1-N} u \ (rx) \left\{ \left(\frac{J_T}{Pr} \right) \frac{\partial^{M+1} H}{\partial \psi^{M+1}} - \frac{J_D^{\,(g)}}{Sc} \ h_g \alpha_g - \right.$$

$$- \frac{J_D^{\,(p)}}{Sc} \ \sum_j \theta_j h_j \beta_j + \frac{(Le-1)}{Pr} \sum_i h_i \frac{\partial^{M+1} \alpha_i}{\partial \psi^{M+1}}$$

$$+ \frac{(Le-1)}{Pr} \sum_j \bar{\theta}_j h_j \frac{\partial^{M+1} \beta_j}{\partial \psi^{M+1}}$$

$$\left. + [\alpha_g (1-^1/Pr) - \sum_j \beta_j \delta_j /Pr] \ \frac{\partial^{M+1} (q^2/2)}{\partial \psi^{M+1}} \right\}$$

$$\text{(A-7$'$)}$$

For ducted jets with no "center-body" the conditions of axial symmetry, i.e., Equation (A-20) still prevail but the free-stream conditions that make up the outer boundary conditions, i.e., Equation (A-21) for the free jet problem must be replaced to reflect the fact that the outer boundary is now the wall of the duct.

Ducted Jet (no centerbody; outer contour prescribed)

$\psi = 0$: same as Equations (A-20) \qquad (A-22)

$\psi = \psi_{wall}$:

$\partial \alpha_i / \partial \psi = \partial \beta_j / \partial \psi = 0 \qquad \Longrightarrow$ impermeable wall

$\partial H / \partial \psi = 0 \qquad \qquad \Longrightarrow$ adiabatic wall
\qquad\qquad or \qquad\qquad\qquad\qquad\qquad\qquad\qquad\qquad (A-23)
$T = T_{wall} \qquad \qquad \Longrightarrow$ prescribed wall temperature

$$\partial u / \partial \psi = - (\psi^M / \rho u y^N)_{wall} \ (\rho u^2 / \mu_g^{(rx)})_{mean} \ (c_f/2)$$

$$\partial (\Gamma/y^3)/\partial \psi = - (\psi^M / \rho u y^{N+1})_{wall} \ (\rho u^2 / \mu_g^{(rx)})_{mean} (\widetilde{\tau}/\widetilde{\mu})_{wall} (c_f/2)$$

The latter two conditions express the fact that in reality
a boundary layer is developing along the wall. Thus, in
effect two length scales define the mixing region, namely
the boundary layer thickness along the wall and the radius
of the duct. Since, the boundary layer thickness is very
small compared to the duct radius, obtaining its detailed
flow structure near the wall would require a highly refined
numerical mesh relative to the mesh needed for good resolution
of the bulk flow field. It is assumed here that the details
of the wall boundary layer are not a dominant influence on
the development of the bulk flow field and in this connection
the gross effects of the wall boundary layer are included by
using these two equations without resorting to unwarranted
detail. Accordingly, the boundary conditions on the velocities,
u = 0, w = 0 are replaced by relations between wall shear and
velocity gradients in terms of the skin friction coefficients
whose values are considered as input into the numerical programs.
Thus, these equations can be derived as follows:

$$\tau^{(rx)} / \mu^{(rx)} = - (\partial u / \partial y)_{wall} = (c_f/2) (\rho u^2)_{mean} / \mu^{(rx)} {}^{*}$$

$$\tau^{(r\theta)} / \mu^{(r\theta)} = - [\partial(\Gamma/y^2)/\partial y]_{wall}$$

(A-24)

with $\quad (c_f/2) \equiv (\tau_{wall}^{(rx)} / \rho u^2)_{mean}$

$$\widetilde{\tau} \equiv [\tau^{(r\theta)} / \tau^{(rx)}]_{wall}$$

$$\widetilde{\mu} \equiv \mu^{(r\theta)} / \mu^{(rx)}$$

---

* Note r and y both reflect the radial coordinate in the case
  where N = 1.

46

For the ducted annular jet, the centerbody is considered as an impermeable wall. As such the outer boundary conditions associated with the previous problem also apply here for the inner wall.

Ducted Annular Jet (Physical centerbody contour prescribed)

$\psi = \psi_{OW}$: Same as Equations (A-23)   (A-25)

$\psi = \psi_{IW}$:

$\partial\alpha_i/\partial\psi = \partial\beta_j/\partial\psi = 0 \implies$ impermeable wall

$\partial H/\partial\psi = 0 \implies$ adiabatic wall

or   (A-26)

$T = T_{IW} \implies$ prescribed wall temperature

$$\partial u/\partial\psi = (\psi^M/\rho u y^N)_{IW} \, (\rho u^2/\mu_g^{(rx)})_{mean} \, (^Cf/2)_{IW}$$

$$\partial\Gamma/y^2/\partial\psi = (\psi^M/\rho u y^{N+1})_{IW} \, (\rho u^2/\mu_g^{(rx)})_{mean} \, (\widetilde{\tau}/\widetilde{\mu})_{IW} (^Cf/2)_{IW}$$

There is a difference however between these two problems and that is for the centerbody problem it is possible for

$$\psi = \psi_{IW} = 0$$

while

$$y = y_{IW} \neq 0$$

which can yield a non-regular behavior along the centerbody if the exponent, M, in Equation (A-1) is other than zero as evidenced by examining the inner wall boundary conditions. For example, if M = 1 as is usual for treating free-jet flows Equations (A-26) for u and Γ would show that $\partial u/\partial\psi_{IW} = \partial(\Gamma/y^2)/\partial\psi_{IW} = 0$ even if $^Cf/2 \neq 0$! This difficulty is circumvented by imposing M = 0 and therefore shows the utility of the generalized stream function as defined by Equation (A-1).

Now, if the so-called centerbody is considered as the
outer bounds of the recirculation zone then the "inner wall"
boundary conditions must reflect the fact that across the
boundary there can exist a diffusive transfer of mass and
momentum as well as energy. In this regard then what is
specified initially along the "dividing streamline" are the
axial distributions of the dependent variables as determined
by the well-stirred reactor analysis. Thus, as a first iterate,
interaction across the dividing streamline will be unidirectional
and the kinetics associated with the recirculation zone will
affect the processes occurring within the jet mixing region
whereas the reverse situation is, during this first iterative
"pass," not considered. In essence then, the recirculation
zone is treated as a passive source (or sink) of thermal
energy and species.   Once this first "pass" is made, evaluation
of the fluxes of mass, momentum and energy across this dividing
streamline, as discussed in the body of this report, will
define a new recirculation zone state for treatment with the
well-stirred reactor analysis and thence the mixing analysis
can be repeated. Accordingly the boundary conditions for this
sub-problem are:

Ducted Annular Jet (Recirculation Zone Contour Prescribed)

$\psi = 0$:   Same as Equation (A-20)

$\psi = \psi_{OW}$:   Same as Equation (A-23)

$\psi = \psi_{IW}$:

$$u = u(x, \psi_{IW})$$

$$\alpha_i = \alpha_i(x, \psi_{IW})$$

$$\beta_j = \beta_j(x, \psi_{IW})$$

$$T = T(x, \psi_{IW})$$

$$\Gamma = \Gamma(x, \psi_{IW})$$

48

Essentially this completes the analyses required for all the options and submodels associated with the mixing model. However, as TABLE I indicates, the ducted jet submodel can also treat problems where instead of providing a prescribed outer wall contour one can impose a prescribed pressure. In this connection, the unknown contour is deduced from the calculations by imposing conservation of mass at each axial station.

In addition, the equations, as set forth here, were grouped for ease in the discussion and in formulating their finite-difference counterparts. However, the actual computer program logic need not reflect blocks of calculations commensurate with the internal groupings within the equations as are shown here.

APPENDIX B - FINITE-DIFFERENCE FORM OF GOVERNING EQUATIONS

The governing partial differential equations describing the conservation of mass, momentum, and energy within the flow field and along the axis can be readily put in an explicit finite-difference form. A backward-difference scheme is employed for the axial derivatives and a central-difference scheme for the radial derivatives.

Consider the flow field divided into a grid in ψ, x coordinates. Then the derivatives of an independent variable, say F, will be evaluated by
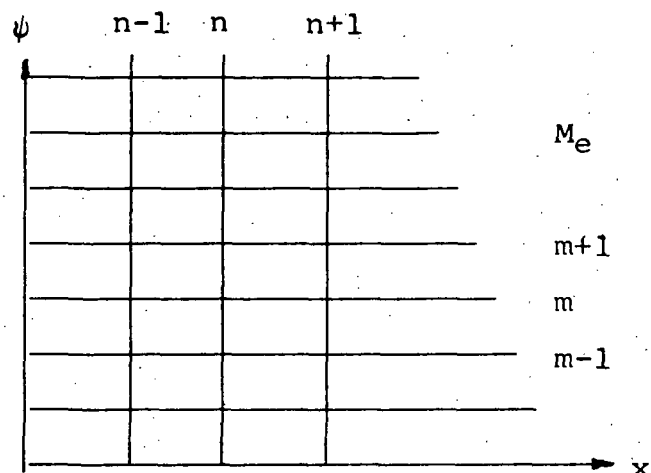
$$(\partial F / \partial x)_{n+1,m} = \frac{F_{n+1,m} - F_{n,m}}{\Delta x} = \frac{\Delta(F)_{n+1,m}}{\Delta x} \tag{B-1}$$

$$\left(\frac{\partial F}{\partial \psi}\right)_{n,m} = \frac{F_{n,m+1} - F_{n,m-1}}{2\Delta \psi} = \frac{\Phi(F)_{n,m}}{\Delta \psi} \tag{B-2}$$

$$\left[\frac{\partial}{\partial \psi}\left(a \frac{\partial F}{\partial \psi}\right)\right]_{n,m} = \frac{a_{n,m+\frac{1}{2}}(F_{n,m+1} - F_{n,m}) + a_{n,m-\frac{1}{2}}(F_{n,m-1} - F_{n,m})}{(\Delta \psi)^2}$$

$$= \left[\Psi(a_{n,m} <F>_{n,m})\right] \bigg/ (\Delta \psi)^2 \tag{B-3}$$

where

$$a_{n,m\pm\frac{1}{2}} = (a_{n,m} + a_{n,m\pm1})/2 \qquad \text{(B-4)}$$

The M+1-ordered derivatives required for the equations along the axis are put into the form

$$\frac{\partial^{M+1}F}{\partial\psi^{M+1}}\bigg|_{n,m} = \frac{F_{n,m+1} - 2M\, F_{n,m} + F_{n,m-1}}{(2-M)(\Delta\psi)^{M+1}} \qquad \text{(B-5)}$$

Accordingly, using the formalism as described by the above equations, we have

$$\Delta(\alpha^{i})_{n+1,m} = \Delta x\left\{\frac{(\dot{w}_q)^{i}}{\rho u}\quad \frac{\Sigma(\dot{w}_p)^{ij}}{\rho u}\right\}_{n,m} + \frac{\Delta x}{\psi^{M}(\Delta\psi)^2}\cdot$$

$$\Psi\left\{\left[(A)\quad \left(\frac{Le}{Pr}\right)_g (1-J_{D_i})\right]_{n,m}\!\!<\alpha^{i}>_{n,m}\right\} \qquad \text{(B-6)}$$

$$\Delta(\beta^{j})_{n+1,m} = \Delta x\left\{\frac{(\dot{w}_p)^{j}}{\rho u}\right\}_{n,m} + \frac{\Delta x}{\psi^{M}(\Delta\psi)^2}$$

$$\Phi\left\{\left[(A)\quad \left(\frac{Le}{Pr}\right)_g \theta_j (1-J_{D_j})\right]_{n,m}\!\!<\beta^{j}>_{n,m}\right\} \qquad \text{(B-7)}$$

$$(\Delta u)_{n+1,m} = \Delta x\left\{\left(\frac{dy}{dx}\right)_{n+1,m}\left(\frac{\Gamma^2}{y^3 u}\right)_{n,m} - \left(\frac{dp}{dx}\right)_{n+1,m}\left(\frac{1}{\rho u}\right)_{n,m}\right\} + \frac{\Delta x}{\psi^{M}(\Delta\psi)^2}\cdot$$

$$\Psi\left\{\left[(A)\quad J_m^{(x)}\right]_{n,m}\!\!<u>_{n,m}\right\} \qquad \text{(B-8)}$$

$$(\Delta\Gamma)_{n+1,m} = \frac{\Delta x}{\psi^{M}\Delta\psi^2}\Psi\left\{[A\tilde{\mu}\, J_M^{(\theta)}]<\Gamma>_{n,m}\right\}_{n,m} - \frac{\Delta x}{\psi^{M}\Delta\psi}\Phi\left\{\Gamma\tilde{\mu}^{(rx)}\right\}_{n,m}$$

$$\text{(B-9)}$$

51

$$(\Delta H)_{n+1,m} = \frac{\Delta x}{\psi^M \Delta \psi^2} = \left\{ \Psi \left\{ \left[\frac{AJ_T}{P_r}\right]_{n,m} <H>_{n,m} \right\} + \Psi \left\{ \sum_i \left[\frac{A(L_e-1)}{P_r}\right]_{n,m} h_i <\alpha^i> \right\} \right.$$

$$+ \Psi \left\{ \sum_j \left[\frac{A(L_e-1)}{P_r}\right]_{n,m} \theta_j h_j <\beta_j>_{n,m} \right\}$$

$$+ \Psi \left\{ \left[A(\alpha_g(\widetilde{\mu}_g-1) - \sum_j \beta_j \delta_j \widetilde{\mu}_j/\widetilde{u})\right]_{n,m} <q^2/2> \right\}$$

$$\left. + \Phi \left\{ \left[A(\alpha_g(\widetilde{\mu}_g-1) - \sum_j \beta_j \sigma_j \widetilde{\mu}_j/u_g)\right]_{n,m} <w^2/2>_{n,m} \right\} \right\}$$

$$- \frac{\Delta x}{\psi^M \Delta \psi} \left\{ \Phi \left\{ A \frac{J_D^{(g)} h_q \alpha_q}{S_c} \right\}_{n,m} + \Phi \left\{ A \frac{J_D^{(p)}}{S_c} \sum \theta_j h_j \beta_j \right\}_{n,m} \right.$$

$$\left. + \Phi \left\{ A\mu^{(rx)} J_M^{(\theta)} \widetilde{\mu} w^2 \right\}_{m,m} \right\} \qquad (B-10)$$

The radial momentum, i.e.,

$$\partial p/\partial \psi = \psi^M r^2 /uy^4 \qquad (B-11)$$

can be obtained by simple quadrature and the quantity A in the above equations is defined as

$$A = y^{2N} \mu_g^{(rx)} \rho u/\psi^M \qquad (B-12)$$

Application of the finite-difference forms, i.e., Equations B1 through B4 are also applied to the requisite boundary conditions that have been discussed in Appendix A.

52

The axial step size, Δx, must be kept small to ensure stability. This is done by setting Δx equal to the smallest of the triplet $(\Delta x_1, \Delta x_2, \Delta x_3)$ where the following criteria is used to establish their values:

(1) For $\psi_{m=2} \leq \psi \leq \psi_{m=M_e}$

$$\Delta x_1 = \frac{\psi^N (\Delta \psi)^{M+1}}{3\left[\left(\frac{A}{S_c}\right)_{n,m+\frac{1}{2}} + \left(\frac{A}{S_c}\right)_{n,m-\frac{1}{2}} \right]} \qquad (B-13)$$

(2) For $\psi = \psi_{m=1}$

$$\Delta x_2 = \frac{(\Delta \psi)^{M+1}}{3 \left[2^{(N+1)} (\rho u)_{n,m}^{(1-N)} \left(\frac{u}{S_c}\right)_{n,1} \right]} \qquad (B-14)$$

(3) $\qquad \Delta x_3 = \text{minimum } (\Delta y)_m \qquad\qquad (B-15)$

Then $\Delta x = \min (\Delta x_1, \Delta x_2, \Delta x_3)$ and accordingly Δx is directly related to $\Delta \psi$ (an input) and inversely related to the local value of eddy viscosity.

APPENDIX C - NOMENCLATURE

A   factor which differentiates between diffusion-controlled combustion (A=1) and droplet evaporation (A=0), Equation (24)

A_j cross sectional area of lateral jet; dilution hole analysis, Equation (51), m^2

B   transfer number in droplet combustion analysis, Equation (24)

C_f skin-friction coefficient

C_{ij} mole fractions

C_p specific heat, $J/kg/^{\circ}K$

d   droplet diameter, m
D   jet diameter, m
d_j dilution hole diameter, m
E   activation energy, k cal/mole/$^{\circ}K$
$\dot{E}$ total rate of energy flux across dividing streamline, Equation (49), J/kg

$\dot{e}$ energy flux across dividing streamline/unit surface area, Equation (47), $J/kg/m^2$

$\bar{H}$ heat of combustion, Equation (24), J/kg

H   total enthalpy of mixture, J/kg

$(h)_g$ enthalpy of gas-phase mixture in multi-component system, J/kg

h_k static enthalpy of specie k , J/kg

h   mixture enthalpy or width of lateral jet, Equation (51), J/kg
J   defined in Equations (A-9) through (A-15)
k   thermal conductivity, J/m sec $^{\circ}K$

k_{fp} , k_{bp} forward and backward reaction rates for reaction p

54

$k_{c,p}$ reaction rate constant for reaction p

$k(s)$ empirically determined constants used in eddy viscosity models of mixing subprogram, Equation (54)

Le   Lewis number

$\dot{M}_T$ total rate of mass flux across dividing streamline, kg/sec

$\dot{m}$ mass flow rate within stirred reactor, kg/sec

N   geometric parameter, N=0 implies 2-D flow, N=1 implies axisymmetric flow, or number of gas-phase species

N_j total number of dilution holes at an axial station or number density

$\bar{N}$ stoichiometric oxygen/fuel ratio

p   pressure, N/m^2

Pr   Prandtl number

$\dot{Q}$ net rate of external heat addition

Q   heat of vaporization

$\dot{q}$ ratio of dilution hole momentum flux to primary stream momentum flux, Equation (50)

q   component of velocity in x,r plane, m/sec

R   gas constant, $J/^{\circ}k/mol$

$r_{\frac{1}{2}}$ jet "half radius" based upon location of the mean velocity within mixing region, m.

s   swirl factor, = angular momentum flux/axial momentum flux times nozzle radius.

Sc   Schmidt number

T   temperature, $^{\circ}K$

t   time, sec

u, v, w	components of the velocity vector in the axial (x), radial $(y$ or $r)$, and tangential (θ) directions, m/sec
V	volume of stirred reactor, m^3
V_j	average velocity of lateral jet, Equation (53), m/sec
W_k	molecular weight of specie k, kg/kg_{mole}
$\dot{W}_k$	volumetric rate of production of specie k, $kg\ m^3/sec$
$(\dot{W}_g)_i$	production of the ith gas-phase specie due to homogeneous gas-phase reactions, $kg/m^3/sec$
$(\dot{w}_p)^F_{ij}$	production of the ith gas-phase specie from the jth particle class due to evaporation or heterogeneous reactions, $kg/m^3/sec$
$(\dot{w}_p)^F_j$	production of the jth particle class, $kg/m^3/sec$
$(y_i)_g$	mass function of species i in the gas-phase subsystem
y_{IW}	radius of dividing streamline of innerwall of annular combustor
y_{OW}	radius of outerwall of combustor, m
(Δy)	"Effective" ring width due to dilution hole efflux, m
α_k	mass fraction of gaseous specie k
α_g	mass fraction of all <u>gas-phase</u> species in multi-component system
β_k	mass fraction of particulate species k
β_p	mass fraction of all solid (or liquid) phase species in multicomponent system
Γ	circulation, $\Gamma = wy$, m^2/sec
δ	droplet or bulk density , kg/m^3
$\epsilon_D, \epsilon_V, \epsilon_T$	turbulent gas-phase exchange coefficients of mass, momentum and energy, respectively
$\theta_j, \delta_j, \sigma_j$	ratio of particle-to-gas phase eddy diffusitives of mass, momentum and energy

56

λ	burning or evaporation rate constraint, Equation (23)
μ	eddy viscosity , N-sec/m²
$\tilde{\mu}$	ratio of eddy viscosities in the rx-plane to the rθ-plane
ν	molecular kinematic viscosity, N-sec/m²
ν'_{ip}	stoichiometric coefficients of reactants i in reaction p
ν''_{ip}	stoichiometric coefficients of reaction products i in reaction p
ρ	density, kg /m³
τ	residence time within stirred reactor, sec
$\tilde{\tau}$	ratio of shear stress in (rx) to (rθ) planes
Φ	equivalence ratio = fuel-air ratio/φ
φ	stoichiometric fuel-air ratio
ψ	stream function

Subscripts

[ ]	molar concentration, moles/cc
( )$_\ell$	implies liquid state
( )$_g$	implies gaseous state
( )$_o$	conditions along axis
( )$_{OW}$	outer wall
( )$_{IW}$	inner wall or dividing streamline
( )$_p$	implies particulate state
( )$_\infty$	free stream conditions
( )$_m$	maximum value

Superscripts

( )^I	implies inflow state for Recirculation Zone Model
( )^O	implies outflow state for Recirculation Zone Model
( )$^{B.P.}$	boiling point
( )^{rx}	rx-component of ( )
( )$^{r\theta}$	rθ-component of ( )

57

REFERENCES

1. George, R.E., Verssen, J.A. and Chass, R.L., "Jet Aircraft: A Growing Source of Pollution," J. Air Pollution Control Ass'n., 19, No. 11, pp. 847-855, 1969.

2. Bastress, E. K., "Nature and Control of Aircraft Engine Exhaust Emissions," APCA Paper No. 69-190, 1969.

3. Lozano, E.R., Melvin, W.W. and Hochheiser, S., "Air Pollution Emissions from Jet Engines," J. Air Pollution Control Ass'n., 18, No. 6, pp. 392-394, 1968.

4. Bogdon, L. and McAdams, H. T.,"Analysis of Aircraft Exhaust Emission Measurements," Cornell Aero. Lab. Report NA-5007-K-1, October 1971.

5. Schnell, E., "Analysis of Small Gas Turbine Engine Components," ADARD LS-46-71, "Small Gas Turbines for Helicopters and Surface Transport," May 1971.

6. Vaught, J. M., "Collection and Assessment of Aircraft Emission Base-Line Data - Turboprop Engines," Allison Report 756-A-15 (Detroit Diesel Allison Report Number EDR7200), September 1971.

7. Grobman, J., "Effect of Operating Variables on Pollutant Emissions from Aircraft Turbine Engine Combustors," NASA Lewis Research Center Report NASA TMX-67887, 1971.

8. Niedzwiecki, R. W. and Jones, R. E., "Pollution Results of a Swirl-Can Combustor," NASA Lewis Research Center Report NASA TMX-68160, 1972.

9. Edelman, R. Fortune, O. and Wielerstein, G., "Some Observations on Flows Described by Coupled Mixing and Kinetics," General Motors Research Labs., Symposium on Emissions from Continuous Combustion Systems, September 27-28, 1971, also Plenum Press, New York.

10. Fenimore, C. P., "Formation of NO in Premixed Hydrocarbon Flames," 13th Symposium (International) on Combustion, The Combustion Institute, 1971, p. 373.

11. Edelman, R. and Fortune, O., "A Quasi-Global Chemical Kinetic Model for the Finite Rate Combustion of Hydrocarbon Fuels," AIAA 69-86.

12. Engleman, V., Edelman, R. B.; Bartok, W. and Longwell,J.P., "Experimental and Theoretical Studies of NO_x Formation in a Jet-Stirred Combustor," The 14th Symposium (International) on Combustion, Pennsylvania State University, August 1972.

13. Skinner, G. B., Lifshitz, A., Scheller, K. and Burcat,A., "Kinetics of Methane Oxidation," J. Chem. Phys. 56, 6, April 1972.

14. Bowman, C. T. and Seery, D., "Investigations of NO Formation Kinetics in Combustion Processes: The Methane-Oxygen-Nitrogen Reaction, "Presented at the Symposium on Emissions From Continuous Combustion Systems, General Motors Research Labs., Warren, Mich.,September 27-28,1971.

15. Chinitz, W., Pyrodynamics, 3, 1966, p. 196.

16. Beer, J. M., Chigier, N.A., "Combustion Aerodynamics," Chapter 5, John Wiley & Sons, Publisher, New York, 1972.

17. Abramovich, G. N., "The Theory of Turbulent Jets," MIT Press, Cambridge, Mass., 1963, pp. 541-556.

18. Schetz, J. A., Billig, F. S., "Penetration of Gaseous Jets Injected into a Supersonic Stream," Journal of Spacecraft and Rockets, Vol. 3, No. 11, November 1966.

19. Lilley, D. G., Chigier, N. A., "Nonisotropic Turbulent Stress Distribution in Swirling Flows From Mean Value Distributions," Int. J. Heat Mass Transfer, Vol. 14, 1971, pp. 573-585.

20. Lilley, D.G., Chigier, N.A., "Nonisotropic Exchange Coefficients in Turbulent Swirling Flames from Mean Value Distributions," Combustion and Flame, 16, 1971, pp.177-189.

21. Edelman, R., Fortune, O., "An Analysis of Mixing and Combustion in Ducted Flows," AIAA Paper 68-114, presented at the 6th AIAA Aerospace Sciences Meeting, New York, 1968.

22. Fernandez, F. L., Lubard, S. C., "Turbulent Vortex Wakes and Jets," AIAA Paper 71-615, Presented at the AIAA 4th Fluid and Plasma Dynamics Conf., Palo Alto, Calif., June 21-23, 1971.

23. Edelman, R., Economos, C., "A Mathematica Model for Jet Engine Combustor Pollutant Emissions," AIAA Paper No. 71-714, Presented at the AIAA/SAE 7th Propulsion Joint Specialists Conf., Salt Lake City, Utah, June 14-18, 1971.

24. Longwell, J. P. and Weiss, M. A., Ind. Eng. Chem. 47, 1634, (1955).

25. Bartok, W., Englemen, V., Goldstein, R. and del Valle, E.G., "Basic Kinetic Studies and Modeling of Nitrogen-Oxide Formation in Combustion Processes," Presented at the Symposium on Combustion Processes and Air Pollution Control, A.I.Ch.E., 70th Annual Meeting, Atlantic City, N.J., August 1971.

26. Hottel, H. C., Williams, G.C. and Miles, G.A., "Mixedness in the Well-Stirred Reactor," 11th Symposium (International) on Combustion, The Combustion Institute, 1967, pp.771-778.

27. Zeinalov, M.A.O., Kuwata, M. and Essenhigh, R.H., "Stirring Factors in Combustion Chambers: A Finite-Element Model of Mixing Along An Information Flow Path," Presented at the 14th Symposium (International) on Combustion, Pennsylvania State University, August 1972.

28. Bowman, B.R., Pratt, D.J., and Crowe, C. T., "Effects of Turbulent Mixing and Chemical Kinetics on Nitric Oxide Production in a Jet-Stirred Reactor," Presented at the 14th Symposium (International) on Combustion, Pennsylvania State University, August 1972.

29. Klapatch, R. D. and Koblish, T. R., "Nitrogen Oxide Control with Water Injection in Gas Turbines," ASME paper 71/WA/GT-9, November 1971.

30. Shaw, H., "Reduction of Nitorgen Oxide Emissions From a Gas Turbine Combustor by Fuel Modification," for Presentation at the 18th Annual Inernational Gas Turbine Conference and Products Show, Washington, D.C., April 8-12, 1973.

31. Lipfert, F. W., "Correlation of Gas Turbine Emissions Data," ASME Paper 72-GT-60, 1972.

32. Chigier, N. A., Chervinsky, A., "Experimental Investigation of Swirling Vortex Motions in Jets," Technion-Israel Institute of Technology, Dept. of Aeronautical Engineering, TAE Report No. 53, 1966. Also J.Appl'd.Mech. Vol. 34, 1967.

33. Chervinsky, A., "Turbulent Swirling Jet Diffusion Flames," AIAA Journal, Vol. 7, No. 10, October 1969.

TABLE I. — COMPUTATIONS IN MIXING ZONES

I VARIABLE MIXING ZONES	II SPECIFIED INITIAL CONDITIONS	III BOUNDARY CONDITIONS ALONG IMPERMEABLE PART OF OUTER WALL	IV BOUNDARY CONDITIONS ALONG INNER WALL	
Axial Velocity, $u(x,y)$	$u = u(o,y)$ for $y_{IW} < y < y_{OW}$	Specify wall skin friction or shear: $c_{f_{rx}}(x)$ or $\tau_{rx}(x)$	(A) Annular Flow	Same as outer wall
			(I) Imbedded Recirculation Zone	Specify $u_{IW} = u_{IW}(x)$ based upon mean flow through velocity in recirculation zone
Swirl Velocity, $w(x,y)$	$w = w(o,y)$ for $y_{IW} < y < y_{OW}$	Specify wall skin friction or shear: $c_{f_{r\theta}}(x)$ or $\tau_{r\theta}(x)$	(A)	Same as outer wall
			(I)	specify $w_{IW} = w_{IW}(o,y) \cdot w_{IW}(o) \frac{y_{IW}(x)}{y_{IW}(o)}$
Temperature, $T(x,y)$	$T = T(o,y)$ for $y_{IW} < y < y_{OW}$	Specify adiabatic or wall temperature: $\frac{\partial H}{\partial y}\big)_w = 0$ or $T_w(x)$	(A)	Same as outer wall
			(I)	Specify $H_{IW} = H$ recirculation zone
Mass Fraction, $\alpha_{i,j}(x,y)$	$\alpha_{i,j} = \alpha_{i,j}(o,y)$ for $y_{IW} < y < y_{OW}$	Impermeability: $\frac{\partial \alpha_i}{\partial y}\big)_w = 0$	(A)	Same as outer wall
Number density, $N_j(x,y)$	$N_j = N_j(o,y)$ for $y_{IW} < y < y_{OW}$		(I)	Specify $(\alpha_i)_{IW} = (\alpha_i)$ recirculation zone
Droplet (Particle) size $d_j(x,y)$	$d_j = d_j(o,y)$ for $y_{IW} < y < y_{OW}$			
Pressure, $p(x,y)$	$p = p(o,y)$ for $y_{IW} < y < y_{OW}$	Specify $y_{OW}(x)$ and $p_{OW}(x)$ is obtained as part of the solution or obtain $y_{OW}(x)$ if $p_{OW}(x)$ is specified (see Wall Contour below)	(A)	Determined as part of the solution
			(I)	Determined as part of the solution
Wall Contour Outer	$y_{OW} = y_{OW}(O)$	If y_{OW} specified then $p(xy)$ is obtained as part of the solution or obtain $y_{OW}(x)$ if $p_{OW}(x)$ is specified	(A)	Specified; $y_{IW} = y_{IW}(x)$
Inner	$y_{IW} = y_{IW}(O)$		(I)	Specified; $y_{IW} = y_{IW}(x)$

	V AIR INJECTION ALONG THE WALL	
Variable	Slots	Holes
V_I	When the combustor flow reaches a slot, the problem is reinitialized.	When the combustor flow reaches a hole, the penetrations are determined and the flow properties at $x = x_H$ are specified as shown in Column II.
T_I	The "new" initial conditions involve the extension of the profiles at $x = x_s$, as given in Column II, across the slot where the slot width is known by the specification of $y_w = y_w(x)$.	
P_I		For both slots and holes, the state of the air flow (P_I, T_I, V_I) must be specified on the upstream side of the openings. Then, given an estimate for discharge coefficients, the state of flow entering the combustor is determined. The distribution of slots and holes are input information.
A		

* For full flow symmetry conditions are applied on the axis.

TABLE II

EXTENDED C-H-O CHEMICAL KINETIC REACTION MECHANISM

$$k_f = AT^b \exp(-E/RT)$$

REACTION	A	FORWARD b	E/R
1. $C_nH_m + \frac{n}{2}O_2 \to \frac{m}{2}H_2 + n\,CO$	$\dfrac{5.52\times10^8}{p^{.825}} \cdot c_{C_nH_m}^{\frac{1}{2}} c_{O_2}$	1	12.4×10^3
2. $CO + OH = H + CO_2$	5.6×10^{11}	0	$.543 \times 10^3$
3. $CO + O_2 = CO_2 + O$	3×10^{12}	0	25.0×10^3
4. $CO + O + M = CO_2 + M$	1.8×10^{19}	-1	2×10^3
5. $H_2 + O_2 = OH + OH$	1.7×10^{13}	0	24.7×10^3
6. $OH + H_2 = H_2O + H$	2.19×10^{13}	0	2.59×10^3
7. $OH + OH = O + H_2O$	5.75×10^{12}	0	$.393 \times 10^3$
8. $O + H_2 = H + OH$	1.74×10^{13}	0	4.75×10^3
9. $H + O_2 = O + OH$	2.24×10^{14}	0	8.45×10^3
10. $M + O + H = OH + M$	1×10^{16}	0	0
11. $M + O + O = O_2 + M$	9.38×10^{14}	0	0
12. $M + H + H = H_2 + M$	5×10^{15}	0	0
13. $M + H + OH = H_2O + M$	1×10^{17}	0	0
14. $O + N_2 = N + NO$	1.36×10^{14}	0	3.775×10^4
15. $N_2 + O_2 = N + NO_2$	2.7×10^{14}	-1.0	6.06×10^4
16. $N_2 + O_2 = NO + NO$	9.1×10^{24}	-2.5	6.46×10^4
17. $NO + NO = N + NO_2$	1.0×10^{10}	0	4.43×10^4
18. $NO + O = O_2 + N$	1.55×10^9	1.0	1.945×10^4
19. $M + NO = O + N + M$	2.27×10^{17}	-0.5	7.49×10^4
20. $M + NO_2 = O + NO + M$	1.1×10^{16}	0	3.30×10^4
21. $M + NO_2 = O_2 + N + M$	6.0×10^{14}	-1.5	5.26×10^4
22. $NO + O_2 = NO_2 + O$	1×10^{12}	0	2.29×10^4
23. $N + OH = NO + H$	4×10^{13}	0	0
24. $H + NO_2 = NO + OH$	3×10^{13}	0	0
25. $CO_2 + N = CO + NO$	2×10^{11}	-1/2	4×10^3
26. $CO + NO_2 = CO_2 + NO$	2×10^{11}	-1/2	2.5×10^3

Reverse reaction rate, k_r, is obtained from k_f and

the equilibrium constant, K_c.

TABLE III

$CH_4/O/N$ System (Reference 14 , Bowman/Seery)

$$k_f = AT^b \exp(-E/RT)$$

	REACTION	A	FORWARD b	E/R
1.	$CH_4 + M = CH_3 + H + M$	2×10^{17}	0	44.5×10^3
2.	$CH_4 + OH = CH_3 + H_2O$	2.8×10^{13}	0	2.5×10^3
3.	$CH_4 + O = CH_3 + OH$	2×10^{13}	0	4.64×10^3
4.	$CH_4 + H = CH_3 + H_2$	6.9×10^{13}	0	5.95×10^3
5.	$CH_3 + O_2 = H_2O + CHO$	2×10^{10}	0	0
6.	$CH_3 + O = CHO + H_2$	1×10^{14}	0	0
7.	$CHO + OH = CO + H_2O$	1×10^{14}	0	0
8.	$CHO + M = H + CO + M$	2×10^{12}	1/2	14.4×10^3
9.	$O + N_2 = NO + N$	1.4×10^{14}	0	3.79×10^3
10.	$N + O_2 = NO + O$	6.4×10^9	1	3.14×10^3
11.	$N + OH = NO + H$	4×10^{13}	0	0

TABLE IV

GASL $CH_4/O/N$ System

$$k_f = AT^b \exp(-E/RT)$$

REACTION	A	FORWARD b	E/R
1. $CH_4 + M = CH_3 + H$	2×10^{17}	0	44.5×10^3
2. $CH_4 + OH = CH_3 + H_2O$	3.5×10^{14}	0	4.5×10^3
3. $CH_4 + O = CH_3 + OH$	2×10^{13}	0	3.45×10^3
4. $CH_4 + H = CH_3 + H_2$	2×10^{14}	0	5.95×10^3
5. $CH_3 + O = HCHO + H$	1.9×10^{13}	0	0
6.* $CH_3 + O_2 = CHO + H_2O$	2×10^{10}	0	0
7. $CH_3 + O_2 = HCHO + OH$	1×10^{14}	0	0.75×10^3
8.* $CH_3 + O = CHO + H_2$	1×10^{14}	0	0
9. $HCHO + OH = CHO + H_2O$	3×10^{13}	0	0
10. $HCHO + H = CHO + H_2$	1.7×10^{13}	0	1.5×10^3
11. $HCHO + CH_3 = CHO + CH_4$	2.5×10^{10}	1/2	2.65×10^3
12. $HCHO + O = CHO + OH$	3×10^{13}	0	0
13. $HCHO + O_2 = CO_2 + H_2O$	7.3×10^{10}	1/2	0
14. $CHO + O_2 = CO_2 + OH$	7.4×10^{11}	1/2	0
15. $CHO + O = CO_2 + H$	5.4×10^{11}	1/2	0
16. $CHO + O = CO + OH$	5.4×10^{11}	1/2	0
17. $CHO + CH_3 = CH_4 + CO$	2.5×10^{10}	1/2	0
18. $CHO + OH = CO + H_2O$	3×10^{13}	0	0
19.* $HCO + M = H + CO + M$	2×10^{12}	1/2	-14.4×10^3

PLUS ALL REACTIONS IN TABLE II

* These reactions are retained for purposes of
comparing with the mechanism of TABLE III

TABLE V. - OPERATING CONDITIONS FOR TWO-PHASE
RECIRCULATION ZONE COMBUSTION CALCULATIONS

Fuel: C_8H_{18}

Injection Temperature   Fuel: 300° K
                                         Air : 300° K

Equivalence Ratio   1.0

Fraction Liquid Fuel: 0.5 (for all cases
                                             except $d^I = 0$)

Pressure: 1 atm

Variable: Droplet diameter and
                                         $\dot{m}/v$ (residence time)

TABLE VI. - VALUES OF EDDY VISCOSITY AND/OR
SWIRL CONSTANT USED IN PRESENT
CALCULATIONS (see Eq. (54))

Swirl Value	Non-Reacting Runs	Reacting Runs
S	k(s)	k(s)
0.066	0.025	
0.112	0.033	0.023
0.232	0.066	0.045
0.600	*	

$$* \begin{cases} \mu_1 = 6.7\ (10)^{-2}\ N\ sec/m^2 & \text{for } y < y_{peak} \\ \mu_2 = 1.02\ (10)^{-}\ N\ sec/m^2 & \text{for } y \geq y_{peak} \end{cases}$$

TABLE VII. – SWIRLING JET EXHAUST CHARACTERISTICS

s	0.112	0.232	0.06	0.6
u_o (msec)	76.0	103.0	41.0	52.4
w_{mo} (m/sec)	16.7	32.7	4.8	35.6
fuel	LPG	LPG	N/A	N/A
Φ	5.05	5.05	N/A	N/A
$(\alpha)_{fuel}$	0.245	0.245	N/A	N/A
T_o °K	300	300	300	300
$(p_\infty - p_o)$ (kg/m^2)	70	19	1	81
r_{jet} mm	25	25	50	50
p_∞ kg/m^2	$1.03(10)^4$	$1.03(10)^4$	$1.03(10)^4$	$1.03(10)^4$

NOTE: For the combustion experiments, liquified petroleum gas (LPG) was used.

The theoretical calculations used propane as the fuel.

TABLE VIII. — ANNULAR JET INITIAL CONDITIONS
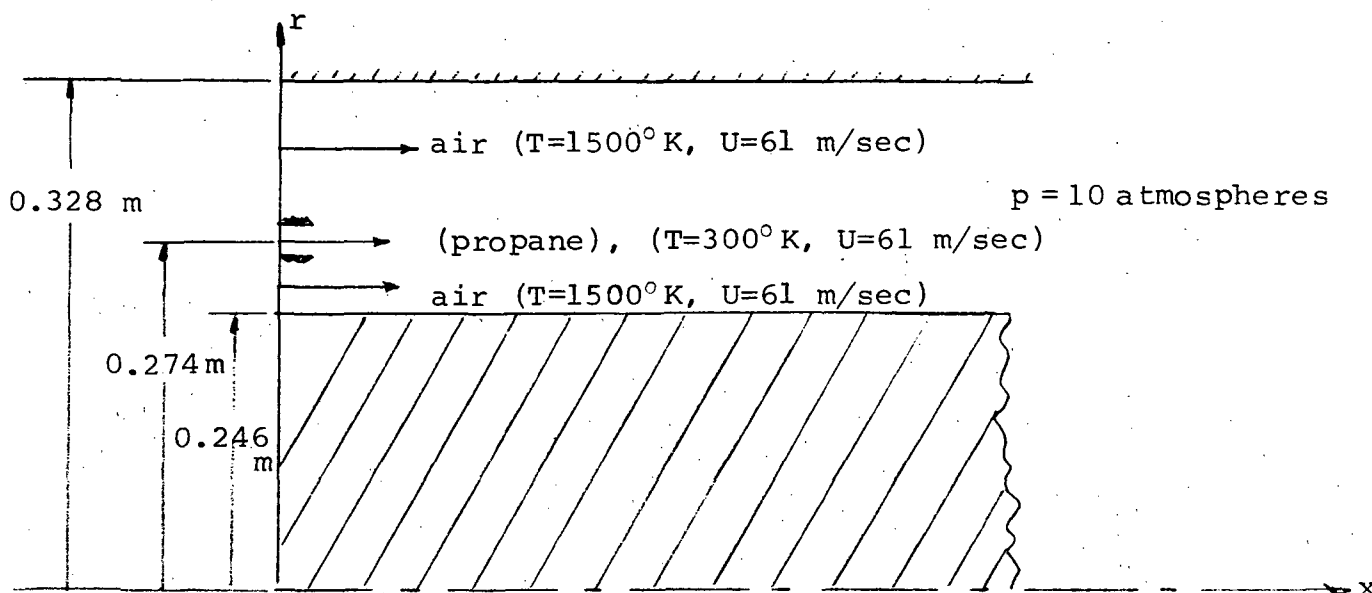
Initial Data

r/r_{wall}	U m/sec	T $^{\circ}K$	α_{N2}	α_{02}	α_{fuel}
.8267	61	1500	.768	.232	0.0
.8309	61	1500	.768	.232	0.0
.8333	61	300	0.0	0.0	1.0
.8338	61	300	0.0	0.0	1.0
.8344	61	300	0.0	0.0	1.0
.8349	61	300	0.0	0.0	1.0
.8373	61	1500	.768	.232	0.0
.8414	61	1500	.768	.232	0.0

geometric constraints

Case 1 p_{wall} = constant = 10 atm.; outer wall contour variable, center body constant

Case 2 p_{wall} is variable , $r_{outer\ wall}$ = constant = 0.328m center body constant

1 – Fuel Cone

2 – Primary Reaction Zone

3 – Reversal Zone

4 – Secondary Zone

5 – Carbon Producing Zone

Secondary Air

Cooling Air

Primary Air

Fuel Spray

Air Swirler

Primary Zone

Secondary Zone
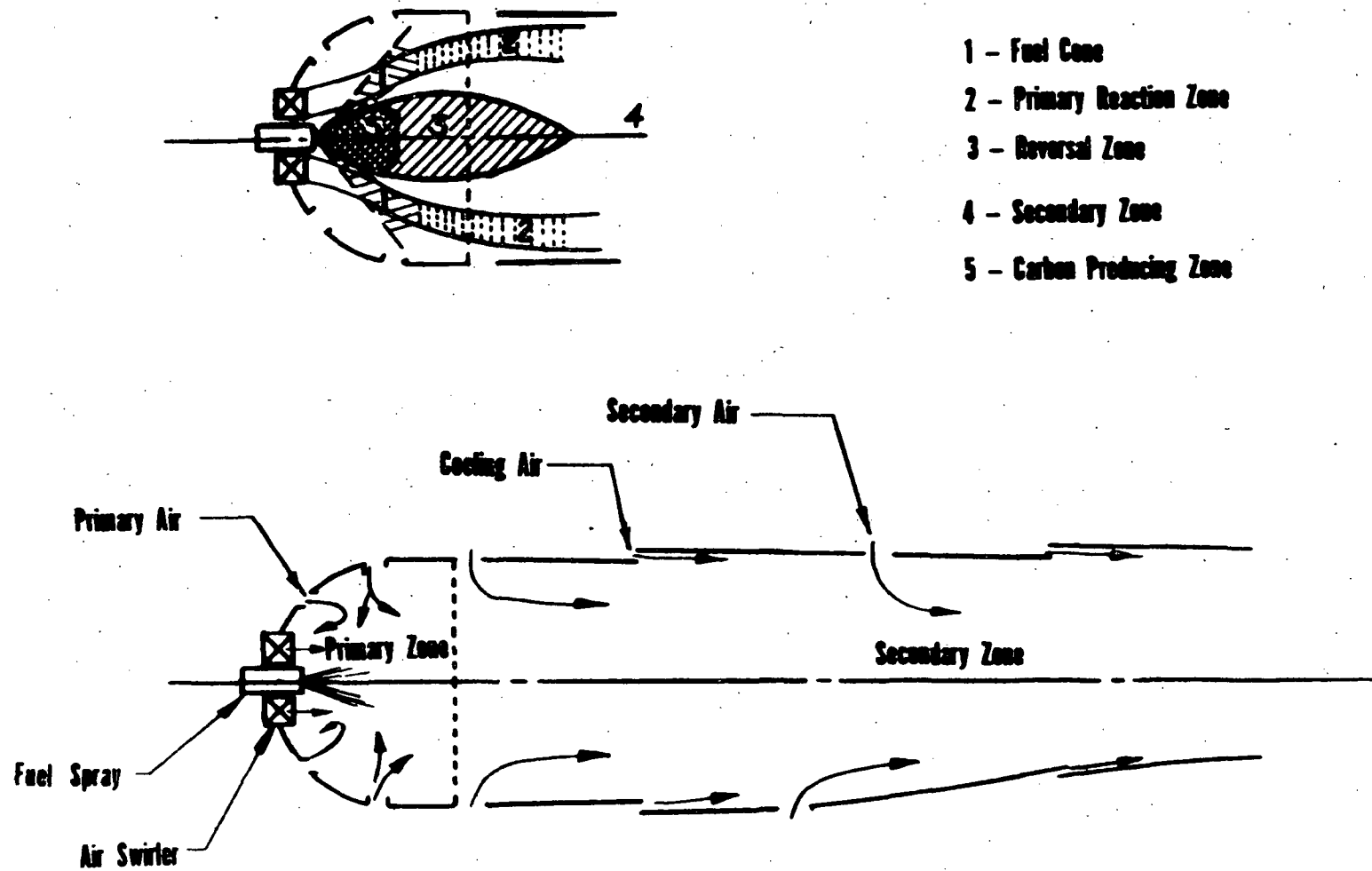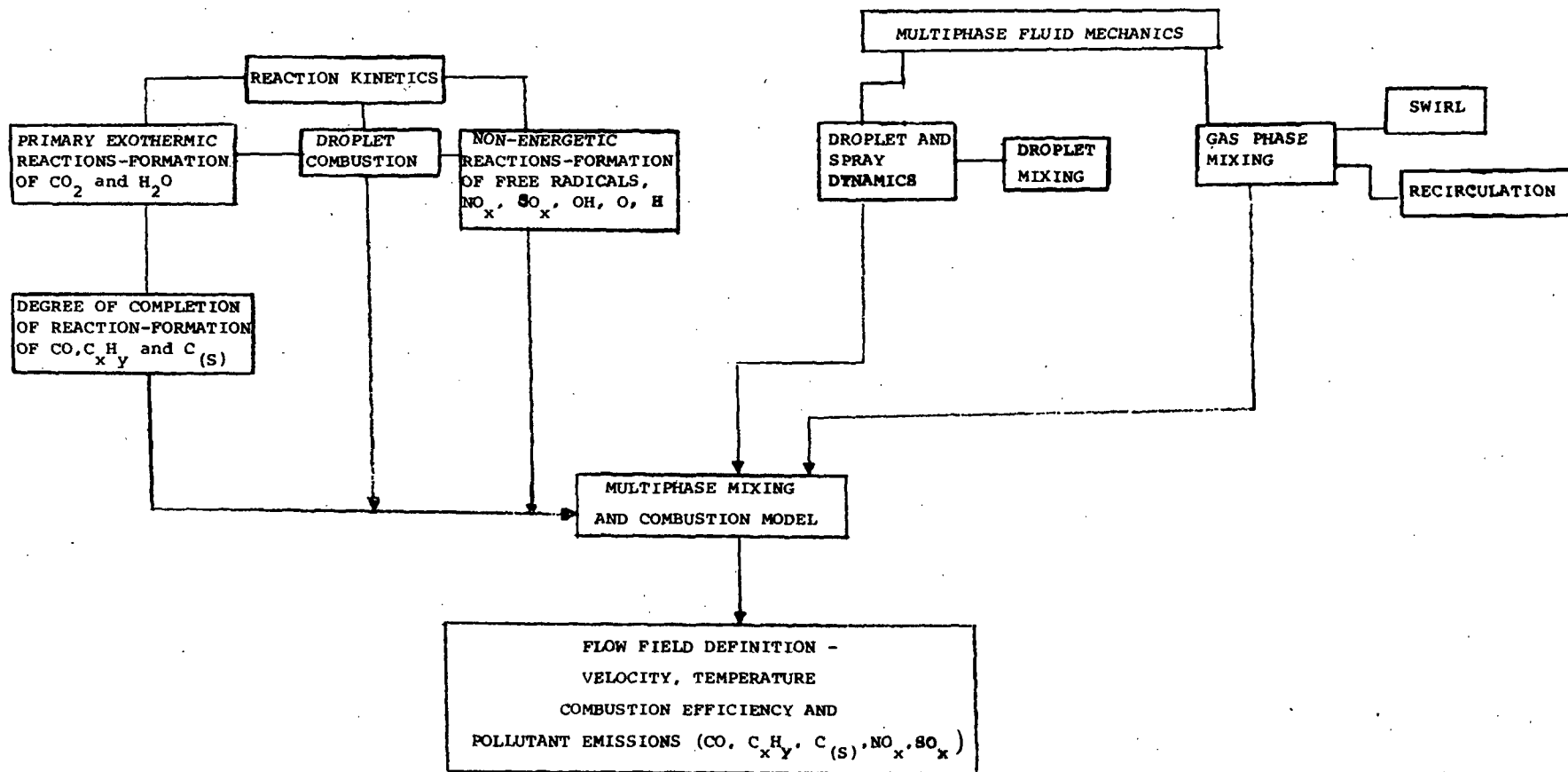
FIGURE 1 GAS TURBINE COMBUSTOR FLOW SCHEMATIC
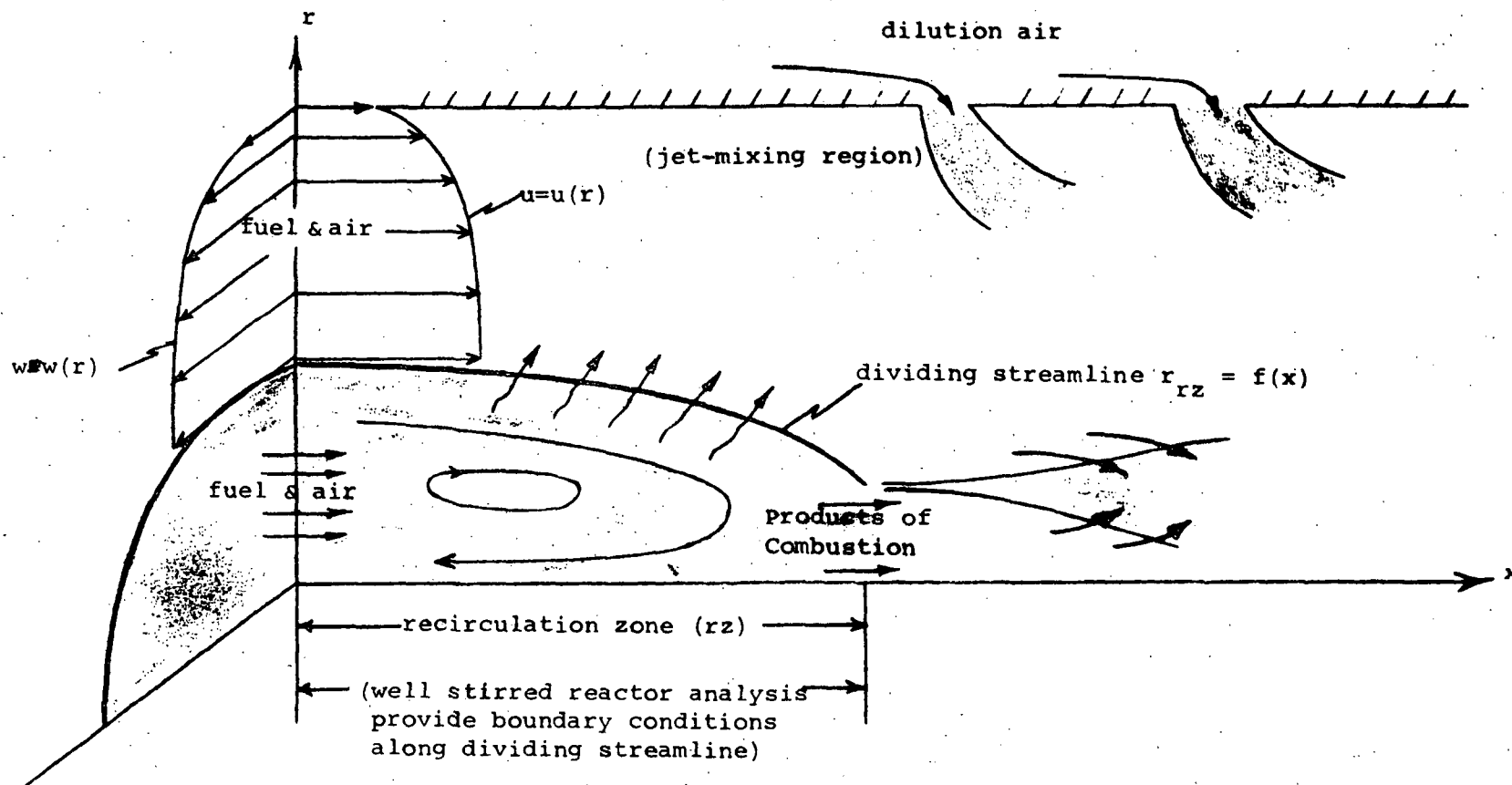
FIGURE 2 - UNIFIED MODEL-MODULAR CONSTRUCTION

FIGURE 3 —   SCHEMATIC OF MODEL COUPLING

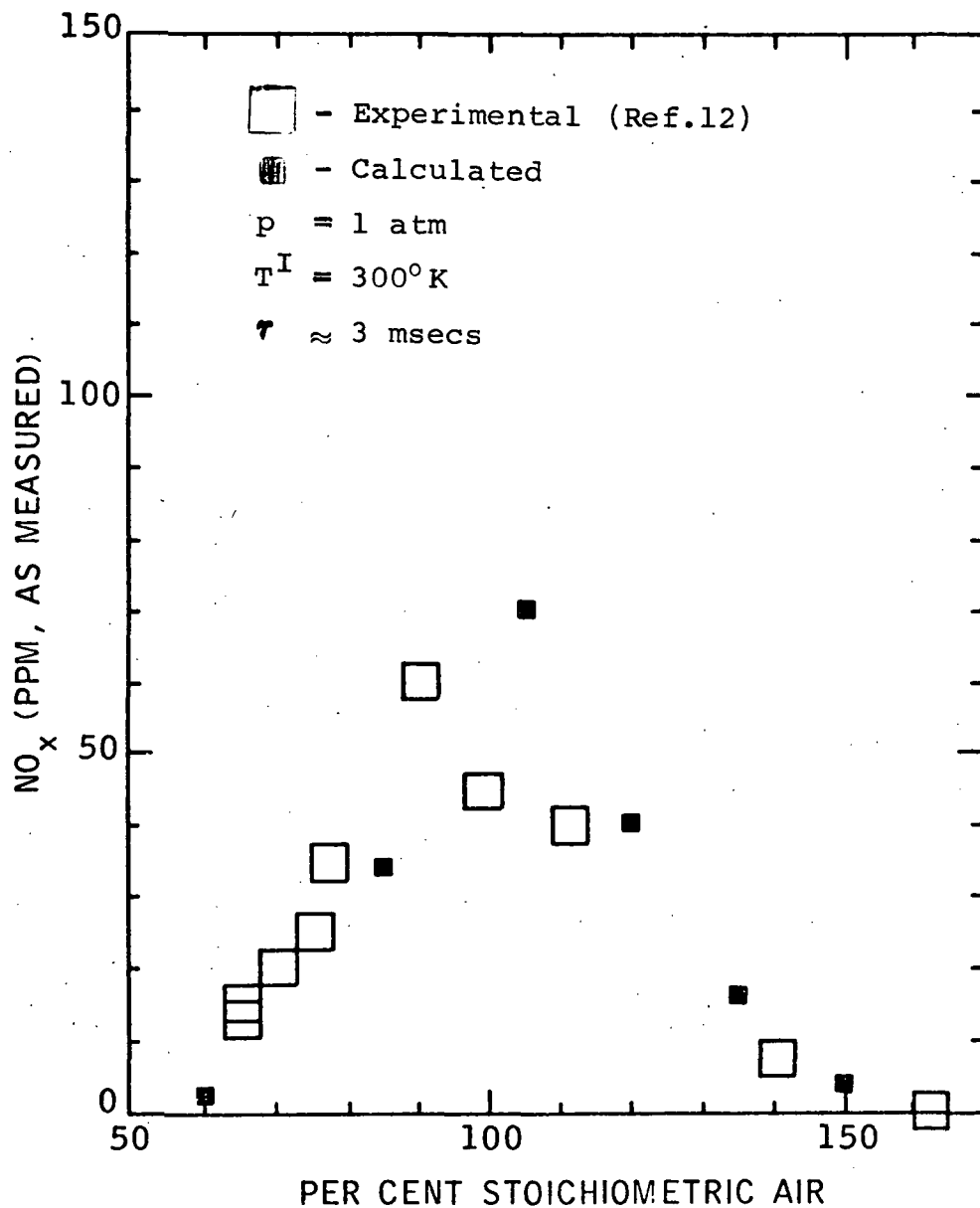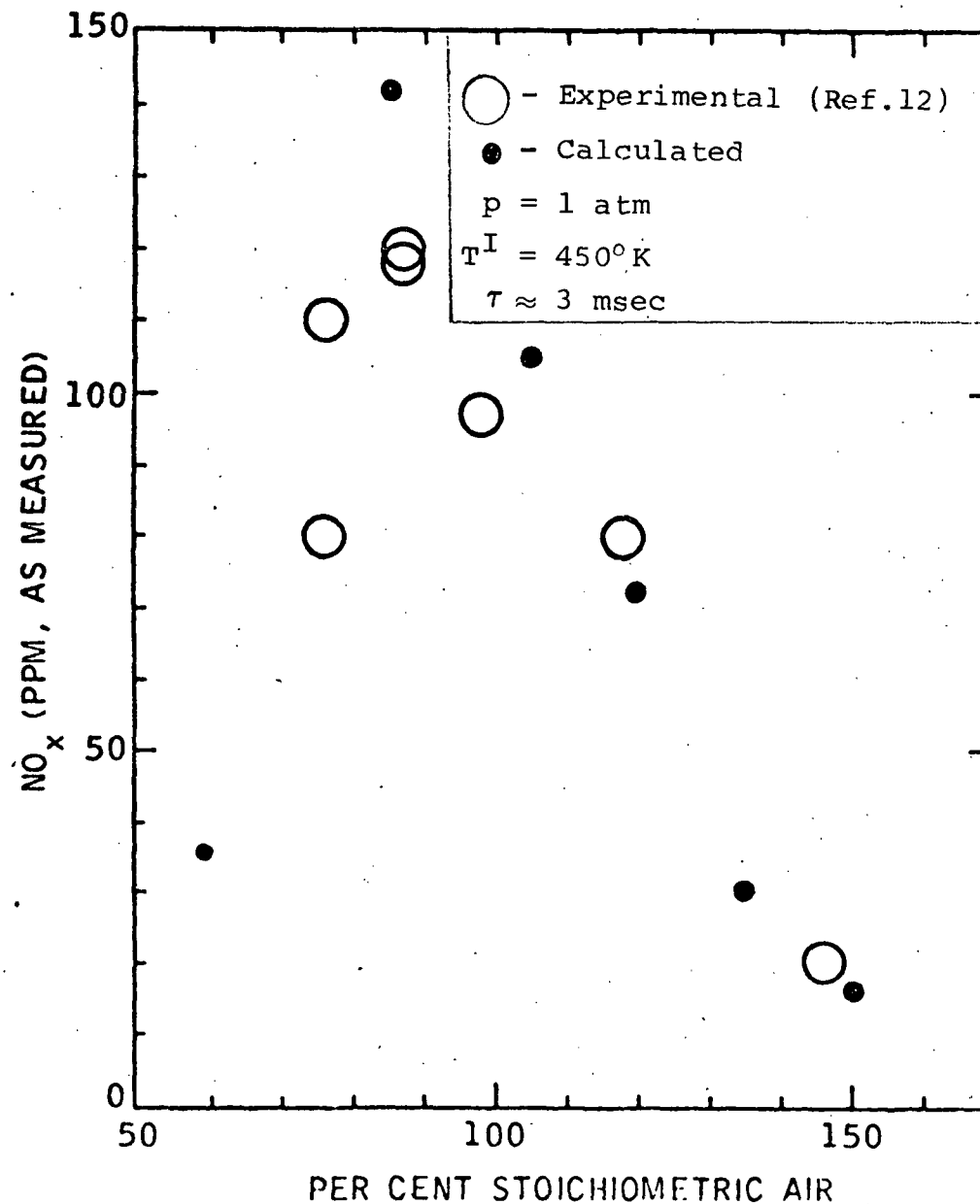FIGURE 4 – COMPARISON OF GASL THEORY WITH NO_x EMISSIONS FROM AN H_2/AIR FIRED JET STIRRED REACTOR

73

FIGURE 5 — COMPARISON OF GASL THEORY WITH NOx EMISSIONS
FROM A CO/AIR FIRED JET STIRRED REACTOR
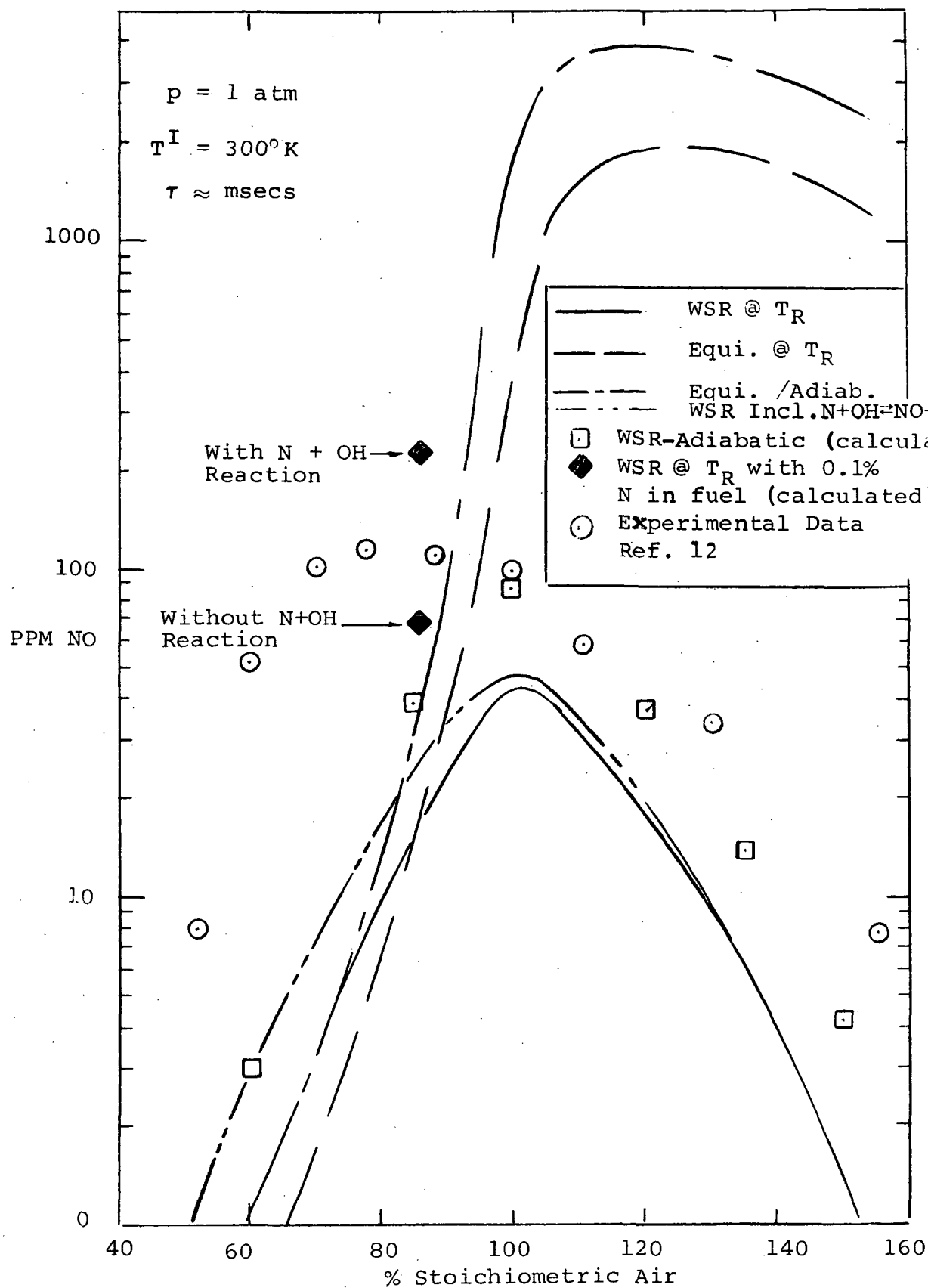WITH H₂ ADDED IN THE AMOUNT OF ½ to 1% (VOLUME) OF CO

FIGURE 6 – COMPARISON OF GASL THEORY WITH NO_x EMISSIONS
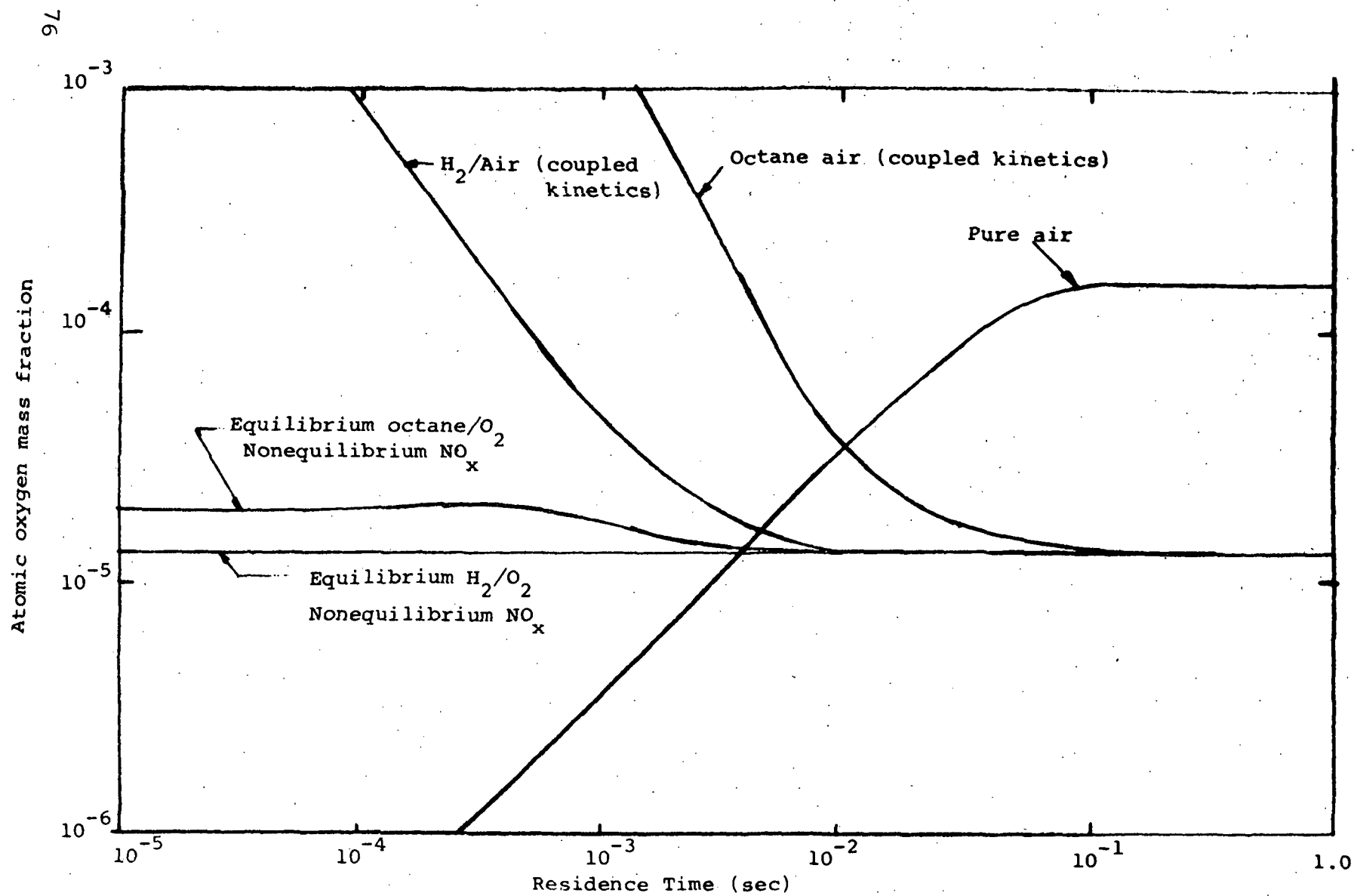FROM A C_3H_8/AIR FIRED JET STIRRED REACTOR
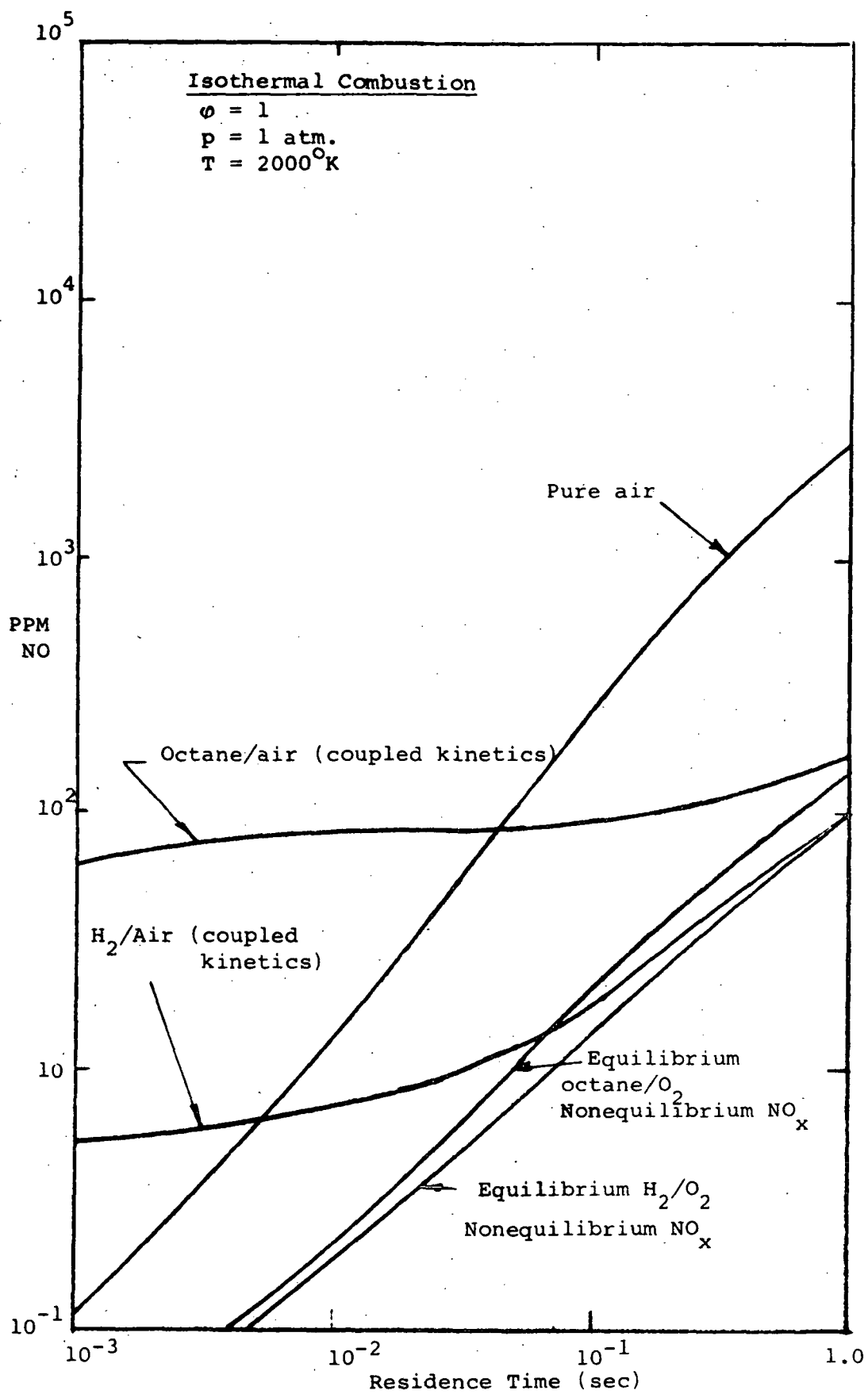
FIGURE 7 - EARLY FORMATION OF O

FIGURE 8 - EARLY FORMATION OF NO

77
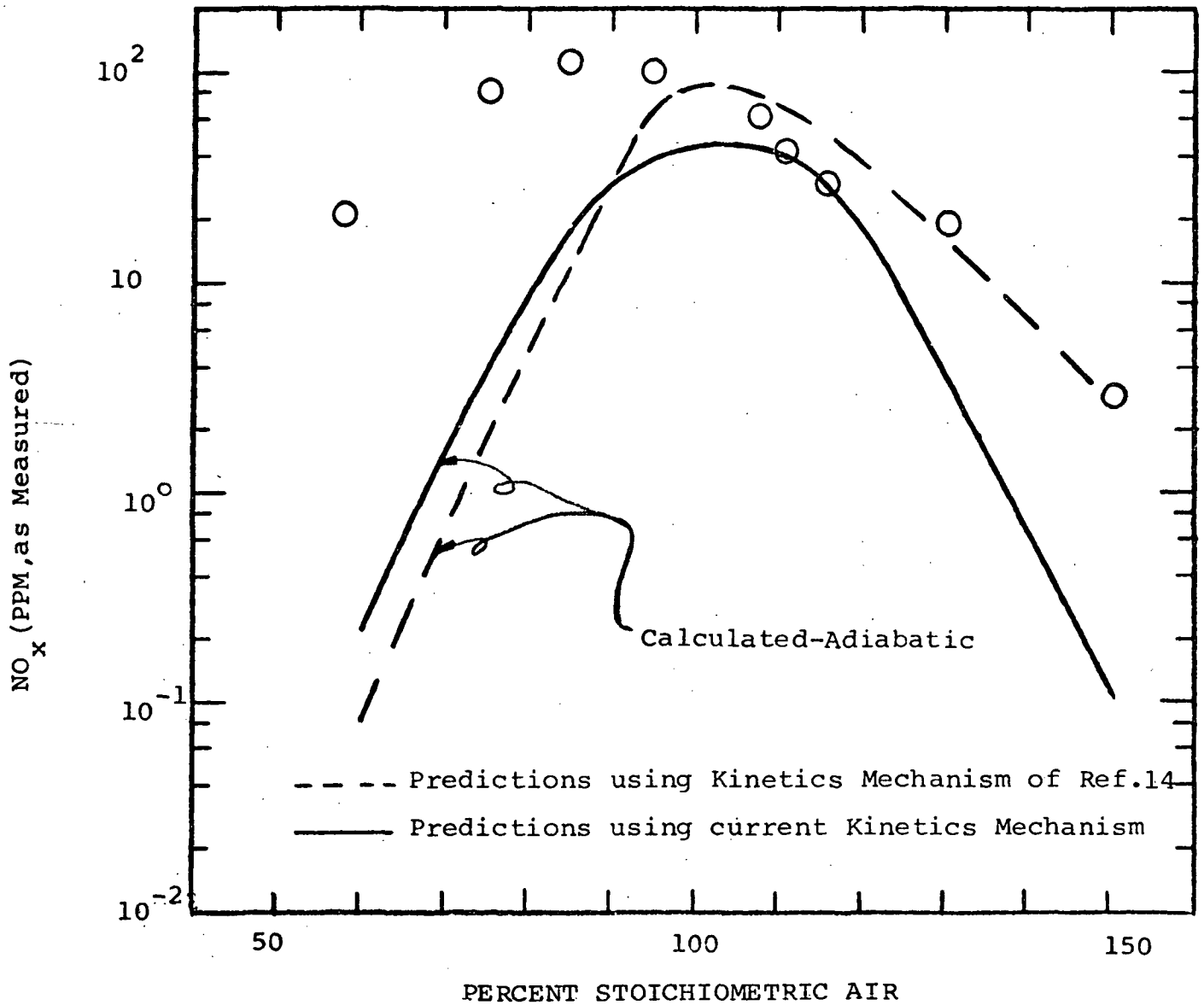
FIGURE 9 — COMPARISON OF GASL THEORY WITH NO$_x$ EMISSIONS FROM A CH$_4$/AIR FIRED JET STIRRED REACTOR
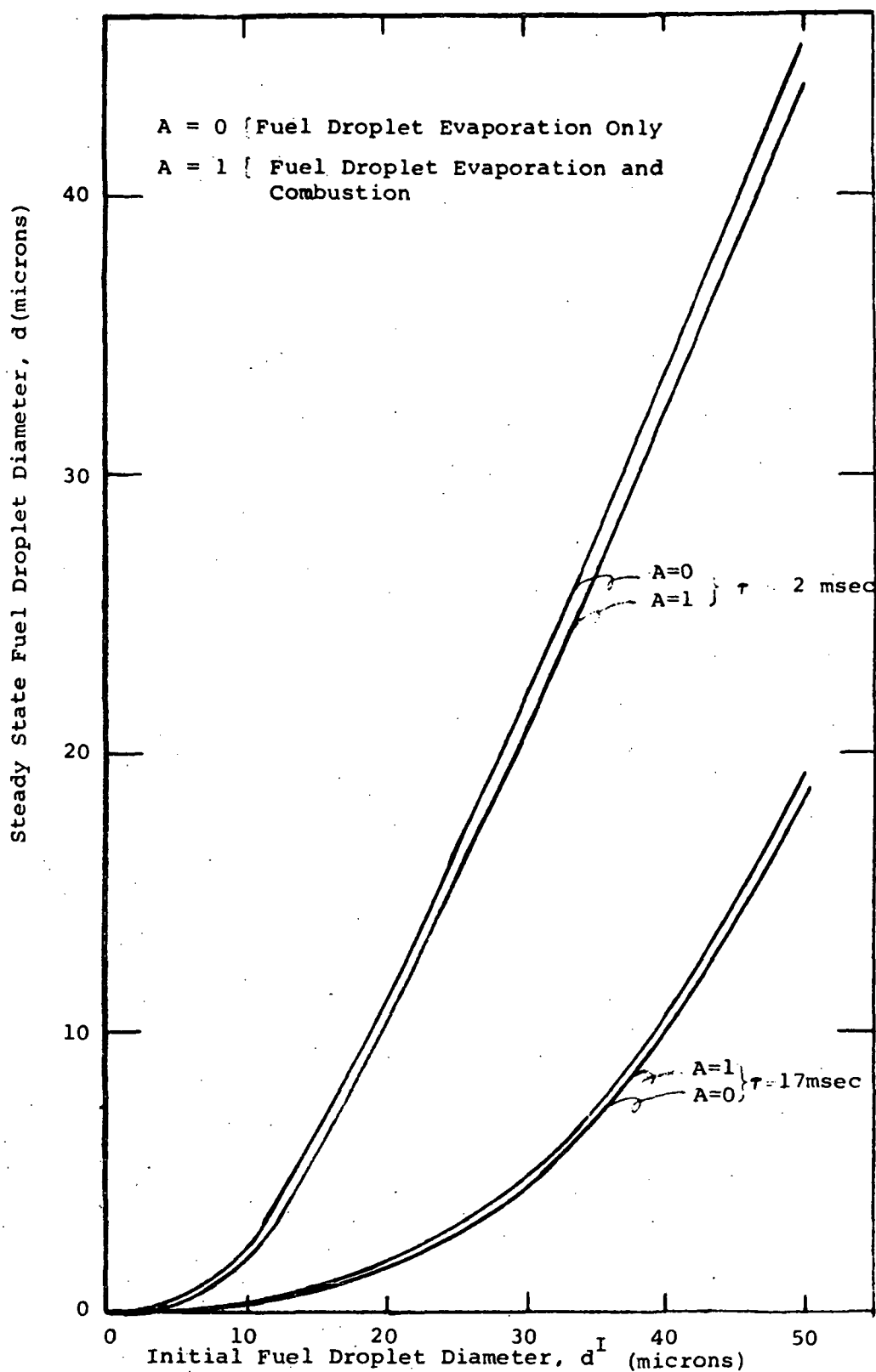
Figure 10 - Effect of residence time upon the fuel droplet
diameter in the recirculation zone as a function
of initial diameter
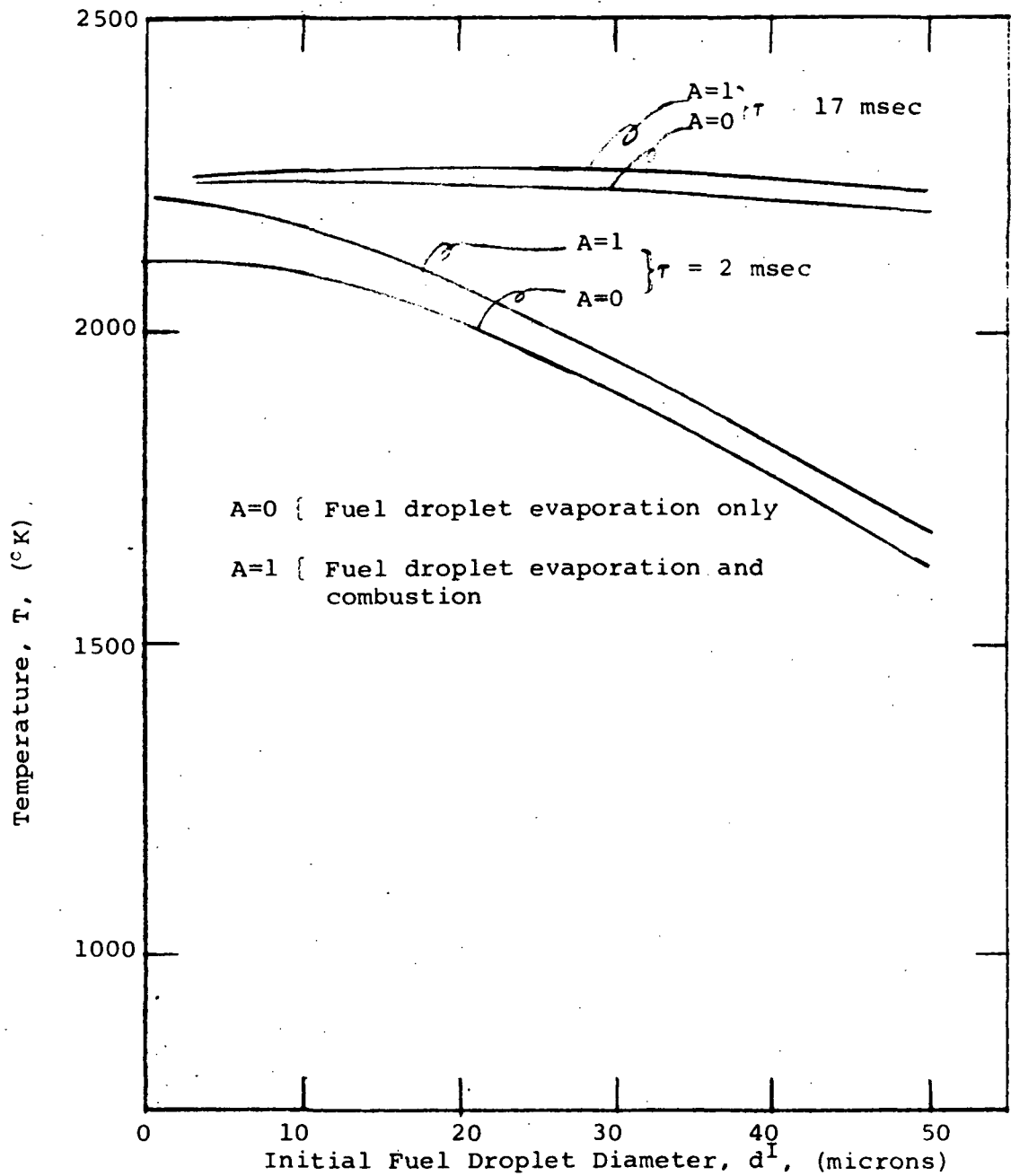
Figure 11 – The effect of residence time upon the recirculation zone temperature as function of initial fuel droplet diameter.
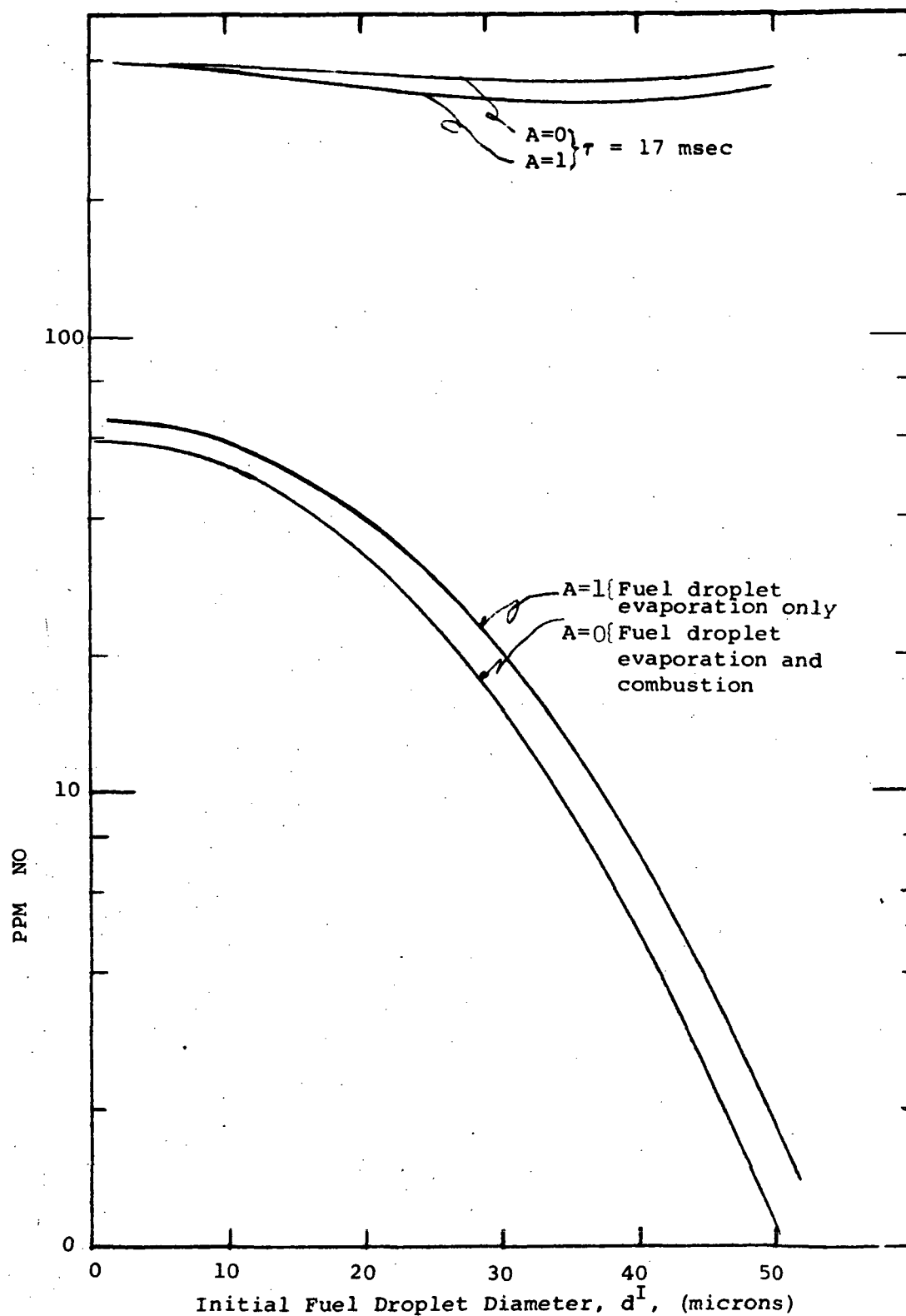
Figure 12 - The effect of residence time upon the recirculation
zone concentration of NO as a function of initial
fuel droplet diameter

FIGURE 13 - COMPARISON, PRESENT THEORY/TURBINE COMBUSTOR DATA - EFFECT OF WATER AND STEAM INJECTION UPON NO_x REDUCTION
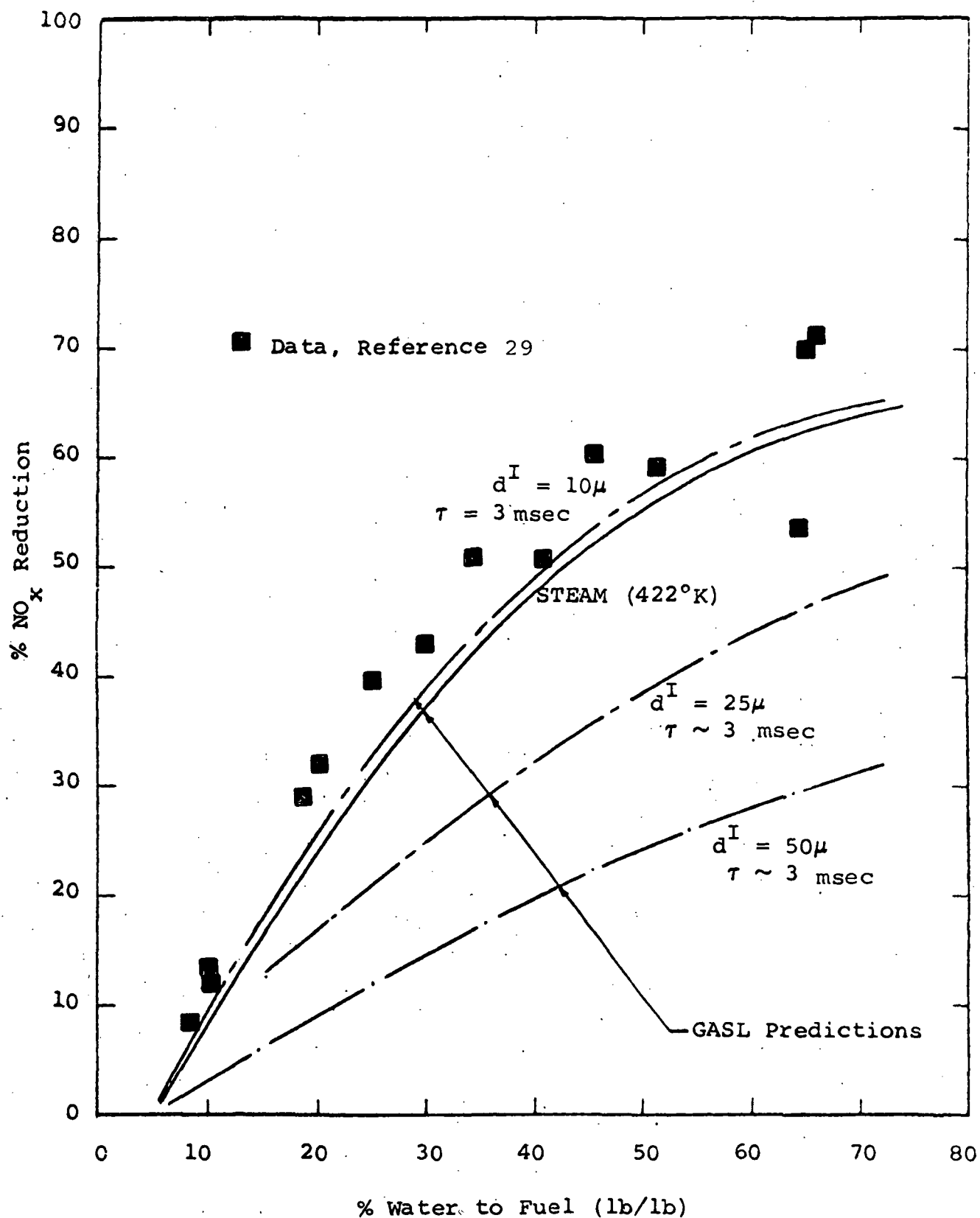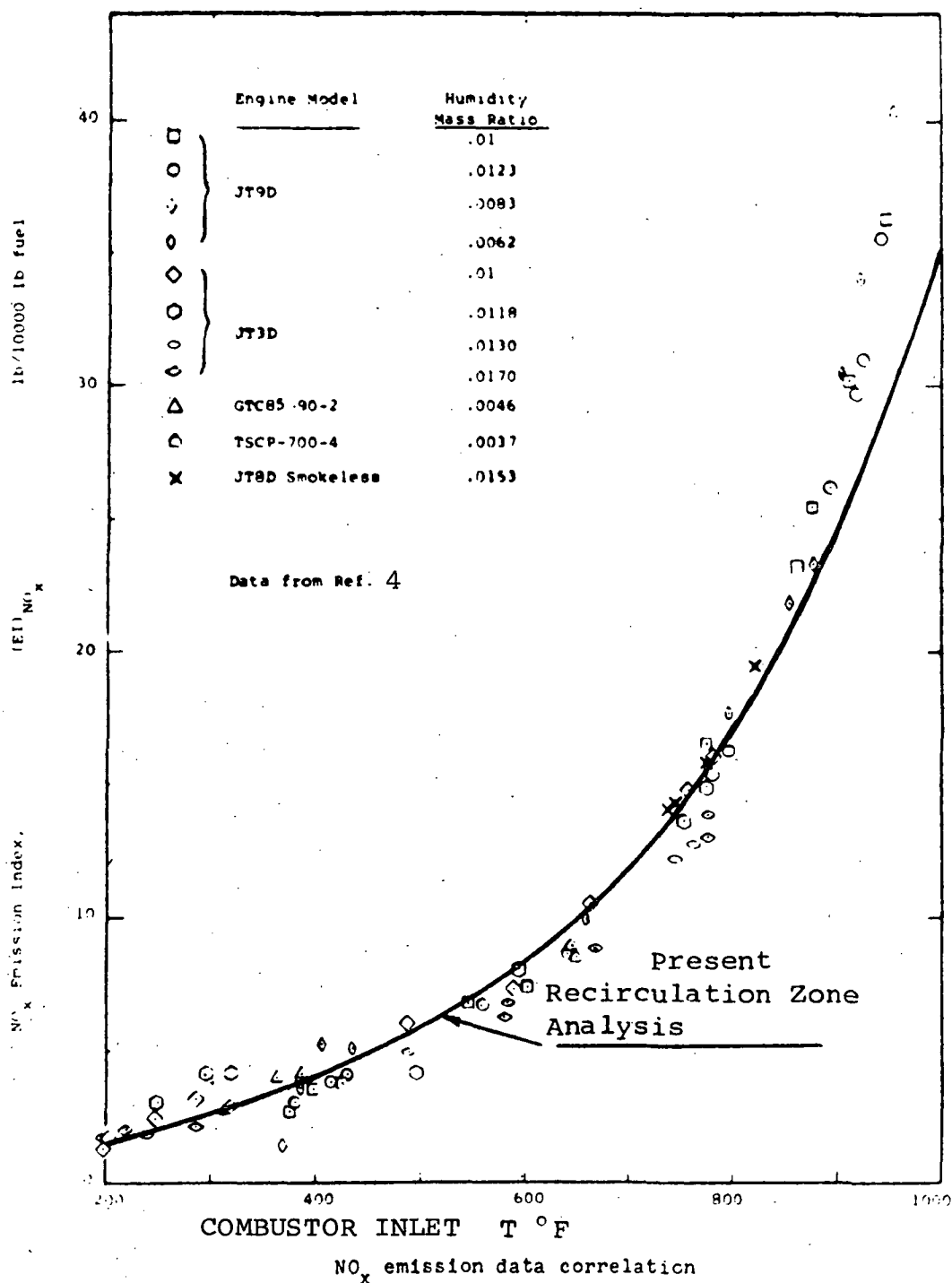
FIGURE 14 - COMPARISON OF THEORY WITH CORRELATION OF REFERENCE 32 FOR TURBOJET ENGINE EMISSIONS DATA
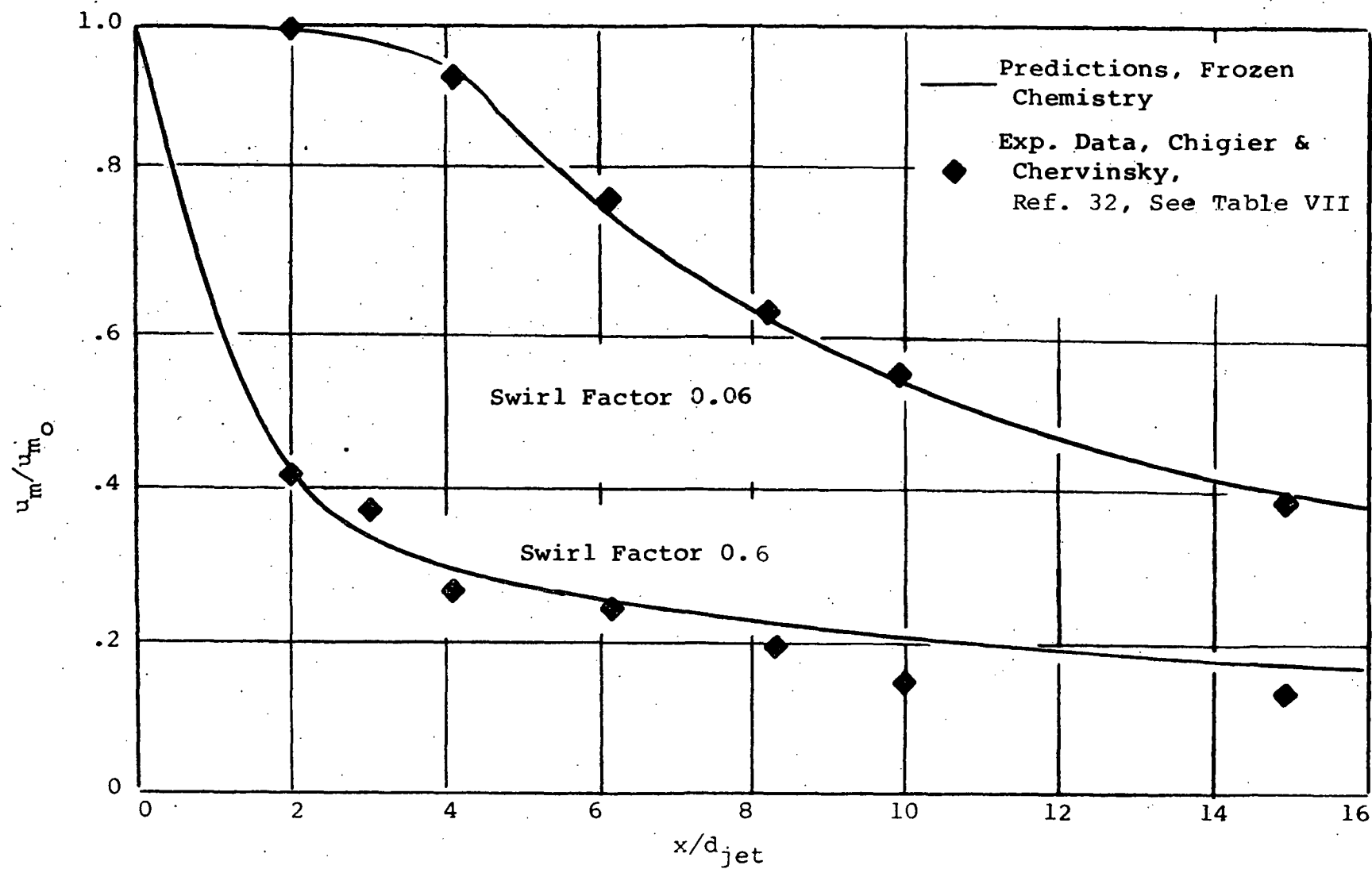
FIGURE 15 - COMPARISON, THEORY/EXPERIMENT, AXIAL VELOCITY DECAY
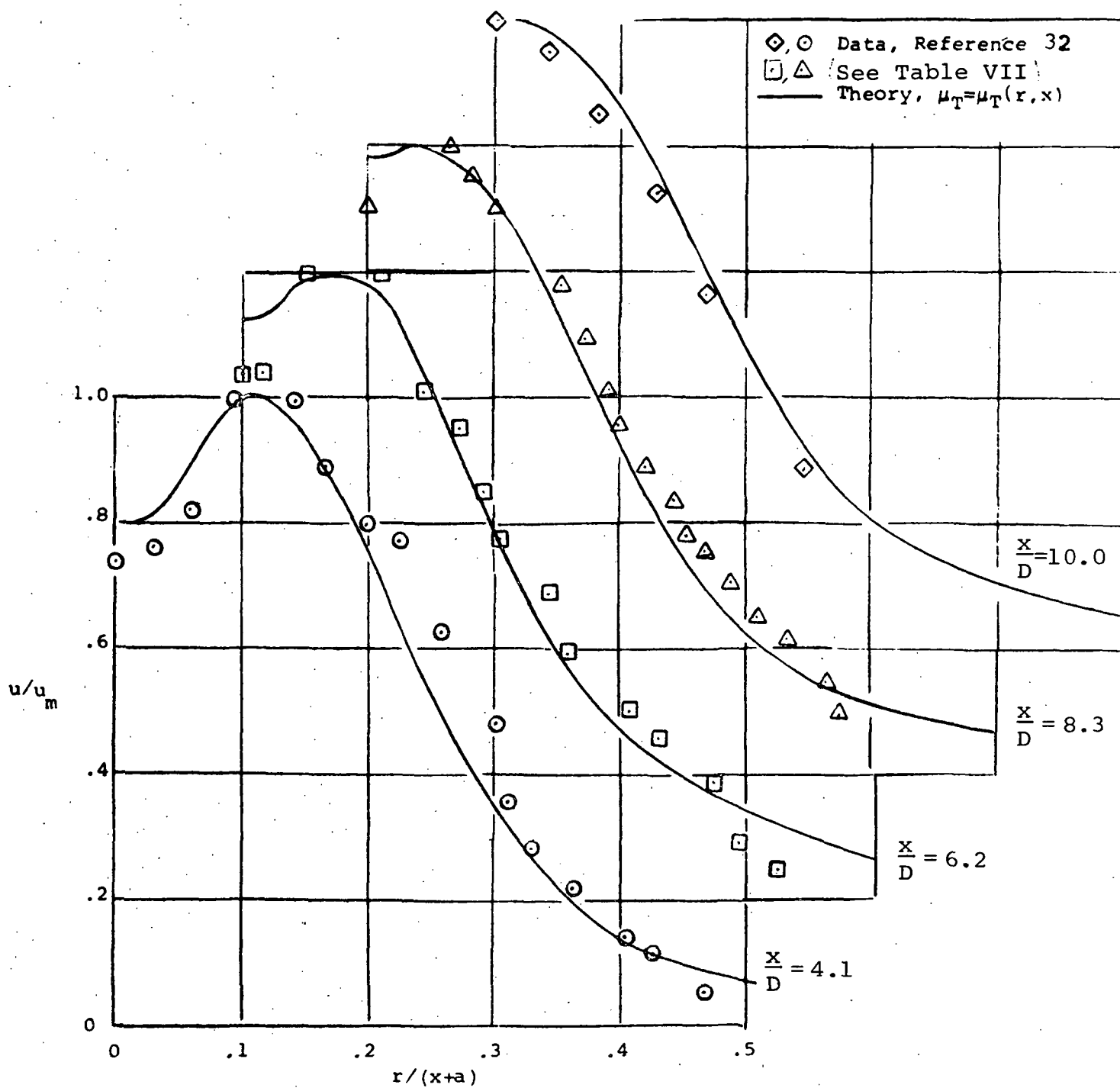
FIGURE 16 - COMPARISON, THEORY/EXPERIMENT, AXIAL VELOCITY

S = 0.6
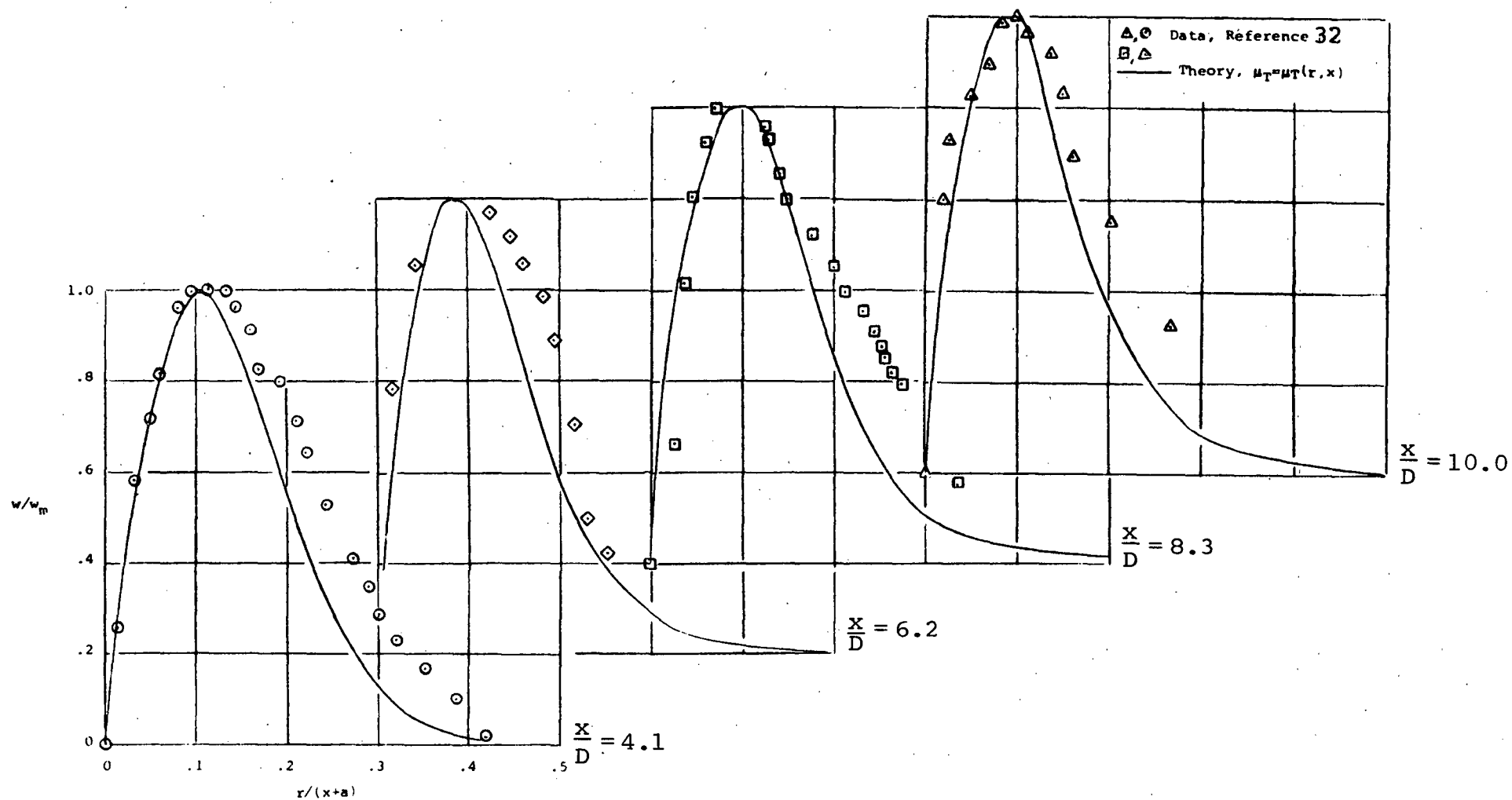
FIGURE 17 — COMPARISON, THEORY/EXPERIMENT, TANGENTIAL VELOCITY

S = 0.6
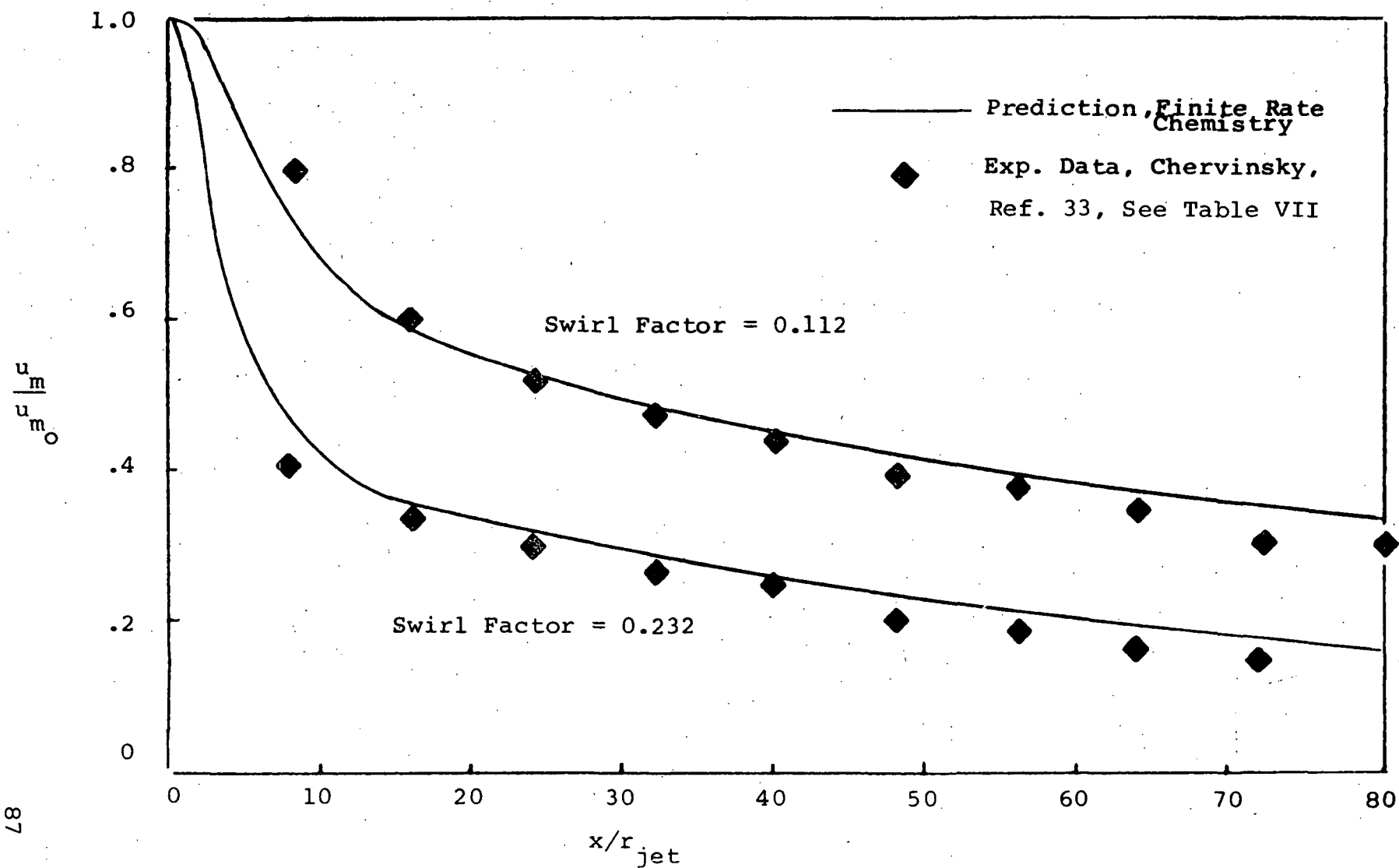
FIGURE 18 - COMPARISON, THEORY/EXPERIMENT, AXIAL VELOCITY DECAY
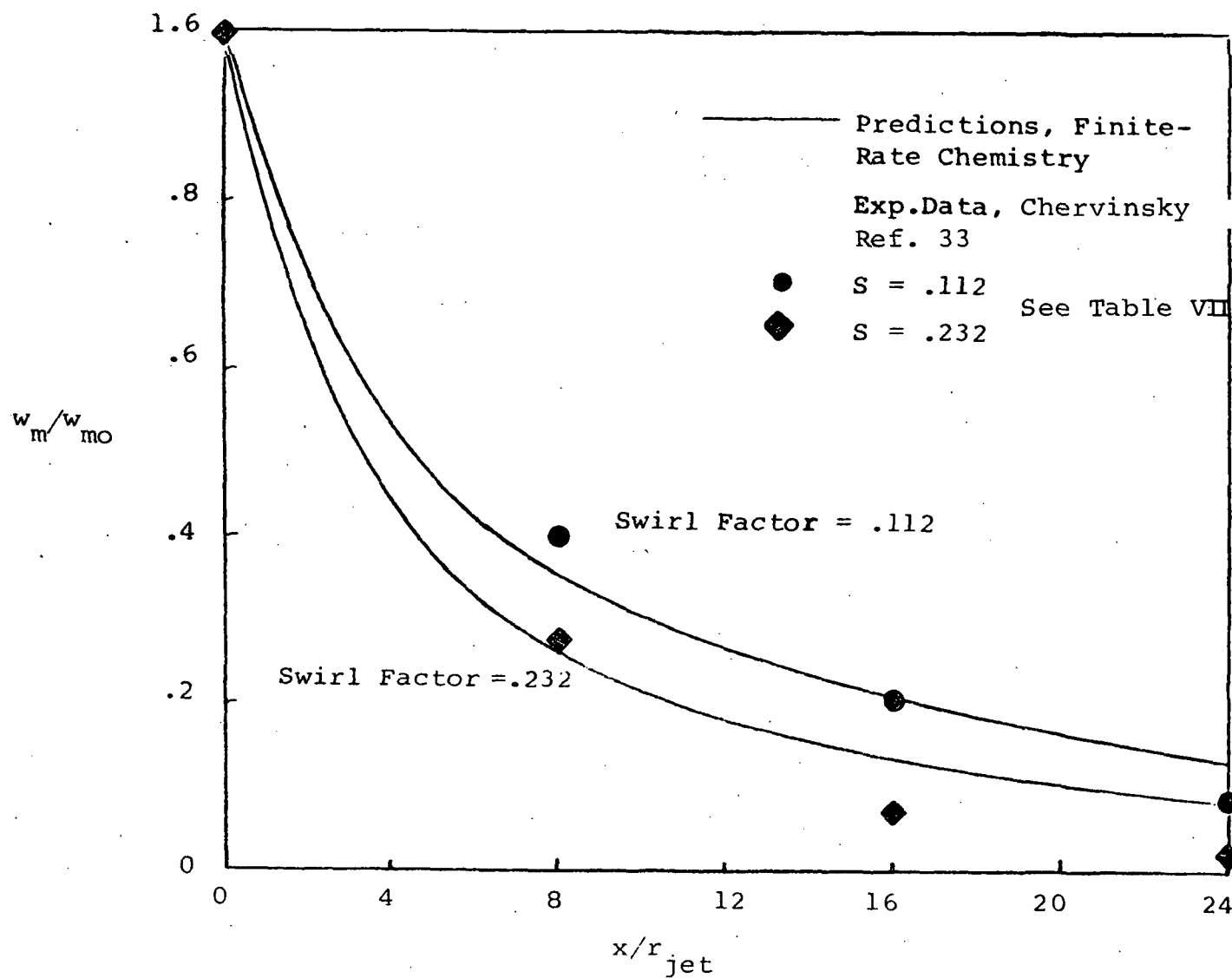
FIGURE 19 -   COMPARISON, THEORY/EXPERIMENT, TANGENTIAL VELOCITY DECAY
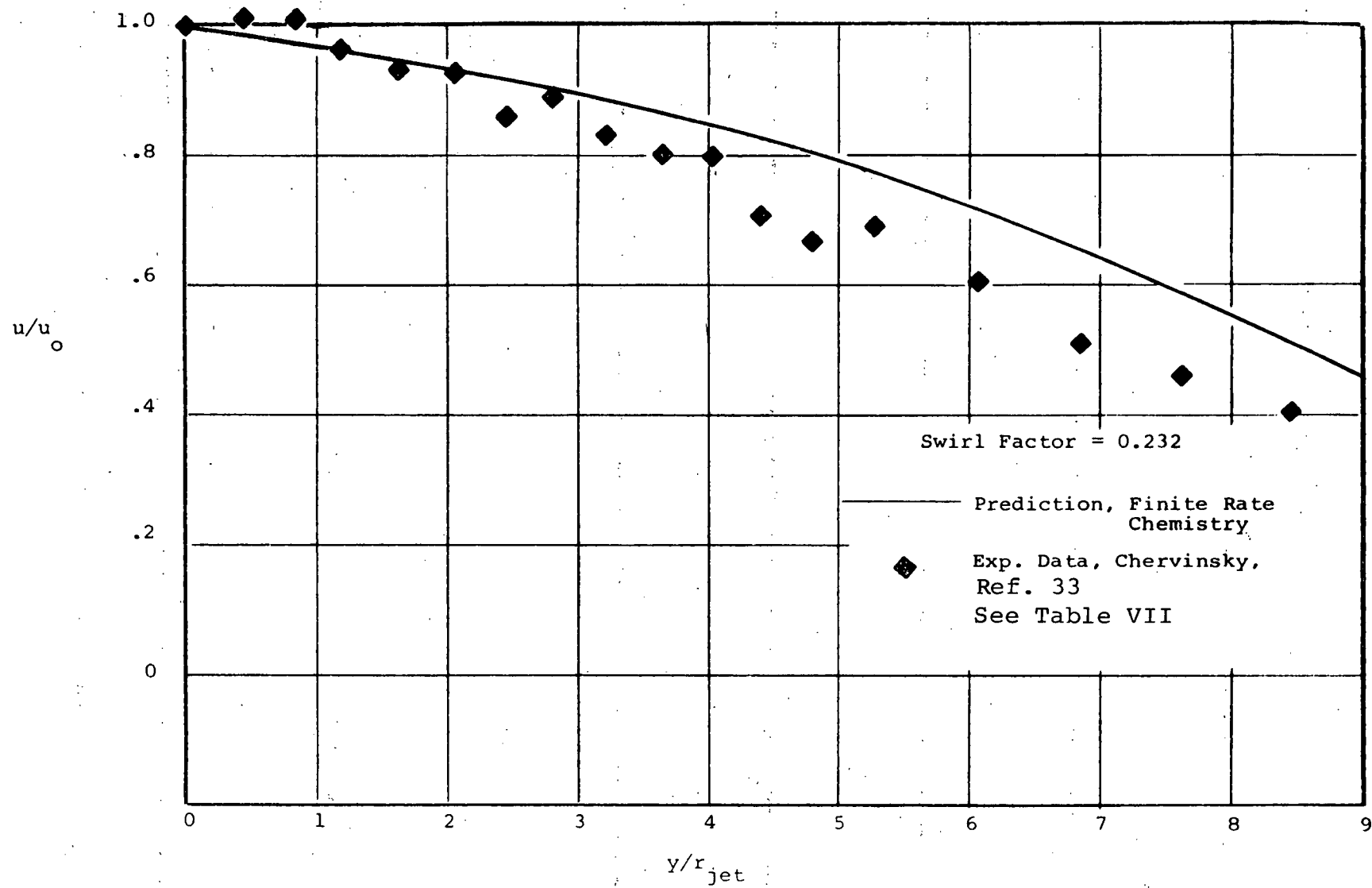
FIGURE 20 - COMPARISON, THEORY/EXPERIMENT, RADIAL VELOCITY PROFILE, x/r_{jet} = 49

Swirl Factor = 0.232

——— Prediction, Finite Rate Chemistry

◆ Exp. Data, Chervinsky, Ref. 33 See Table VII

u/u_o

y/r_{jet}
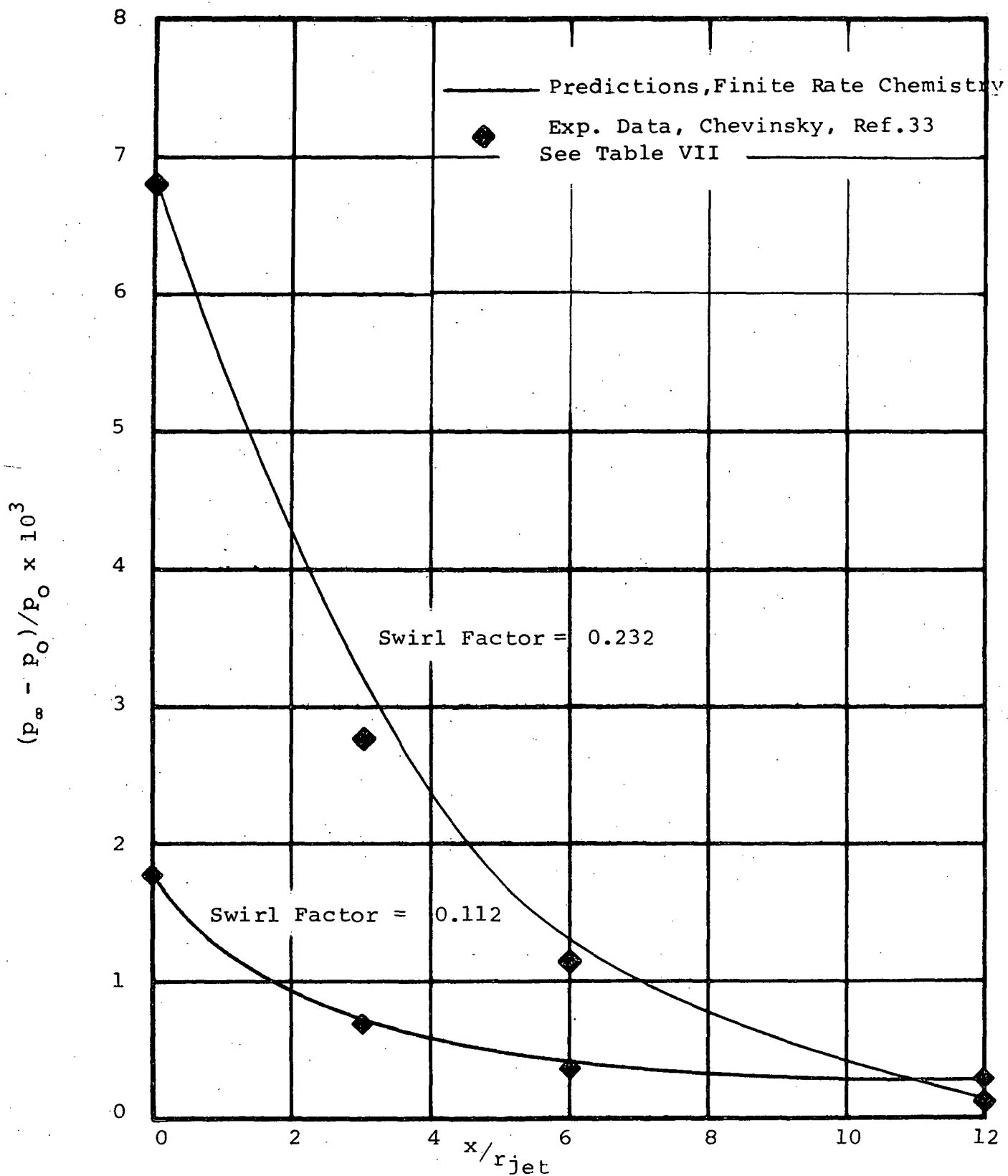
FIGURE 21 - COMPARISON, THEORY/EXPERIMENT, STATIC PRESSURE DECAY

90
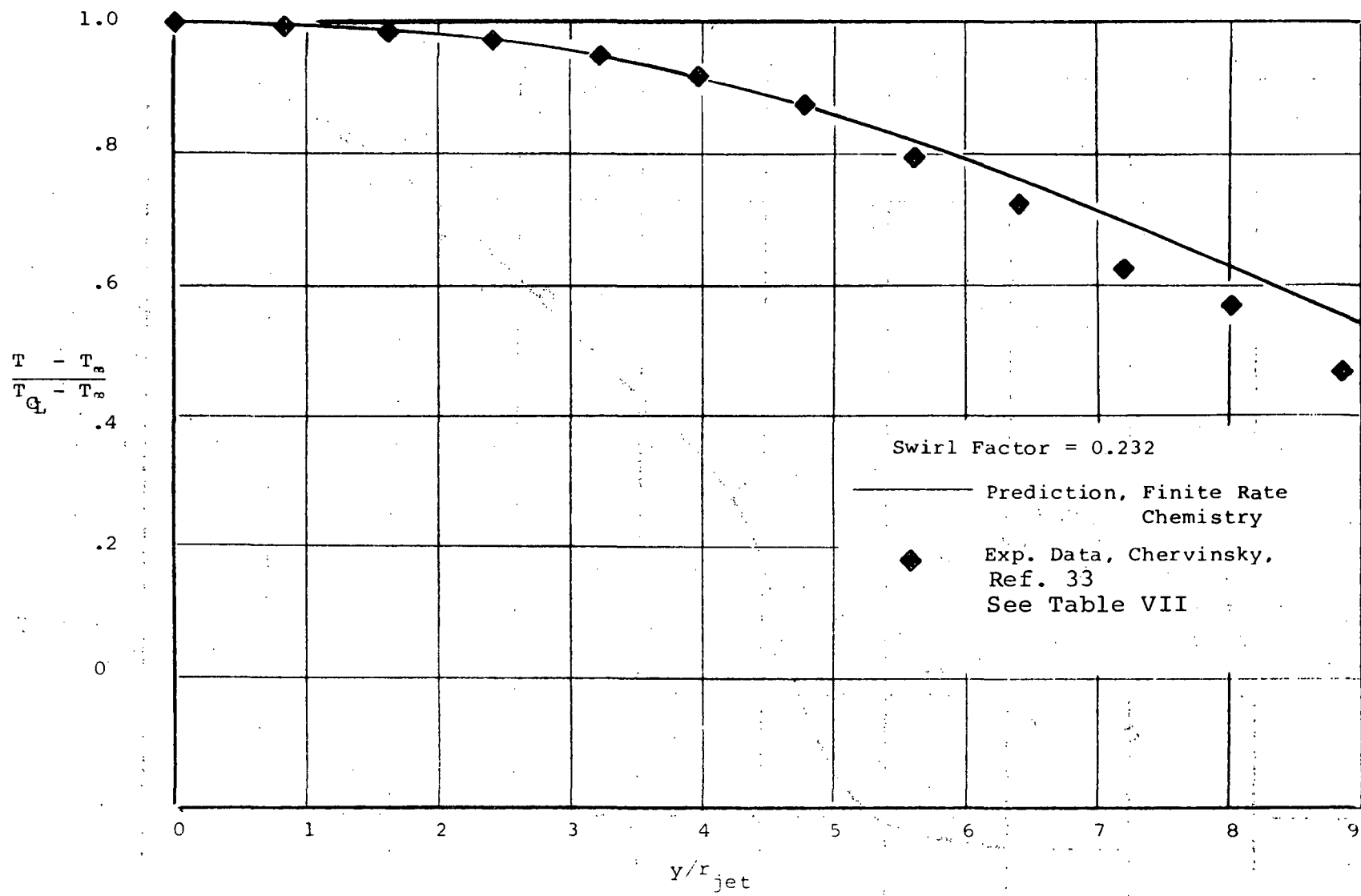
FIGURE 22 - COMPARISON, THEORY/EXPERIMENT, RADIAL TEMPERATURE PROFILE, $x/r_{jet} = 49$
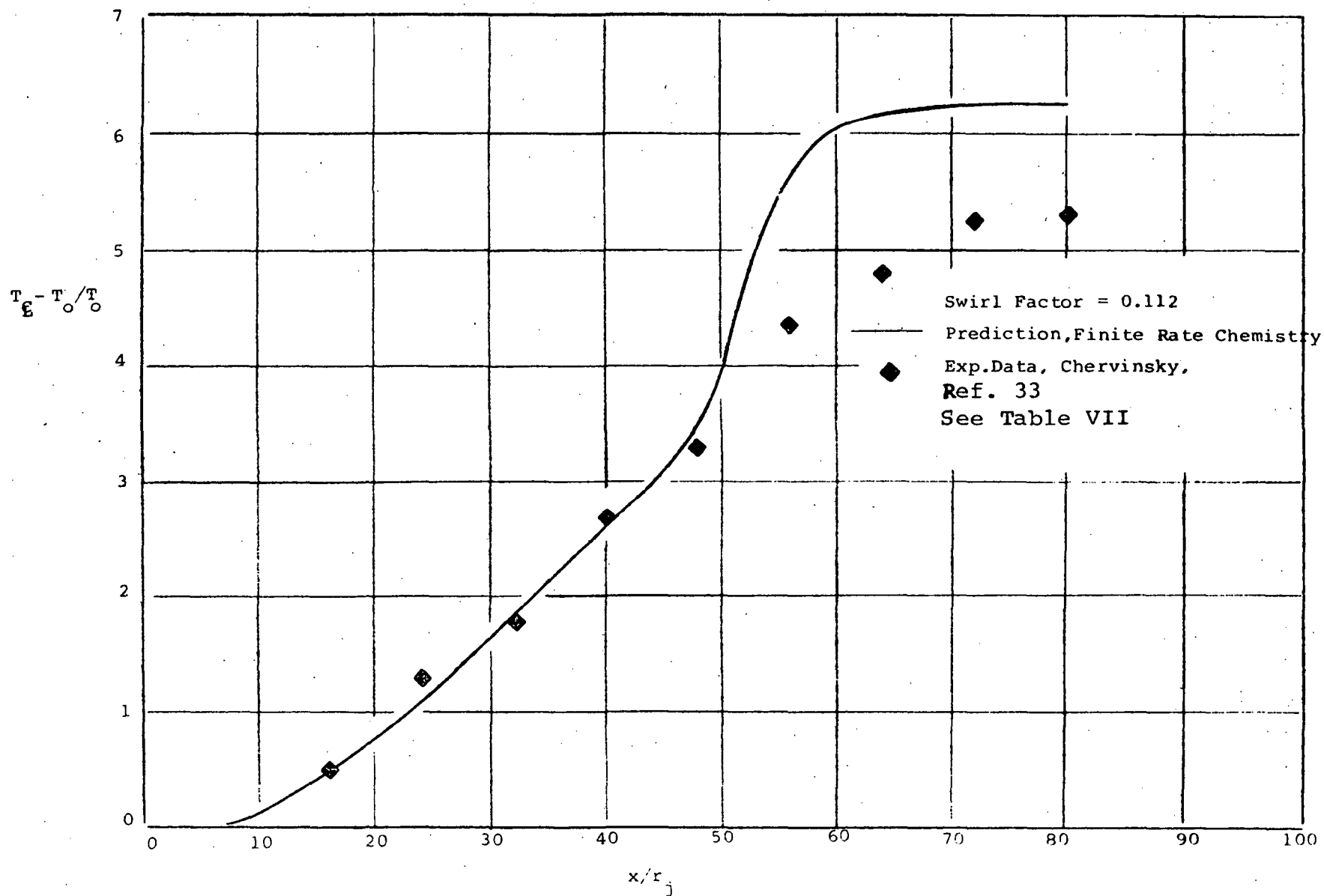
FIGURE 23 - COMPARISON, THEORY/EXPERIMENT, AXIAL TEMPERATURE VARIATION
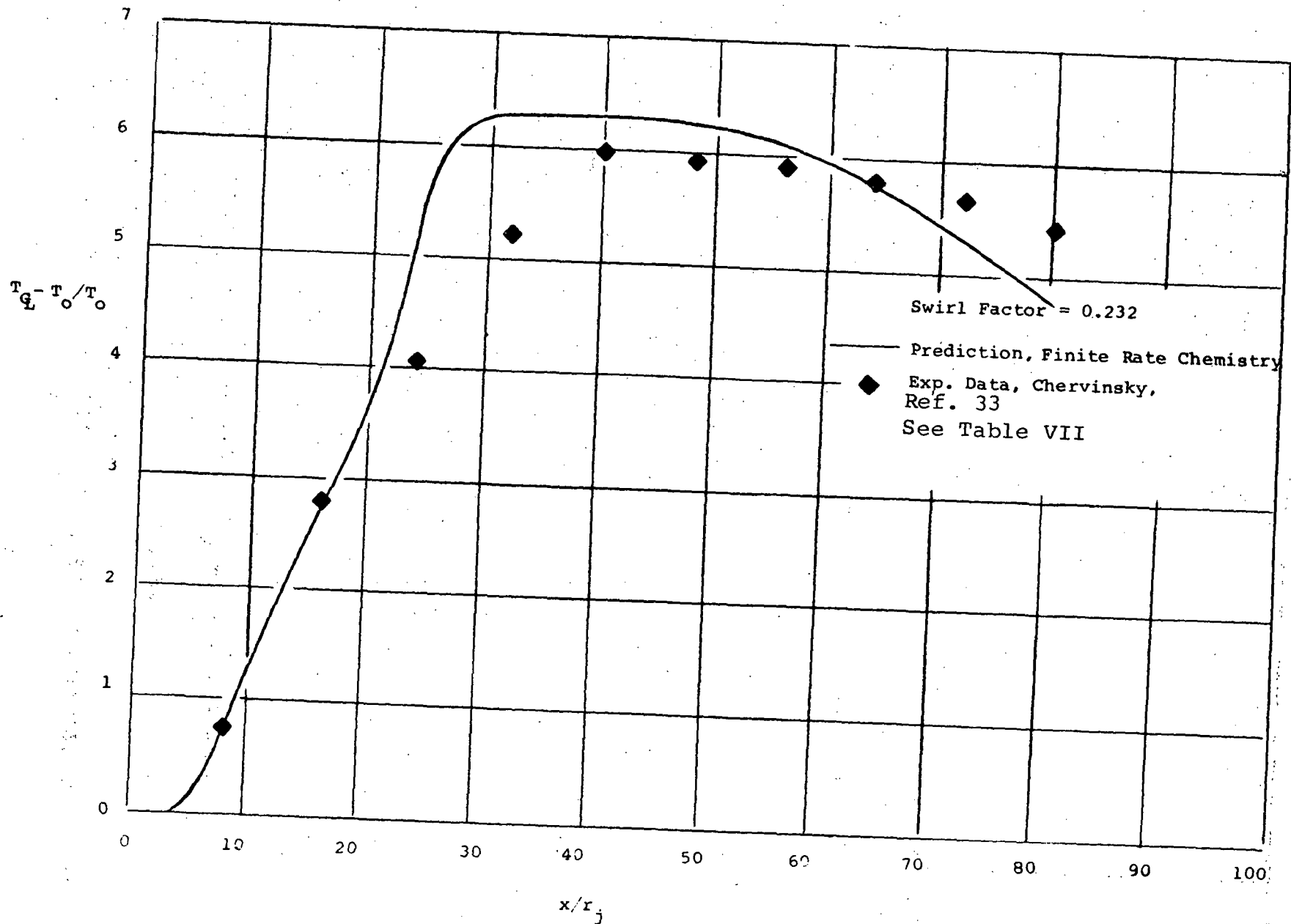
FIGURE 24 — COMPARISON, THEORY/EXPERIMENT, AXIAL TEMPERATURE VARIATION
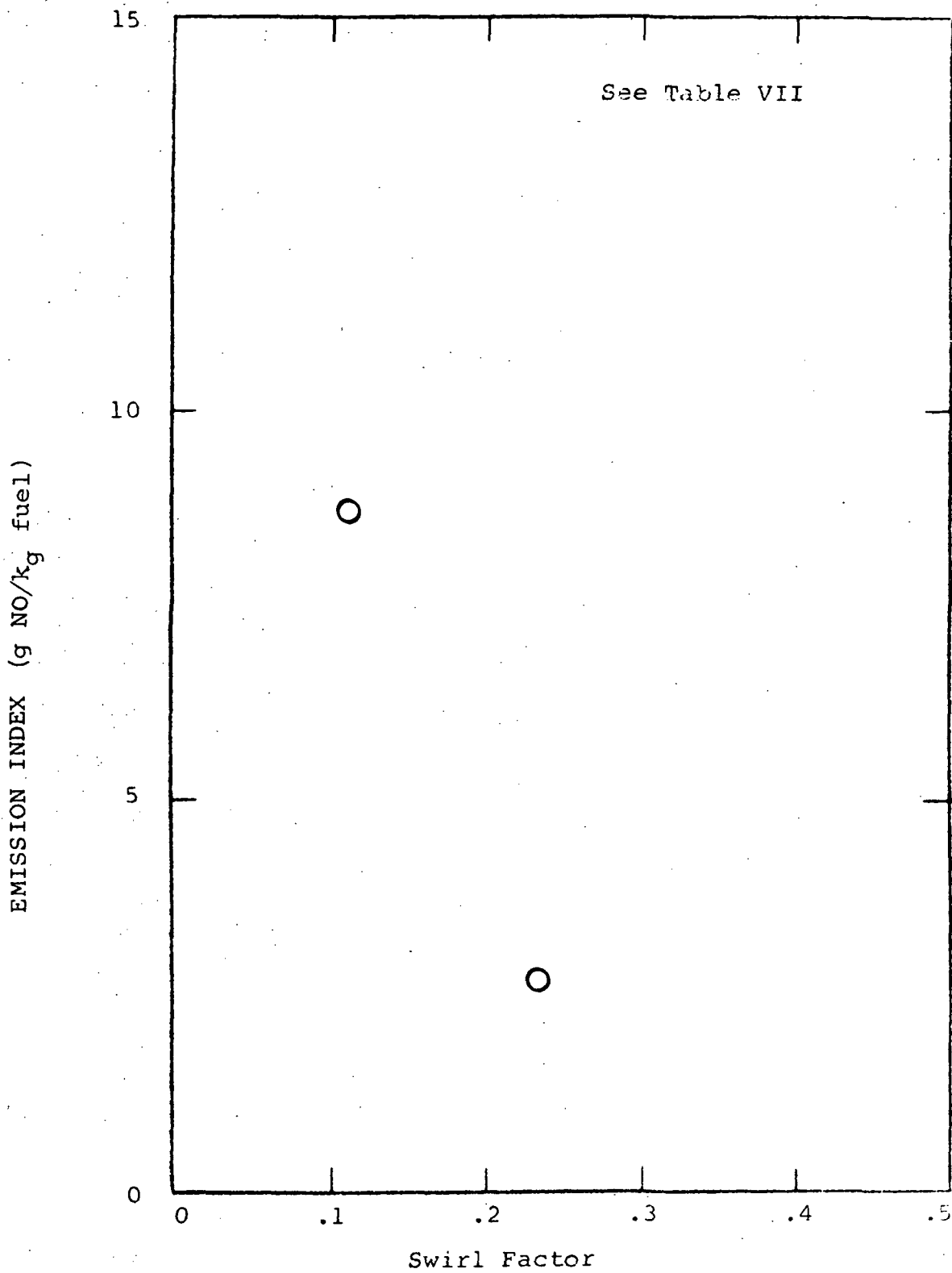
FIGURE 25 - VARIATION OF NITRIC OXIDE EMISSION INDEX WITH SWIRL FACTOR

94
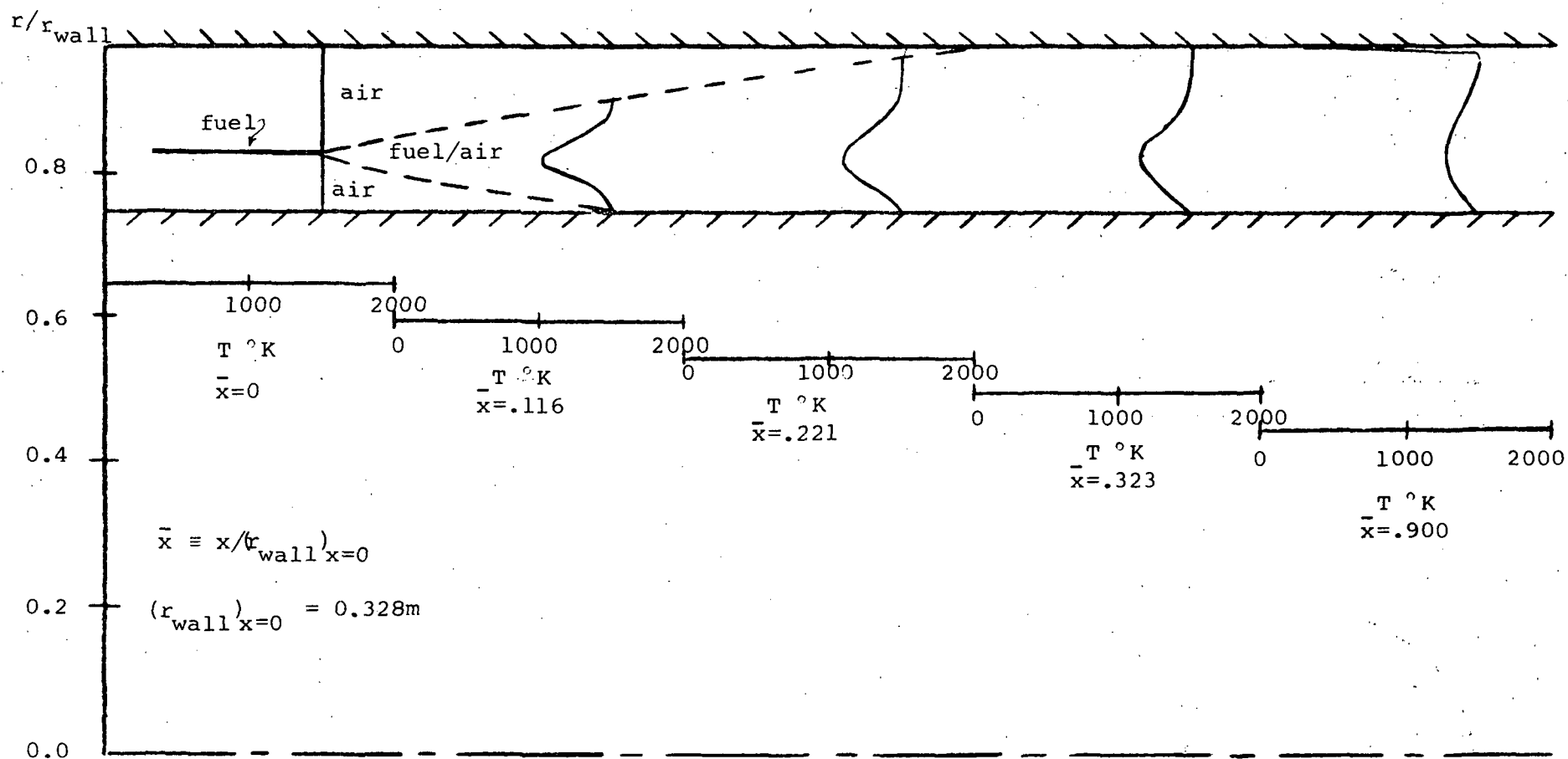
FIGURE 26 — TEMPERATURE PROFILE DEVELOPMENT WITHIN ANNULUS, CASE 1 P = CONST. = 10 ATMOSPHERES
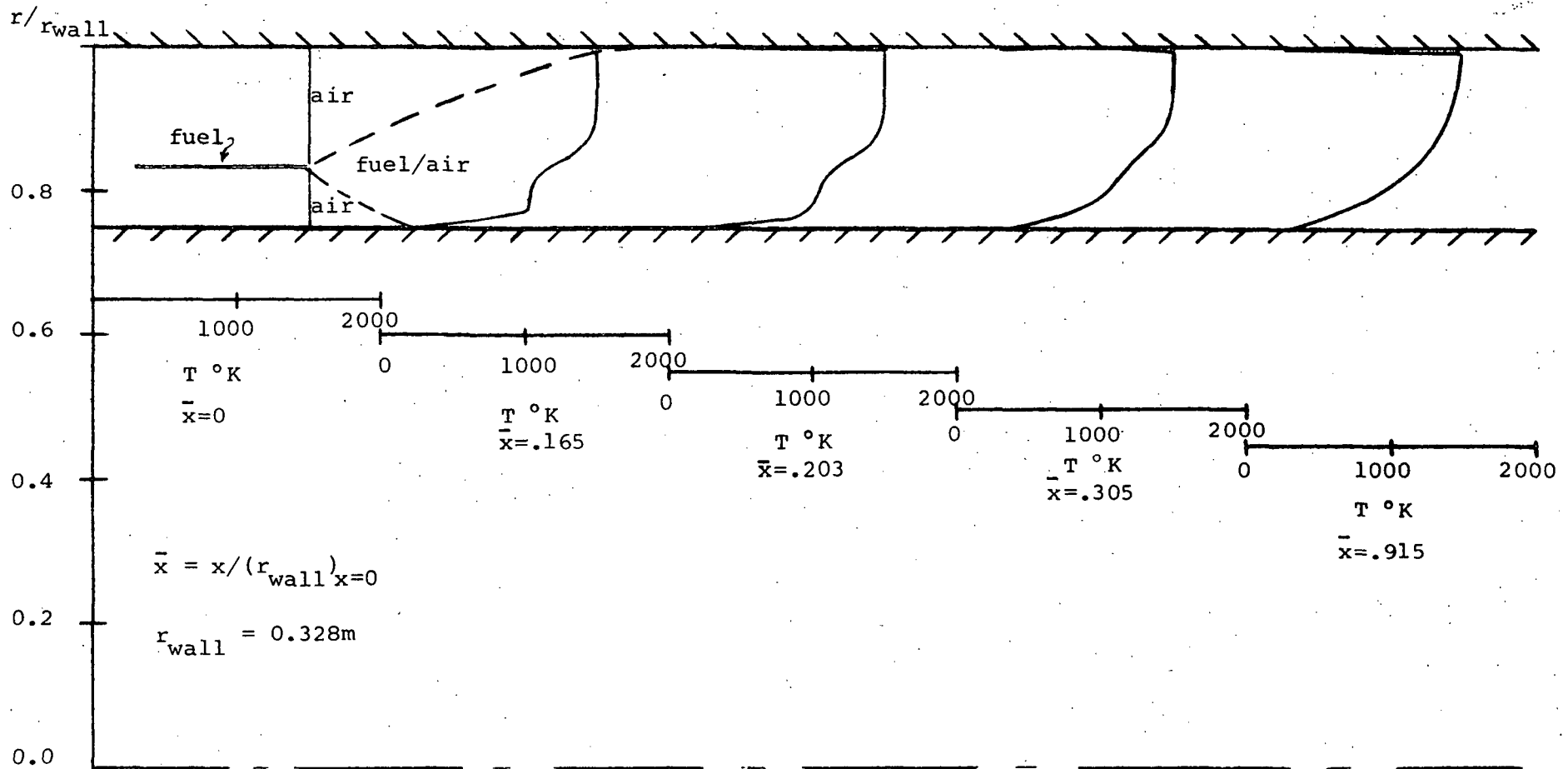
FIGURE 27- TEMPERATURE PROFILE DEVELOPMENT WITHIN ANNULUS, CASE 2, r_{wall} = CONSTANT = 0.328m

1. NASA-Lewis Research Center
   21000 Brookpark Road
   Cleveland, OH 44135
   Attn: Report Control Office   MS 5-5   1
           Technology Utilization   3-19   1
           Library   60-3   2
           L. Schopen   500-206   1
           Fluid Systems Components Div.   5-3   1
           W. L. Stewart   501-5   1
           Seymour Lieblein   501-5   1
           Bernard Lubarsky   3-3   1
           Lt. Col. G. S. Weden   500-317   1
           N. T. Musial   500-311
           J. B. Esgar   60-4   1
           W. T. Olson   3-16   1
           R. A. Rudey   60-6   1
           J. F. Dugan, Jr.   86-1   1
           R. E. Jones   60-6   1
           J. Grobman   60-6   1
           C. J. Marek   60-4   1
           R. Brokaw   301-1   1
           D. N. Anderson   60-4   11

2. NASA Scientific and Technical Information Facility
   P. O. Box 33
   College Park, Maryland 20740
   Attn: Acquisitions Branch   10
           RQT-2448

3. NASA Headquarters
   600 Independence Ave., S.W.
   Washington, D. C. 20546
   Attn: N. F. Rekos (RLC)   1
          W. H. Roudebush (RLN)   1

4. NASA-Langley Research Center
   Langley Station
   Technical Library   1
   Hampton, Virginia 23365
   Attn: M. R Nichols   1
          J. V. Becker   1
          R. J. Margajon   1

5. Environmental Protection Agency
   Office Air and Water Programs
   Advanced Automotive Power
      Systems Development Division
   2929 Plymouth Road
   Ann Arbor, Michigan 48105
   Attn: Mr. William Mirsky   1

6. Environmental Protection Agency
   Control Systems Division
   Research Triangle Park, N. C. 28811
   Attn: Mr. Paul Wieber   1

7. Environmental Protection Agency
   Mobile Source Air Pollution
   Room 639
   West Tower
   Washington, D. C. 20460
   Attn: Mr. George Kittredge   1

8. Naval Air Propulsion Test Center
   Building 600
   Philadelphia Naval Base
   Philadelphia, P. A. 19112
   Attn: Mr. L Magitti   1

9. Aerospace Research Laboratory
   Wright Patterson AFB, Ohio 45433
   Attn: Dr. R. G. Dunn   1

10. Aero-Propulsion Laboratory
    Wright Patterson AFB, Ohio 45433
    Attn: Mr. Robert E. Henderson   1

11. Air Force Office of Scientific Research
    1400 Wilson Boulevard
    Arlington, Virginia 22209
    Attn: SREP   1

12. Department of the Army
    U. S. Army Aviation Material Laboratory
    Propulsion Division (SAUFE-PP)
    Fort Eustis, Virginia 23604
    Attn: J. White   1
          E. T. Johnson   1

13. U. S. Army
    St. Louis, MO 63166
    Attn: L. E. Bell - AVSCOM
          AMSAV-EFP   1

14. Department of the Navy
    Bureau of Naval Weapons
    Washington, D. C. 20025
    Attn: Robert Brown   1

15. Department of the Navy
    Bureau of Ships
    Washington, D. C. 20360   1

16. Defense Documentation Center
    Cameron Station
    5010 Duke Street
    Alexandria, Virginia 22314   1

17. FAA Headquarters
    800 Independence Ave., S. W
    Washington, D. C. 20533
    Attn: William Westfield   1
            Library   1

18. Williams Research Corp.
    2280 W. Maple Road
    Walled Lake, Michigan 48088
    Attn: Arnold Plumley   1

19. United Aircraft Corp.
    Pratt & Whitney Aircraft Division
    400 Main Street
    E. Hartford, Connecticut 06108
    Attn: P. Goldberg   1
            Library   1
            R. Marshall   1

20. United Aircraft Research
    E. Hartford Connecticut
    Attn: Library   1

21. Detroit Diesel Allison Division
    Department 8894, Plant 8
    P. O. Box 894
    Indianapolis, Indiana 46206
    Attn: R. D. Tyler   1
            F. Verkamp   1
            Library   1

22. Northern Research & Engineering Corp.
    219 Vassar Street
    Cambridge, Massachusetts 02139
    Attn: K. Ginwala   1

23. General Electric Company
    Flight Propulsion Division
    Cincinnati, Ohio 45215
    Attn: Technical Information Center   N-32   1
           D. Bahr   1

24. General Electric Company
    1000 Western Avenue
    West Lynn, Massachusetts 01905
    Attn: Dr. C. W. Smith
           Library Building   2-40M   1

25. Curtiss-Wright Corporation
    Wright Aeronautical Division
    Wood-Ridge, New Jersey 07075
    Attn: D. Wagner   1
           W. Walker   1

26. Air Research Manufacturing Company
    402 South 36 Street
    Phoenix, Arizona 85034
    Attn: Robert O. Bullock   1
           J. M. Haasis   1

27. Air Research Manufacturing Company
    9851 Sepulveda Boulevard
    Los Angeles, California 90009
    Attn: L. C. Wright   1

28. AVCO Corporation
    Lycoming Division
    550 S. Main Street
    Stratford, Connecticut
    Attn: Claus W. Bolton   1
           Charles Kuintzle   1

29. Continental Aviation & Engineering Corp.
    12700 Kercheval
    Detroit, Michigan 48215
    Attn: Eli H. Bernstein   1
           Howard C. Walch   1

30. International Harvester Company
    Solar Division
    2200 Pacific Highway
    San Diego, California 92112
    Attn: P. A. Pitt   1

31. Goodyear Atomic Corporation
    Box 628
    Piketon, Ohio
    Attn: C. O. Langebrake   1

32. George Derderian, AIR 53622 B
    Naval Air Systems Command
    Department of the Navy
    Arlington, Virginia 20360   1

33. The Boeing Company
    Commercial Airplane Division
    P. O. Box 3991
    Attn: G. J. Schott   MS 80-66   1

34. The Boeing Company
    Missile and Information Systems Division
    224 N. Wilkinson Street
    Dayton, Ohio 45402
    Attn: Warren K. Thorson   1

35. Aerojet-General Corporation
    Sacremento, California 95809
    Attn: M. S. Nylin   1
          Library   1

36. Cornell Aeronautical Laboratory
    4455 Genessee Street
    Buffalo, New York 14221   1

37. Marquardt Corporation
    16555 Saticoy Street
    Van Nuys, California   1

38. TRW, Inc.
    23555 Euclid Avenue
    Cleveland, Ohio   1

39. Aro, Inc.
    Arnold Air Force Station
    Tennessee   1

40. Cummings Engine Co.
    Cummings Technical Center
    1900 McKinley Avenue
    Columbus, Indiana 47201
    Attn: Curt Dasbach   1
          Mail Code 50142

41. Pratt & Whitney Aircraft
    Florida Research & Development Center
    Box 2691
    West Palm Beach, Florida 33402
    Attn: G. Lewis   1

42. Aerojet General Corporation
    Sacramento Facility
    P. O. Box 15847
    Sacramento, California 95813
    Attn: C. E. Tedmon   1
           Dave Kors   1

43. Eaton Yale and Towne Research Center
    26201 Northwestern Highway
    Southfield, Michigan 48075
    Attn: H. M. Reigner   1

44. Rocketdyne
    North American Rockwell
    6630 Canoga Avenue
    Canoga Park, California 91304
    Attn: S. D. Clapp, Manager
           Propulsion Technology Research Division   1